Characterization of cerebral vascular abnormalities in an Alzheimer's disease mouse model

by

KAAN ELBI BIRON

B.Sc., University of British Columbia, 2002

A THESIS SUBMITTED IN PARTIAL FULFILLMENT OF

THE REQUIREMENTS FOR THE DEGREE OF

DOCTOR OF PHILOSOPHY

in

THE FACULTY OF GRADUATE STUDIES

(Microbiology and Immunology)

THE UNIVERSITY OF BRITISH COLUMBIA

(Vancouver)

April 2011

Abstract

Alzheimer's disease (AD) patients suffer progressive neurodegenerative loss of memory and other intellectual abilities leading to Dementia, the exact cause of this disease is still unknown. A central pathological hallmark of AD is the presence of an aggregated amyloid-beta peptide (abeta). A strong link between brain vascularity dysfunction and AD exits due to evidence of reduced blood-brain barrier (BBB) integrity preceding other AD neuropatholgies. Furthermore, BBB dysfunction could influence cerebral blood flow, which could in turn influence blood clotting mechanisms during AD. Current dogma holds that AD BBB leakiness is likely due to vascular deterioration and apoptosis. I propose an alternative hypothesis: angiogenesis and hypervascularization underlie increased vascular permeability in AD. Cerebrovascular integrity was characterized in Tg2576 AD model mice by examining the expression of tight junction (TJ) proteins (occludin and ZO-1) with markers of apoptosis and angiogenesis. In aged AD mice, a significant increase in the incidence of disrupted TJs was directly linked to an increased microvascular density, but not apoptosis, which strongly supports hypervascularity as a basis for BBB dysfunction. My results demonstrate that AD related BBB disruption is due to neoangiogenesis, resulting in the redistribution of TJs that maintain the barrier thus providing a new paradigm for connecting vascular remodelling with AD. Unique atypical nonvascular TJ expression was also noted in the aged Tg2576 mice including "halos" of ZO-1 expression surrounding dense-core abeta plaques and occludin expression on a subset of astrocytes sometimes associated with plaques. The observed brain TJ-related pathologies appeared to be linked to the presence of abeta. This argument was

strengthened by observations of Tg2576 mice treated with abeta immunotherapy, which showed reduced brain abeta levels. Tg2576 mice actively immunized with abeta had normal BBB TJ morphology, no apparent occlusions, normal angiogenesis and lacked the unique atypical nonvascular TJ expression. An examination of the general status of the clotting abilities of the Tg2576 mouse was examined. Whole blood from aged Tg2576 mice clotted faster than controls. However, the biochemical components of the clotting cascades were normal, suggesting potential platelet involvement. Taken together, the observed BBB abnormalities will provide new entry points for therapeutic intervention.

Preface

Chapter 4 is based on work that has been previously published. **Figure 4.1**, **Figure 4.2**, **Figure 4.3** and **Figure 4.4** were based on work conducted by Dr. Dara Dickstein (formally of the Dr. Wilfred A. Jefferies laboratory, UBC), which has been published. Dickstein, D. L., Biron, K. E., Ujiie, M., Pfeifer, C. G., Jeffries, A. R. and Jefferies, W. A.. (2006) "Abeta peptide immunization restores blood-brain barrier integrity in Alzheimer disease." The FASEB Journal. 20(3): 426-33. I helped to write and was responsible for editing and compiling the manuscript and imaging **Figure 4.2** and **Figure 4.4**. **Figure 4.1** and **Figure 4.3**, reproduced with permission, were included in this thesis in order to provide supporting evidence for Chapter 4 as recommended by Dr. Wilfred A. Jefferies and my thesis committee. **Figure 4.12**, **Figure 4.13** and **Figure 4.14** are based on work conducted by Drs. Jami Bennett (The Biomedical Research Centre, UBC) and Stephen McQuaid (University of Belfast, Ireland) and have been published. Bennett, J., Basivireddy, J., Kollar, A., Biron, K. E., Reickmann, P., Jefferies, W. A. and McQuaid, S.. (2010) "Blood-brain barrier disruption and enhanced vascular permeability in the multiple sclerosis model EAE." Journal of Neuroimmunology. Published online Sept-15-2010 ahead of print, http://dx.doi.org/10.1016/j.jneuroim.2010.08.011 . Figures used from this publication were reproduced as originally published, with permission. I aided in the reagent procurement, study design, organization, coordination, *in vivo* dissections and experimental execution for **Figure 4.12, Figure 4.13** and **Figure 4.14**. All procedures involving mice were approved by the UBC Animal Care Committee, certificate #'s: A07-

0772 (admendments A07-0772-A001), A07-0271 and A07-0269 (admendments A07-0269-A001 and A07-0269-A002).

Table of Contents

List of Tables

List of Figures

List of Abbreviations

Abeta	Amyloid-beta peptide
Abeta1-40	Amyloid-beta 1-40
Abeta1-42	Amyloid-beta 1-42
AD	Alzheimer’s disease
AJ	Adheren junction
APC	Antigen presenting cells
APLP1	APP-like protein-1
APLP2	APP-like protein-2
ApoE	Apolipoprotein E
APP	Amyloid precursor protein
aPTT	Activated partial thromboplastin time
BBB	Blood-brain barrier
BSA	Bovine serum albumin
CAA	Cerebral amyloid angiopathy
CFA	Complete Freund's adjuvant
CFDA-SE	Carboxyfluorescein diacetate succinimidyl ester
CNS	Central nervous system
CSF	Cerebral spinal fluid
CW	Continuous wave
EAE	Experimental autoimmune encephalomyelitis
EDTA	Ethylenediaminetetraacetic acid
EOAD	Early-onset Alzheimer’s disease
H&E	Hematoxylin and eosin stain
HRT	Hormone replacement therapy
ICFA	Incomplete Freund's adjuvant
IFNγ	Interferon gamma
i.p.	Intraperitoneal
i.v.	Intravenous
KPI	Kunitz protease inhibitor
LFB	Luxol fast blue
LOAD	Late-onset Alzheimer’s disease
LRP	Low density lipoprotein receptor-related protein
MOG35-55	Myelin oligodendrocyte glycoprotein peptide 35-55
MS	Multiple sclerosis
MRI	Magnetic resonance imaging
MVD	Microvessel density
NAWM	Normal appearing white matter
NFT	Neurofibrillary tangle
NVU	Neurovascular unit
PBS	Phosphate buffered saline
PCR	Polymerase chain reaction
PFA	Paraformaldehyde
PI	Propidium iodide

PPP	Platelet-poor plasma
PrP	Prion protein
PS1	Presenilin 1
PS2	Presenilin 2
PT	Prothrombin time
PTX	Pertussis toxin
RAGE	Receptor for advanced glycosylation products
ROS	Reactive oxygen species
SEM	Standard error of the mean
SNPs	Single-nucleotide polymorphisms
TBI	Traumatic brain injury
TF	Tissue factor
TFA	Total fluorescence area
Tg/+	Transgenic heterozyous Tg2576 AD mouse
TJ	Tight junction
TNFα	tumor necrosis factor α
tPA	Tissue plasminogen activator
vWF	von Willebrand factor
WM	White matter
ZO-1	Zona occludin-1
+/+	Wild-type mouse

Acknowledgements

Who to thank and in what order?

My family comes first. Thank you Dad, Mom and Ozan. Mom I miss and love you. With all the crap that we went through, my family has been the ONLY constant positive force. No acknowledgement page can do them justice.

I'd like to thank Dr. Kyla Omilusik (at the writing of this she hadn't finished writing her feces but I'm being pre-emptive here). You are like a sister to me. Thank you for being there both good times and bad. I am seriously going to miss you. I'd like to thank KB Choi, you are a very underrated technician, especially with all the shit you have to put up with. I'd like to thank Les Rollins…because…well…RESPECT. I'd like to thank Dr. Mike Long, I love you dog, let's get married sometime. I'd like to thank Clara Ng for well…she knows why. I'd like to thank the BRC's Core Services for providing me with relevant science shit to do sciencey things. I'd like to thank UBC BioImaging Facility, specifically Kevin Hodgson, for everything all related to confocal. I'd like to thank Ana Chavez Steenbock because 143. I'd like to thank Lisa Murphy because she made the right choice. I'd like to thank the Biomedical Research Centre for being a frat house where you can literally do anything and get away with it. I'd like to thank the Jefferies lab. I'd like to thank Helen Dranse because she wanted to be thanked. I'd like to thank Dr. Bernhard Lehnertz because he's German. I'd like to thank Bahareh Ajami and Leslie So for admiring my legs. I'd like to thank Sherie Duncan for being so cute. I'd like to thank Melanie Olson for shooting the shit.

I'd like to thank Dr. Dara Dickstein for providing me with a sympathetic scientific ear. FYI, Wilf believes that I'm madly in love with you (and he meant romantically). You are an amazing mentor and thank you for your help. I'd like to thank Dr. Stephen McQuaid for providing the initial stepping stones into completing this thesis. FYI, you were literally 5min away from receiving a $250,000 private donation so that I could complete this thesis far far sooner. Unfortunately, egos got in the way. For the person that's reading this right now and has no clue as to what I'm referring to…the moral of the story is to keep your fucking ego in check. I'd like to thank my thesis committee (Drs. Ninan Abraham, Fumio Takei, Marc Horwitz) for putting up with my shit. I wish my relationship with them could have been more productive. I'd like to thank Dr. Wilf Jefferies for his supervisorial support.

Dedication

I dedicate this thesis to:

♥ Aunt Myrna (1940-1998) – Who urged me into science.
♥ Aunty Valerie (1948-2002) – Who urged me to stay in science.
♥ My Mom (1948-2009) – Who urged me out of science.

I miss you.

Chapter 1: Introduction

1.1 Alzheimer's disease

Recently, the Alzheimer's Association released a report detailing the projected costs of caring for sufferers of Alzheimer's disease (AD) from 2010 to 2050 in the United States (http://www.alz.org/alzheimers_disease_trajectory.asp) [1]. In 2010, it is estimated that the cumulative cost of care for AD patients will be $172 billion. This value is expected to balloon to over $1 trillion by 2050 in the US alone. Comparable costs are expected in Canada. Many do not realize that the majority of the estimated costs are for the care of patients in the late stages of the disease who require more expensive, intensive around-the-clock care. The study concludes that even modest hypothetical treatment improvements will significantly reduce the financial and social impact of AD. The ultimate solution is to solve the chronic underfunding of research in order to facilitate the development of therapeutics agents for AD. With a rapidly aging Western population, the saying "it takes a village to raise a child" will be reversed to "it takes a village to care for the elderly". Time, as inevitable as it is, will tell if the warnings are heeded.

1.1.1 In the beginning

In 1901, Auguste Deter, a woman in her early 50's, was committed by her husband to a Frankfurt mental institution [2]. She was examined by Dr. Alois Alzheimer, who described her as having severe cognitive disorders relating to memory, language and social interaction. Upon her death in 1906, Alzheimer began the neuropathological

characterization of her brain [3]. He noted two major neuropathologies: senile plaques (a structure that had been previously noted by others) and neurofibrillary tangles (a previously uncharacterized pathology of neurons) [4]. In 1910, Alzheimer's senior colleague, Emil Kraepelin, eponymously gave Alzheimer the credit for characterizing the disease [5]. Nevertheless, there is controversy regarding Kraepelin's motives for giving Alzheimer sole credit for the description of a disease that may have been exaggerated to be "new" [6]. Kraepelin may have been partly motivated financially, in order to secure more research funding for "discovering" a new disease, and politically, in order to dampen competing researchers' interests.

1.1.2 A brief description of Alzheimer's disease

AD is categorized as a type of dementia [7], an umbrella term used to describe non-specific symptoms relating to cognitive function. Dementia affects memory, attention, personality, language and problem solving abilities. AD is a progressive neurodegenerative disorder and is described as the most common form of dementia [8] that, as of 2008, affects nearly 500,000 Canadians [9]. Neurodegeneration is another umbrella term for the loss of structure and function of neurons. The basic definition of a neuron is a specialized cell type of the central nervous system (CNS) that communicates information electrically and chemically throughout the body. These signals can relate information regarding movement, the senses and memory. As loss of neurons mount, patients affected with AD typically survive 3-10yrs with the average being six [10]. There are two forms AD: familial and sporadic. The familial form, also referred to as early-onset Alzheimer's disease (EOAD), accounts for <5% of the diagnosed cases [11]

has a strong genetic component and tends to strike early in age (prior to ages 60-65yrs). Sporadic AD, also referred to as late-onset Alzheimer's disease (LOAD), has a complex and multifactorial etiology but generally strikes an aging brain (>65yrs) [11].

Diagnosing AD is complex. A singular test for AD does not yet exist. A patient presenting with "noticeable" gradual cognitive decline will be put through a battery of imaging (PET and or MRI) procedures, neurological, blood and psychological tests [11]. Furthermore, so-called secondary causes of dementia, such as vascular or HIV-associated dementia, must be ruled out. Even after being put through a multitude of tests, an AD diagnosis is not absolute. This diagnosis will still be labeled as "possible" or "probable" AD [12]. Only after death, when the brain is examined for the microscopic neuropathies associated with AD, can a definitive diagnosis be made. It has been estimated that the accuracy of diagnosing living patients compared to autopsy is about 87% [13]. Upon diagnosis, a patient is categorized according to the severity of their disease and palliative treatment options will be given. A cure for AD currently does not exist.

1.1.3 Alzheimer's disease pathology

During the post-mortem examination of Auguste Deter's brain, Dr. Alzheimer noted two major microscopic neuropathologies that would become hallmarks of the disease bearing his name: amyloid plaques and neurofibrillary tangles (NFT) [14]. In a basic sense, both of these hallmarks can be described as protein aggregation pathologies. Amyloid plaques represent the aberrant extracellular aggregation of the amyloid-beta peptide (abeta). NFTs are the intracellular neuronal aggregation of a protein called tau. Whether abeta plaques

and or NFT are a cause or a side-effect of AD remains to be demonstrated. Both pathologies are believed to contribute to a cascade of events that lead to neuronal death and the symptoms of AD. How this occurs is still debated. But several instigators have been examined including abeta, oxidative stress and neuroinflammation.

1.1.3.1 Amyloid-beta

Abeta is a 4kDa peptide that was first identified from AD senile plaques in the early 1980's and subsequently in similar plaque deposits in brains of individuals with Down's syndrome [15-17]. The Down's syndrome connection to abeta eventually led to cloning of the amyloid precursor protein (APP) [18], from which abeta is ultimately derived. Abeta is a proteolytic cleavage product of APP and the cleavage pathway has been extensively characterized **Figure 1.1** (reviewed by [19]).

Figure 1.1: Processing of APP by the secretases.
APP is capable of being cleaved by two separate but functional pathways. (a) In the nonamyloidogenic pathway, APP is first cleaved by alpha-secretase within the abeta sequence, which releases the APPs-α ectodomain. Further processing at the carboxyl terminal of the abeta domain, by gamma-secretase, results in the release of the p3 fragment. (b) The amyloidogenic pathway begins with the beta-secretase cleavage of APP at the amino terminus of abeta domain, releasing the APPs-β ectodomain. Further processing at the carboxy-terminal fragment of the abeta domain, by gamma-secretase, results in the release of abeta. (c) The amino acid residues where the various secretases cleave APP. Abeta and p3 fragments of differing lengths are produced by processing of APP at two different sites by gamma-secretase. The location of the Swedish mutation (KM670/671NL), in the blue box, is noted. Abbreviations: abeta, amyloid-beta peptide; APP, amyloid precursor protein; APPs-α, soluble amyloid precursor protein-α; APPs-β, soluble amyloid precursor protein-beta; C83, carboxy-terminal fragment 83; C59, carboxy-terminal fragment 59; C99, carboxy-terminal fragment 99. Adapted by permission from Macmillan Publishers Ltd: Nature Reviews: Neurology (http://www.nature.com/nrneurol/index.html) [20], copyright (2010).

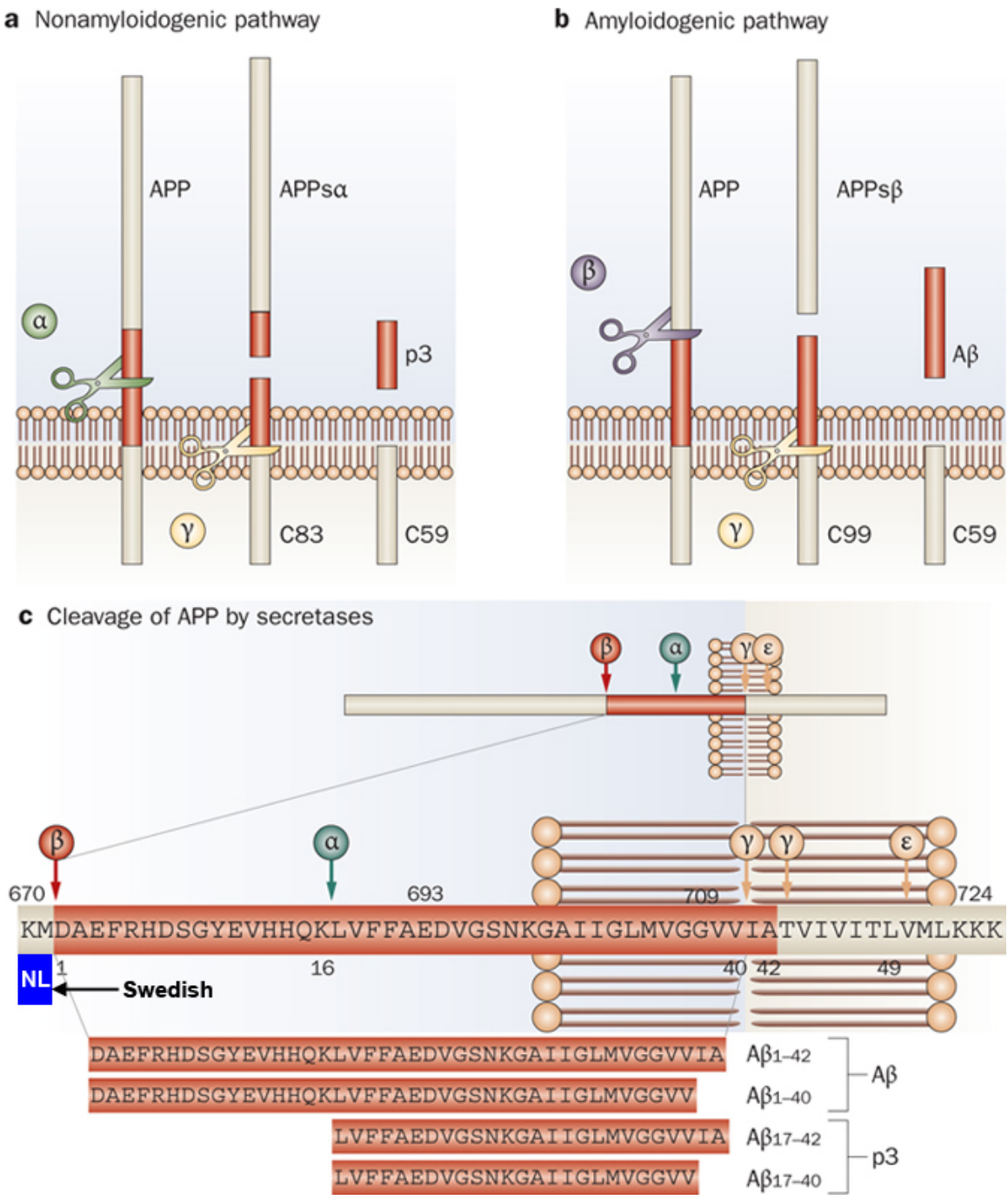
a Nonamyloidogenic pathway
APP
APPsα
p3
α
γ
C83
C59
b Amyloidogenic pathway
APP
APPsβ
β
Aβ
γ
C99
C59
c Cleavage of APP by secretases
β
α
γ
ε
γ
γ
ε
670
693
709
724
KMDAEFRHDSGYEVHHQKLVFFAEDVGSNKGAIIGLMVGGVVIATVIVITLVMLKKK
NL
1
16
40
42
49
Swedish
DAEFRHDSGYEVHHQKLVFFAEDVGSNKGAIIGLMVGGVVIA
Aβ1–42
DAEFRHDSGYEVHHQKLVFFAEDVGSNKGAIIGLMVGGVV
Aβ1–40
Aβ
LVFFAEDVGSNKGAIIGLMVGGVVIA
Aβ17–42
LVFFAEDVGSNKGAIIGLMVGGVV
Aβ17–40
p3

APP is a type 1 integral membrane protein that belongs to an evolutionary conserved gene family [21] found on chromosome 21 in humans. In mammals, the APP gene produces three major isoforms: APP695, APP751 and APP770. Although APP is ubiquitously expressed, certain isoforms are predominant in some tissues. For example, APP695 is mainly found in the brain [18], while APP751 and APP770 are highly expressed in platelets [22, 23]. All APP isoforms have a large extracellular N-terminal portion and a shorter cytoplasmic C-terminal sequence [24]. The major difference between the different APP isoforms is the presence or absence of a Kunitz protease inhibitor (KPI) domain, which is absent from APP695. This domain is capable of inhibiting blood clotting [25-28]. Homologs of APP have also been identified and have been labeled as APP-like protein-1 [29] and -2 [30] (APLP1 and APLP2). They have similar protein structures, similar predicted proteolytically cleavage patterns to APP but do not make abeta. The relevance of the APP isoforms to AD is unclear.

1.1.3.1.1 Amyloid-beta production

Cleavage of APP into its various products occurs sequentially using a combination of three different secretase enzymes (gamma and alpha or beta) [19]. Depending on the combination of secretase enzymes used, two major APP processing pathways can result. Under the non-amyloidogenic pathway **Figure 1.1a**, alpha and gamma-secretases preclude the production of abeta. Under the amyloidogenic pathway **Figure 1.1b**, beta and gamma-secretases liberate soluble abeta. It has been estimated that 90% of APP is cleaved via the non-amyloidogenic pathway under normal physiological conditions [31]. The pathway liberating abeta is the minor 10%. The physiological functions of the

various cleavage products of either pathway are not clear. Some cleavage products like the soluble APP alpha-secretase cleavage product (APPs-α) **Figure 1.1a** are thought to be neuroprotective [31, 32]. The exact physiological function of APP is unclear. However, APP and its homologs may have roles in variety of biological roles including neuronal growth and survival, cell adhesion and insulin and glucose homeostasis (reviewed briefly by [21]). APP null mice are viable but have a number of phenotypes including metabolic and behavioral deficits [33]. However, these mice can be rescued by reintroducing the APPs-α fragment [33]. Mice lacking all three APP homologs (APP, APLP1 and APLP2) are not viable [34]. This suggests that APP, and its related proteins, are physiologically important.

Pathologically, the beta and gamma-secretase cleavage pathway has received the most attention as secreted soluble abeta is released. However, abeta is secreted under normal physiological conditions [35-37], suggesting a yet to be clarified biological role for the peptide. Abeta has several different liberated sizes ranging from 38 to 43 amino acids in length. The most common abeta fragment is 40 amino acids in length (abeta1-40) **Figure 1.1c** and is estimated to be 90% of the abeta species produced [38]. The slightly longer 42 amino acid species (abeta1-42), and more toxic, is a minor product. The length of the abeta species produced results from two gamma-secretase cleavage sites that are two amino acids apart. The amyloidogenic pathway is enhanced by specific mutations found either on APP or the subunit components that make up the gamma-secretase enzyme complex. These mutations are associated with the rarer EOAD (summarized by http://www.molgen.ua.ac.be/ADMutations/) and favor the increased specific

production of abeta1-42 [39, 40]. For example, the so-called Swedish double mutation results in the near six-fold increase in abeta1-42 [41, 42] due to increased beta-secretase processing [43]. These mutations have been the basis of AD-like transgenic mice models where the increased production of abeta can lead to AD, in the case of EOAD. The pathologic trigger for LOAD, which occurs in the vast majority of patients, is unknown.

Abeta has the ability to spontaneously form aggregates ranging in size from dimers to larger oligomers. The oligomers may multimerize into protofibrils, which can further aggregate into insoluble dense-core abeta plaques, a hallmark of AD. The mechanics, biochemistry and physics behind amyloid aggregation have been extensively studied and are reviewed by [44]. The abeta1-42 species is believed to be far more toxic and has a higher ability to form aggregates [45] while abeta1-40 is soluble. Abeta1-42 is also believed to make up the bulk of the plaques and vascular deposits of abeta seen in the disease [46, 47]. Current thinking suggests that the extracellular dense-core abeta plaques are not the cause of AD related dementia, but the soluble abeta oligomers are [48] because there has been no direct correlation between the number of plaques and the severity of dementia in AD [49]. Studies *in vitro* and *in vivo* have demonstrated that oligomers of abeta are more neurotoxic than the insoluble plaques [50-53]. While the mechanism(s) of oligomer formation and toxicity are still unclear, it is known that the process can occur both extra- and intracellularly (reviewed by [48]).

1.1.3.1.2 The amyloid cascade hypothesis

Prior to 1992, explanations and causes for pathogenesis of AD were unfocused. Even today, the exact cause of AD is still heavily debated. The amyloid cascade hypothesis was proposed [54, 55] in order to provide direction to AD research. Several observations led to the formation of the hypothesis. Plaques were identified to be comprised of abeta, which was later found to be a cleavage product of APP. Identifying the APP gene led to its discovery on human chromosome 21. Diseases involving gene duplications of chromosome 21, like Down's syndrome (trisomy 21), develop AD-like symptoms. Finally, EOAD is associated with specific mutations in the APP gene and enzymes that proteolytically cleave APP. Although only a hypothesis, it is the best defined and the most studied conceptual framework for AD [56] but it is not universally accepted. In its basic form, the hypothesis states that abeta is the cause of all AD pathogenesis including NFTs **Figure 1.2**.

Figure 1.2: AD pathogenesis according to the amyloid cascade hypothesis.
The hypothesis suggests that altered metabolism of abeta, in particular aggregation-prone abeta species like abeta1-42, initiates AD pathogenesis. Oligomeric assemblies of abeta trigger aggregation of tau and the formation of NFTs, but also inflammation and oxidative stress, by unclear mechanisms. These downstream processes give rise to progressive neurodegeneration, which ultimately results in dementia. The main pathogenic pathway of AD is illustrated with red arrows, whereas minor contributory pathways are shown with thinner brown arrows. The experimental support for the hypothesis comes mainly from studies of families in which AD is inherited as a dominant trait due to mutations in APP, PS1 or PS2. The evidence that the hypothesis applies to sporadic AD is less solid, although risk factors such as age and ApoE genotype both strongly impact on abeta aggregation in transgenic models and post mortem AD brain. FEBS Journal, 2010, with permission [57] (https://www.interscience.wiley.com).

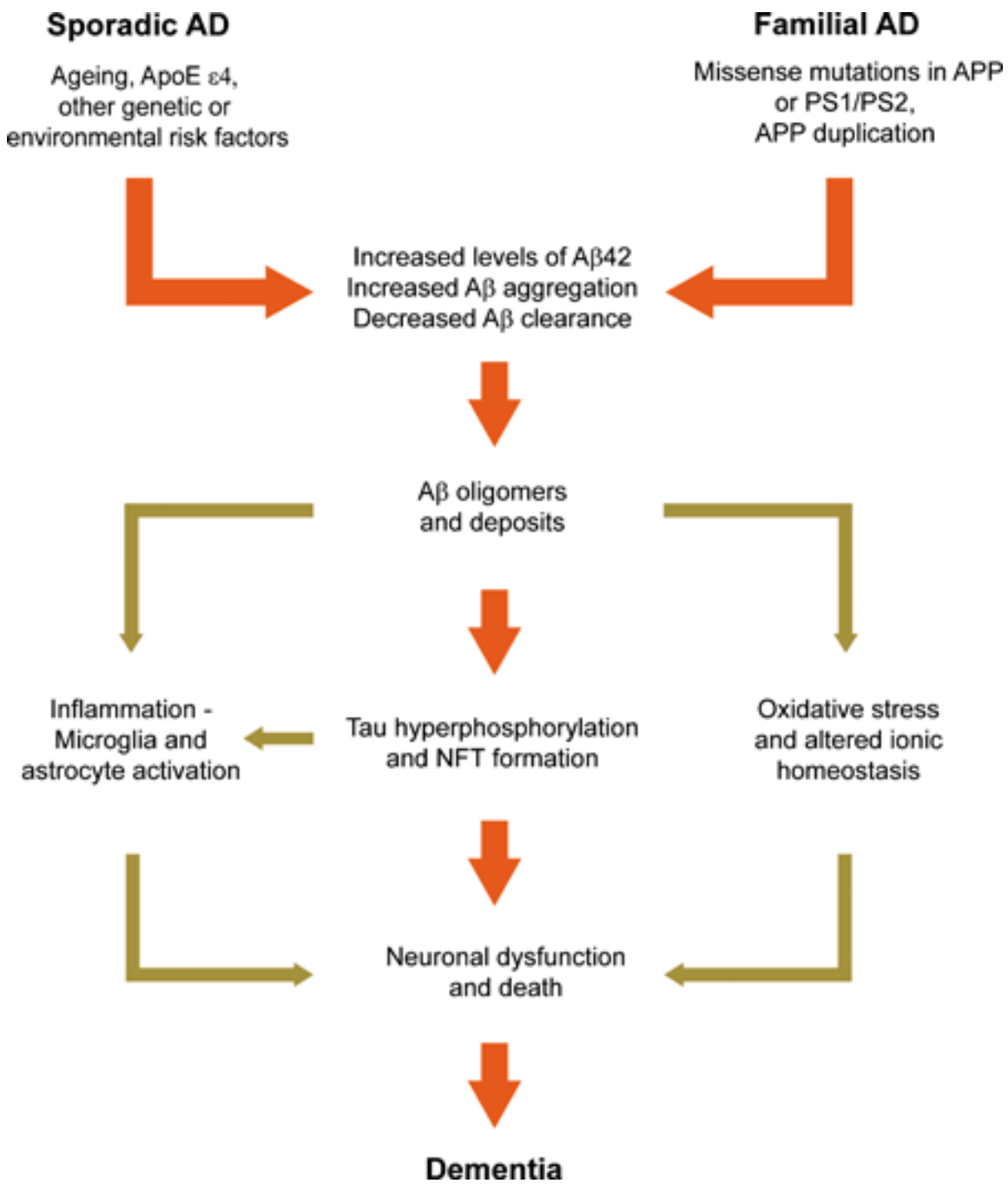
Sporadic AD
Ageing, ApoE ε4, other genetic or environmental risk factors
Familial AD
Missense mutations in APP or PS1/PS2, APP duplication
Increased levels of Aβ42
Increased Aβ aggregation
Decreased Aβ clearance
Aβ oligomers and deposits
Inflammation - Microglia and astrocyte activation
Tau hyperphosphorylation and NFT formation
Oxidative stress and altered ionic homeostasis
Neuronal dysfunction and death
Dementia

Since the proposal of the amyloid cascade hypothesis, several predictions have been generated that have been heavily scrutinized and criticized [56, 58]. Abeta is predicted to cause ALL of the disease symptoms associated with AD. This prediction has yet to be fulfilled. For example, transgenic animal models based on various mutations associated with EOAD only replicate some of the pathologies of AD (discussed below). Abeta should be toxic. As discussed above, current thinking suggests that abeta oligomers are the toxic species. But the mechanism(s) of formation and toxicity are still unclear. Furthermore, *in vitro* studies demonstrating toxicity have been difficult to translate *in vivo*. Removing abeta should eliminate ALL disease pathology and symptoms. This prediction has been tested with limited success. Abeta immunotherapy has successfully treated various AD transgenic mouse models, which are incomplete descriptions of AD. Human abeta immunotherapeutic clinical trials had mixed results and interpretations are incomplete (discussed later). Although, the hypothesis has not met all expectations, it has clearly demonstrated that AD is complex and multifactorial. A variation of the amyloid cascade hypothesis, proposed by Hardy [58], suggests the involvement of vascular damage in combination with abeta. Damage to the vascular endothelial could cause or exacerbate amyloidosis leading to disease.

1.1.3.2 Inflammation and oxidative stress

Abeta may influence neuropathology either directly or indirectly through oxidative stress and or inflammation. Reactive oxygen species (ROS) are highly chemically reactive molecules containing oxygen that can be organic or inorganic [59]. ROS belong to a class of chemicals called free radicals, which have one or more unpaired valence shell

electrons. They are termed “free” because they have an independent existence. ROS are continually created as a by-product of the various normal cellular metabolisms within cells, especially in the brain due to its high oxygen requirement (reviewed by [59]). ROS are capable of inducing oxidative cellular damage by destroying proteins, nucleic acids and lipids, which can drastically affect normal cellular functions. In response, cells and tissues have evolved complex mechanisms to detoxify and cope with ROS related damage [59]. Upsetting the balance towards pro-ROS generation will result in oxidative stress [60], which contributes to ageing [61]. During AD, oxidative stress is increased and plays role in neuropathology (reviewed by [62]). Briefly, vascular and mitochondrial dysfunctions, presence of metals associated with abeta plaques and abeta itself have been demonstrated to influence or directly participate in ROS-related neuronal damage in AD.

Increased oxidative stress in the AD brain can activate inflammatory processes that may damage neurons [63]. However, it is not clear whether neuroinflammation is a cause or a result of neuronal death in AD. Several pro-inflammatory mechanisms within the brain are believed to participate in the AD inflammatory process. Abeta itself can trigger inflammation by activating microglia [64, 65], the resident brain macrophages, which are associated with amyloid plaques. Astrocytes can stimulate inflammation [66]. Following internalization of abeta [67], astrocytes have been shown to secrete pro-inflammatory cytokines resulting in the stimulation of microglia [68]. Antibody independent complement reactions are also known to be activated by abeta [69] and can further stimulate inflammation. The role of NFTs influences in inflammation is less defined; however pro-inflammatory conditions may induce tau hyperphosphorylation, as suggest

by [70], causing tau to create pathological aggregates. Taken together, a positive inflammatory feedback loop is potentially involved in AD [63]. Abeta activates microglia creating pro-inflammatory conditions. The activated microglia can further release pro-inflammatory cytokines, which can activate astrocytes. Local astrocytes can also secrete pro-inflammatory mediators, which in combination with microglia, abeta, and oxidative stress may damage neurons. The damaged neurons might further exacerbate the inflammatory response by releasing pro-inflammatory signals. With increased AD associated inflammation, anti-inflammatory therapy has been explored but with disappointing results [65]. It is believed that the therapeutic failure is in part due to the fact that microglia activity may not be directly affected by the drugs used in the various studies.

1.1.4 Risk factors for Alzheimer's disease

AD is a chronic complex neuropathology that involves multiple factors. A search for risk factors that are associated with the disease is ongoing and depending on the form of AD, either familial or sporadic, the risk factors for the disease are different. EOAD is directly associated with a strong genetic component involving mutations that affect the metabolism of APP. These mutations can be highly penetrant (summarized by http://www.molgen.ua.ac.be/ADMutations/). The most common mutations are associated with APP directly and two different proteins that make up the gamma-secretase enzyme complex, presenilin 1 and 2 (PS1 and PS2), [71]. As mentioned above, these mutations increase the metabolism of APP, generating the more toxic and

aggregatable abeta1-42. It has been estimated that mutations in PS1 could be present in up to 70% of patients with EOAD [72].

Two risk factors for sporadic AD have received greater attention over the past few years, the apolipoprotein E (ApoE) genotype and vascular abnormalities. ApoE is a soluble secreted lipoprotein that is a ligand in the delivery of cholesterol and has been extensively studied in relation to the pathobiology of AD (reviewed by [73]). In the brain, ApoE is produced mainly by astrocytes [74] and aids in the maintenance of neuronal synapses [75]. Genetically, ApoE has three major isoforms, resulting from single-nucleotide polymorphisms (SNPs), referred to as ApoE2, ApoE3 and ApoE4 [76]. The risk for developing sporadic AD increases significantly to nearly 12 times depending on the number of allelic copies of ApoE4 compared to the other ApoE isoforms [77]. How the increased risk for AD is influenced by ApoE4 is not clear because ApoE has both neurodestructive and neuroprotective properties. For example, ApoE (sometimes further enhanced by ApoE4) is known to bind and act as a chaperone for abeta [78], promote abeta aggregation [79], influence APP metabolism [80] and abeta clearance [81].

Prior to the 1900's, vascular abnormalities were recognized as a precursor event to development of what would eventually be labeled as Alzheimer's disease [82]. The exact involvement of vascular disorders with AD is hotly debated. However, it is accepted that there is a strong correlation between the risk factors for vascular disorders and AD (reviewed by [83-85]). These risk factors include the brain injuries, ApoE4 allele and cardiovascular disease. Traumatic brain injuries (TBIs) have been linked to AD [86]. For

example, professional athletes that receive a disproportionate number of head injuries have an increased risk for AD [87]. Reasons for this link are still under investigation but it is important to note that abeta plaques are found in patients who died from acute TBI [88]. As mentioned earlier, the ApoE4 allele is a strong genetic risk factor for AD. Due to the involvement of ApoE in cholesterol metabolism, it is also implicated as a risk factor for various cardiovascular diseases [89] like stroke. Furthermore, ApoE4 is also a significant risk factor for another separate abeta vascular disorder cerebral amyloid angiopathy (CAA). Described as a protein elimination disorder, CAA occurs in at least 90% of patients with AD [90] and is characterized by abeta deposits on the cerebral arteries [91]. The consequence of the vascular deposition of abeta during AD and CAA is the interruption of cerebral blood flow, which can directly impact the cognitive functions of the brain. Cardiovascular disease is a broad umbrella term for a class of diseases that affect the heart and blood vessels. Since the brain's blood supply is entirely dependent on the heart, any disorders of the heart will impact the brain. Therefore, risk factors for cardiovascular diseases are also associated with AD [92], which includes hypo- and hypertension, smoking and increases in cholesterol. Many of the vascular related risk factors for AD are considered to be exclusion criteria for the diagnosis of the disease. As research into AD progresses, the interconnectivity of these seemingly unrelated disorders will eventually translate into viable treatment options.

1.1.5 Alzheimer's disease mouse models

Several unknowns have made it difficult to model AD accurately. The knowledge of the physiological functions of abeta and APP is still unknown. The exact involvement of the

neuropathological mechanism(s) of abeta and NFTs in AD is also unclear. Furthermore, the cause of the sporadic form of AD has yet to be clarified. However, according to the amyloid cascade hypothesis, altered abeta metabolism leads to several downstream effects including the formation of NFTs, inflammation and oxidative stress resulting in neuronal dysfunction and death seen in AD. The bulk of the support for the hypothesis is largely based on studies using various AD mouse models incorporating the genetics of the familial form of AD. To date, there are well over 30 different strains of AD mouse models (a detailed list can be found at http://www.alzforum.org/res/com/tra/default.asp) currently available to researchers. A short list of the most popular mice is summarized in **Table 1.1** and **Table 1.2**.

Table 1.1: Neuropathological characteristics of some common AD transgenic mouse models.
+++, extensive phenotype; +, detectable; −, not detected; nr, not reported. FEBS Journal, 2010, with permission [57] (https://www.interscience.wiley.com).

Model [Ref]	Transgene	Promoter	Age of plaque onset (mo)	Neuritic plaques	Diffuse plaques	CAA	Intraneuronal abeta accumulation	CNS specific expression	Neuro-degeneration	N-terminal truncated abeta
Bri-wt-Abeta1-42A [93]	Human integral membrane protein 2B (ITM2B)/mouse/human APP	Mouse PrP	3	+++	+++	+	nr	+	-	nr
PDAPP [94]	APP minigene V717F (Indiana)	PDGF	6–8	+++	+++	+	nr	+++	-	nr
APP-London [95]	Human APP695 cDNA V642I (London)	Mouse Thy1	> 12	+++	+++	+	nr	+++	-	nr
Tg2576 [96]	APP695 cDNA KM670/671NL (Swedish)	Hamster PrP	9–11	+++	+	+	+	+	-	+
$APP^{NLh/NLh}$ [97, 98]	Mouse APP with humanized abeta containing Swedish mutation	Endogenous mouse APP	> 22	nr	nr	nr	nr	-	-	nr
C3-3 [99]]	Mouse APP with humanized abeta containing Swedish mutation	Mouse PrP	18	+	+	nr	nr	+	-	nr
R.1.40 [100]	YAC with 300kb human APP gene with Swedish mutation	Mouse APP	14	+++	+++	+	nr	-	-	nr
APP23 [101]	APP751 cDNA with Swedish mutations	Murine Thy1	6	+++	+	+	nr	+++	-	nr
Tg-CRND8 [102]	human APP695 cDNA with Swedish/Indiana mutations	Hamster PrP	3	+++	+	+	nr	+	-	nr
APPDutch [103]	human APP751 cDNA with E693Q (Dutch) mutation	Mouse Thy1	22–25	-	+	+++	+	+++	-	nr

Table 1.2: Continued neuropathological characteristics of some common AD transgenic mouse models.
+++, extensive phenotype; +, detectable; −, not detected; nr, not reported. FEBS Journal, 2010, modified with permission [57].

Model [Ref]	Transgene	Promoter	Age of plaque onset (mo)	Neuritic plaques	Diffuse plaques	CAA	Intraneuronal abeta accumulation	CNS specific expression	Neuro-degeneration	N-terminal truncated abeta
Tg-SweDI [104]	Human APP cDNA with Swedish/ Dutch/D694N (Iowa) mutations	Mouse Thy1	3	-	+++	+++	nr	+++	-	nr
Tg-ArcSwe [105]	Human APP695 cDNA with Swedish/E693G (Arctic) mutations	Murine Thy1	6	+++	+	+	+++	+++	-	nr
APParc [106]	Human APP695 with Arctic mutation	Murine Thy1	> 12	+	+	+	-	+++	-	nr
PSAPP [107]	APP695 cDNA with Swedish + PS1 (M146L) mutations	hamster PrP + Rat PDGF b-chain	6	+++	+	+	nr	+	-	nr
3xTg-AD [108]	Human APP695 cDNA with Swedish + PS1 (M146V) + tau (P301L)	Mouse Thy1	6	+++	+++	+	+++	+++	-	nr
5xFAD [109]	Human APP695 cDNA with Swedish/London/I71 6V (Florida) mutations + PS1 (M146L and L286V)	Mouse Thy1	2	+++	+	nr	+++	+++	+	nr
APP/PS1 KI [110]	Human APP751 cDNA with Swedish/London mutations + PS1 (M233T and L235P) knockin	Mouse Thy1	2–3	+++	+	nr	+++	+++	+	+++
TBA2 [111]	Mouse thyrotropin-releasing hormone-Abeta fusion protein	Mouse Thy1	2	nr	+++	-	+++	+++	+++	+++

Nearly all the available AD mouse models are based on the genetics of familial form of AD (reviewed by [57]), even though this form of AD only represents <5% of all AD cases. Therefore, the bulk of these mice are technically models of the predementia phase of familial AD rather than the more prevalent sporadic form. The mutations in APP, PS1 and PS2, isolated from families with familial AD, affect the processing and metabolism of APP. A variety of transgenic mice have been created that over-express the mutant variants of APP, PS1 and or PS2 genes in an attempt to recapitulate the pathologies of AD. The resulting AD mouse models perform this task with varying levels of success. No mice that over-express mutant variants of APP, PS1 or PS2 have been known to develop NFTs. Furthermore, to date there is no mouse expressing a single gene that displays all known AD pathologies.

One example of a familial AD mutation that has gained popularity is the double Swedish mutation found on APP **Figure 1.1c**, which was originally identified in 1992 from a Swedish family [112]. The mutation is located on two consecutive amino acids (KM670/671NL) just outside the N-terminus of the abeta domain on APP. The Swedish mutation increases production of total abeta by nearly six to eight times *in vitro* [41] by favouring processing by beta-secretase [43]. Subsequently, the Swedish mutation was used to identify the beta-secretase enzyme, BACE1 [113]. Several transgenic mice have been created that incorporate the Swedish mutation. In the knockin mouse model $APP^{NLh/NLh}$ **Table 1.1**, the abeta domain of the endogenous mouse APP was humanized and incorporated with the Swedish mutation [97]. This created a mouse that expresses mouse APP (under its natural promoter) with the Swedish mutation generating

humanized abeta. However, after 22 months of age the $APP^{NLh/NLh}$ mice failed to develop abeta plaque pathology [98]. The APP23 mouse **Table 1.1** over-expresses the Swedish mutation in the APP751 isoform under the control of a mouse specific neuron promoter Thy-1 [101]. This mouse develops abeta plaques by six months of age and is known to develop cognitive defects [114] and CAA associated blood-brain barrier leakage [115]. Finally, the most popular AD mouse model, Tg2576 **Table 1.1**, also incorporates the Swedish mutation but on the APP695 isoform under the control of the hamster prion promoter [96, 116]. The Tg2576 mouse develops many of the common abeta related pathologies seen in AD including abeta plaques beginning by nine months of age [96], CAA [96, 117], cognitive defects [96], cerebrovascular defects [118-121], astrogliosis [122], microglosis [123], oxidative stress [124] and dystrophic neuritis [122]. However, this mouse does not develop tau pathologies or neuronal loss and is therefore a useful but incomplete model of AD.

1.2 The blood-brain barrier

The blood-brain barrier (BBB) is the anatomical description of the extensive network of capillary blood vessels that permeate the entire brain (reviewed extensively by [125]) **Figure 1.3** and is estimated to be over 600 km in total length in humans [126].

Figure 1.3: The blood-brain barrier.
(a) The blood–brain barrier (BBB) is formed by endothelial cells at the level of the cerebral capillaries. These endothelial cells interact with perivascular elements such as basal lamina and closely associated astrocytic end-feet processes, perivascular neurons (represented by an interneuron here) and pericytes to form a functional BBB. (b) Cerebral endothelial cells are unique in that they form complex tight junctions (TJ) produced by the interaction of several transmembrane proteins that effectively seal the paracellular pathway. These complex molecular junctions make the brain practically inaccessible for polar molecules, unless they are transferred by transport pathways of the BBB that regulate the microenvironment of the brain. There are also adherens junctions (AJ), which stabilize cell–cell interactions in the junctional zone. In addition, the presence of intracellular and extracellular enzymes such as monoamine oxidase (MAO), gamma-glutamyl transpeptidase (gamma-GT), alkaline phosphatase, peptidases, nucleotidases and several cytochrome P450 enzymes endow this dynamic interface with metabolic activity. Large molecules such as antibodies, lipoproteins, proteins and peptides can also be transferred to the central compartment by receptor-mediated transcytosis or non-specific adsorptive-mediated transcytosis. The receptors for insulin, low-density lipoprotein (LDL), iron transferrin (Tf) and leptin are all involved in transcytosis. P-gp, P-glycoprotein; MRP, multidrug resistance-associated protein family. Reprinted by permission from Macmillan Publishers Ltd: Nature Reviews: Drug Discovery (http://www.nature.com/nrd/index.html) [127], copyright (2007).

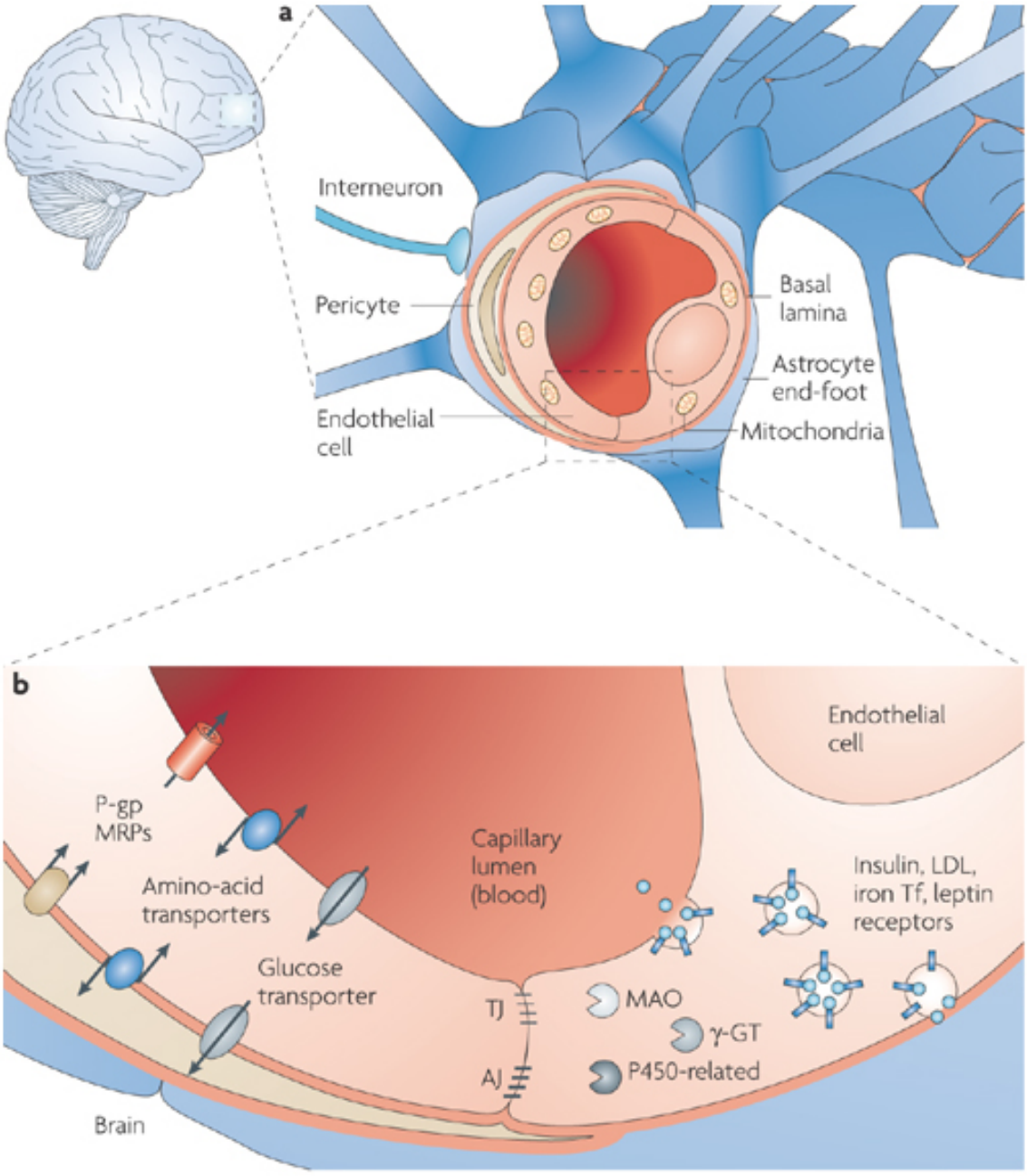

Nature Reviews | Drug Discovery

These blood vessels are comprised of highly specialized endothelial cells that compartmentalize the brain from the peripheral blood. The endothelial cells form a tight sealing monolayer that prevents the passive exchange of solutes between the blood and the brain. The seal between endothelial cells are maintained by tight junction (TJ) proteins **Figure 1.3b** that helps strengthen the barrier that compartmentalizes the brain from the peripheral blood. The BBB has several functional consequences (reviewed by [128]). It serves to prevent potentially toxic substances like the peripheral immune system, pathogenic organisms and their related toxic by-products from damaging the sensitive tissues within brain. Compartmentalizing the brain prevents neuroactive molecules, like neurotransmitters that are capable of affecting the brain and peripheral tissues, "cross-talking" between tissues. Furthermore, compartmentalization creates an optimal microenvironment in the brain by restricting ion and fluid movement. The metabolic requirements of the brain are directly influenced by highly specific transport proteins and mechanisms on the BBB that efflux nutrients and waste products into and out of the brain. These include glucose, amino acid and multidrug resistance-associated transporters. Although the cerebral endothelial cells may physically create the barrier, the concept of the BBB is antiquated because it represents a component in the larger structure, the neurovascular unit (NVU).

1.2.1 The neurovascular unit

The NVU is comprised of multiple cellular subunits that work in concert to maintain proper brain function [125] **Figure 1.3a**. The cellular subunits include neurons, endothelial cells creating the BBB, astrocytes, pericytes and microglia. Although the

BBB is central to the NVU, proper functioning of the endothelia is maintained by intercellular signaling of the adjacent cells [129]. Pericytes surround the endothelium and provide structural stability to the blood vessel by regulating BBB gene expression and influencing astrocyte function [130]. Astrocyte foot processes encircle the pericyte-endothelial cell structure and provide a direct cellular link to neurons [130, 131]. Furthermore, astrocytes help maintain the physical and metabolic requirements of the BBB. Microglia are the resident brain macrophages that act to protect the brain from immune insults. Finally, the bulk of the metabolic demands in the brain are due to the neurons, which can directly influence cerebral blood flow. A dysfunction in any component of the NVU can have disastrous consequences for brain function.

1.2.2 Junctional complexes

The integrity of the BBB is maintained by several different inter-endothelial junctional complexes (reviewed by [125, 128]) **Figure 1.4**.

Figure 1.4: Endothelial cell–cell junctions of blood-brain barrier microvessels.
The diagram shows the major components and organization of the junctional complexes found within the endothelium of the BBB. The major components of the adheren and tight junctions include transmembrane junctional proteins (named in cell 1) and scaffolding proteins and junction-associated proteins involved in mediating the interaction with the actin cytoskeleton (cell 2) are depicted. With kind permission from Springer Science+Business Media: Seminars in Immunopathology, v31, 2009, p497, Engelhardt, B. and Sorokin, L., Fig 2, [132].

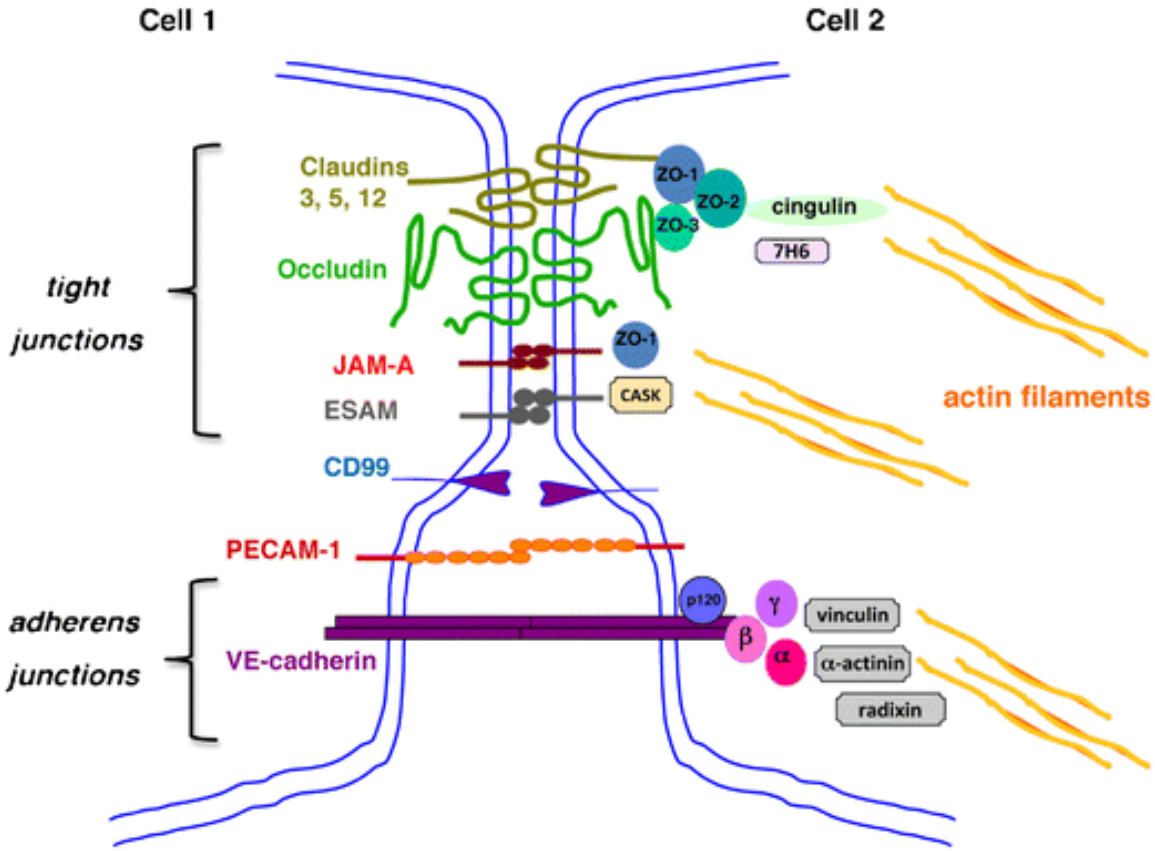

The junctional complexes are comprised of a variety of plasma membrane spanning proteins, scaffold cytoplasmic proteins and the actin cytoskeleton. One type of junctional complex is the adheren junction (AJ) that physically joins adjacent endothelial cells together while providing structural support by anchoring to the cytoskeleton. VE-cadherin is an example of an AJ protein that mediates cell-cell adhesion, and it is linked to the cytoskeleton by various catenins. AJs are critical for the formation of TJs [128]. The physical seal of the BBB is maintained by TJs that act as a "fence" and a barrier. The fence property creates the apical and basolateral polarity of an individual endothelial cell. The barrier function prevents cells and solutes from passing between adjacent cells.

Found near the apical side of a cell barrier, TJ proteins fall into several classes depending on the molecular structure of the membrane protein. For example, occludins are TJ proteins that have a short cytoplasmic N-terminal region, four transmembrane spanning domains and a long cytoplasmic C-terminal region [133]. Other TJ proteins include claudins and JAM-A. Identical TJ proteins from adjacent cells will associate with each other to create the physical barrier. Multidomained cytoplasmic adaptor proteins, like Zona occludin-1 (ZO-1), bind to occludin and other TJ proteins, and provide a direct link to anchor the cytoskeleton. Aside from maintaining barrier functions, many of the junctional complex proteins are also involved signaling cascades relating to morphogenesis, proliferation, differentiation and cell polarity [134]. Various disease conditions are also noted to have BBB dysfunction either as a direct or indirect result of pathology.

1.2.3 The blood-brain barrier and disease

Several infectious, cancerous, inflammatory and neurodegenerative diseases can disrupt the BBB. Mechanisms for BBB dysfunction can be varied and the effect on the barrier can be mild and transient or chronic. Abolishment of the strict exclusion properties of the BBB can have profound effects on the CNS as a result of disease pathology. The neurodegenerative disease, AD, and the autoimmune inflammatory disease, Multiple sclerosis (MS) will be briefly discussed.

1.2.3.1 Alzheimer's disease

As discussed earlier, a growing amount of evidence strongly suggests a vascular connection to AD [85]. However, direct investigation on the dysfunction of the BBB during AD has not been explored until recently. AD patients have been noted to have varying levels of BBB dysfunction as assessed by various high resolution imaging techniques, like magnetic resonance imaging (MRI), and biochemical studies (reviewed by [135, 136]). Defects in BBB transport of brain metabolites have also been noted in AD. For example, reduced transport of glucose across the BBB occurs [137, 138], suggesting faulty energy metabolism during AD. Furthermore, the normal receptor-mediated transport of abeta through the BBB is also believed to be disrupted during AD (reviewed by [125]), leading to accumulation of abeta inside the brain. Briefly, the influx of abeta is dependent on the receptor for advanced glycosylation products (RAGE) [139]. The efflux of abeta is dependent on the low density lipoprotein receptor-related protein (LRP)-1 [140]. During AD, increased RAGE and reduced LRP-1 expression is seen, resulting in the net influx of abeta into the brain [139, 141]. Increased brain abeta accumulation is believed to contribute to AD pathology [125]. Several animal studies including those

utilizing the Tg2576 mouse [118-121] have documented BBB dysfunction. What has yet to be examined is whether BBB dysfunction in either humans or AD mouse models occurs at the level of the TJs, as seen in MS. What can be concluded is BBB dysfunction does occur in AD and the effects are mild and transient.

1.2.3.2 Multiple sclerosis

MS is considered to be an autoimmune disorder characterized by chronic neuroinflammation [142]. During the course of MS, the insulating myelin sheaths that wrap around neurons are attacked by the immune system causing demyelination. The progressive loss of the myelin sheath results in loss of neuron conduction. The improper neuron function can affect patients in a wide variety of symptoms that result in physical and cognitive disability. The CNS is considered to be an immune privilege site due to the highly restrictive properties of the BBB. A key factor in the progression of MS is the breakdown of the BBB resulting in the infiltration of T-cells. The cause of the BBB dysfunction is unknown; however, the invasion of the peripheral immune system is believed to precipitate chronic neuroinflammation. The loss of cerebrovascular occludin and ZO-1 expression in MS patients [143, 144] and in the mouse model for MS, experimental autoimmune encephalomyelitis (EAE) [145-147], has been observed. Whether the BBB dysfunction is a cause or an effect of MS is still unknown.

1.3 Blood clotting

The clotting of blood is a highly sophisticated defense mechanism to prevent death by blood loss. This mechanism has cellular and biochemical components that occur

simultaneously. One of the initiating cellular mechanisms, upon blood vessel damage, is local vasoconstriction. The sympathetic nervous system (a neuronal response that automatically controls stress responses) and paracrine effects are activated, releasing powerful vasoconstrictors [148, 149]. This is the body's attempt to stem the flow of blood. The presence of damaged blood vessels activates hemostasis, which directly leads to the coagulation of blood. Primary hemostasis refers to the activation and deposition of platelets to create a hemostatic plug. Secondary hemostasis refers to the complex enzymatic cascade resulting in the polymerization of the fibrin clot. Both mechanisms of hemostasis occur simultaneously to clot blood.

Under normal circumstances the blood is in a liquid state despite the presence of an excess of coagulation proteins and platelets. Primary and secondary clotting mechanisms are only activated under highly specific and controlled circumstances. Control of coagulation extends to several levels. First, inactive clotting proteins involved in secondary hemostasis circulate in the blood. Second, brisk blood flow ensures unused activated proteins are immediately swept away for disposal in the liver. Third, activation of hemostasis mechanisms requires the exposure of the circulating blood to the subendothelium of damaged blood vessels.

1.3.1 Platelet activation

The subendothelium contains pro-hemostatic elements that are not found on the inside of intact blood vessels, namely collagen and the protein tissue factor (TF). During primary hemostasis, platelets adhere to the site of the damaged endothelium via several receptors.

Vascular injury can expose collagen and von Willebrand factor (vWF) in the subendothelium. Platelets adhere to the site of injury through the binding of vWF to the platelet receptor GPIb-IX-V. They also bind collagen via GPVI (the major collagen receptor on platelets) and α2-β1, another platelet collagen receptor [150]. Adherent platelets can become activated by two independent mechanisms, depending on pathology, but the consequence of platelet activation is the same. One mechanism involves exposed collagen and the other a downstream enzymatic element of secondary hemostasis cascade, thrombin [151]. Activated platelets release the contents of their granules into the plasma, which activates other platelets and blood cells to mediate clotting and tissue repair [152]. Activated platelets will then degranulate releasing fibrinogen aiding the coagulation cascade.

1.3.2 The coagulation cascade

The secondary hemostasis pathway has two interconnected enzymatic cascades that result in the generation of a fibrin clot **Figure 1.5**.

Figure 1.5: A simplified model of the enzymatic cascade of secondary hemostasis.
The contact activation pathway is encircled in red. The tissue factor (TF) pathway is encircled in blue. Unactivated clotting proteases, referred to as factors, are indicated by the letter "F" followed by Roman numerals and activated factors by Roman numerals followed by "a". Open arrows indicate activation reactions involving contact activation pathway proteases. Black arrows indicate activation of proteases in the TF pathway of coagulation. The merged common outcome of both pathways, encircled in green, is the activation of thrombin resulting in the formation of a fibrin clot. Journal of Thrombosis and Haemostasis, 2007, modified with permission [153] (https://www.interscience.wiley.com)..

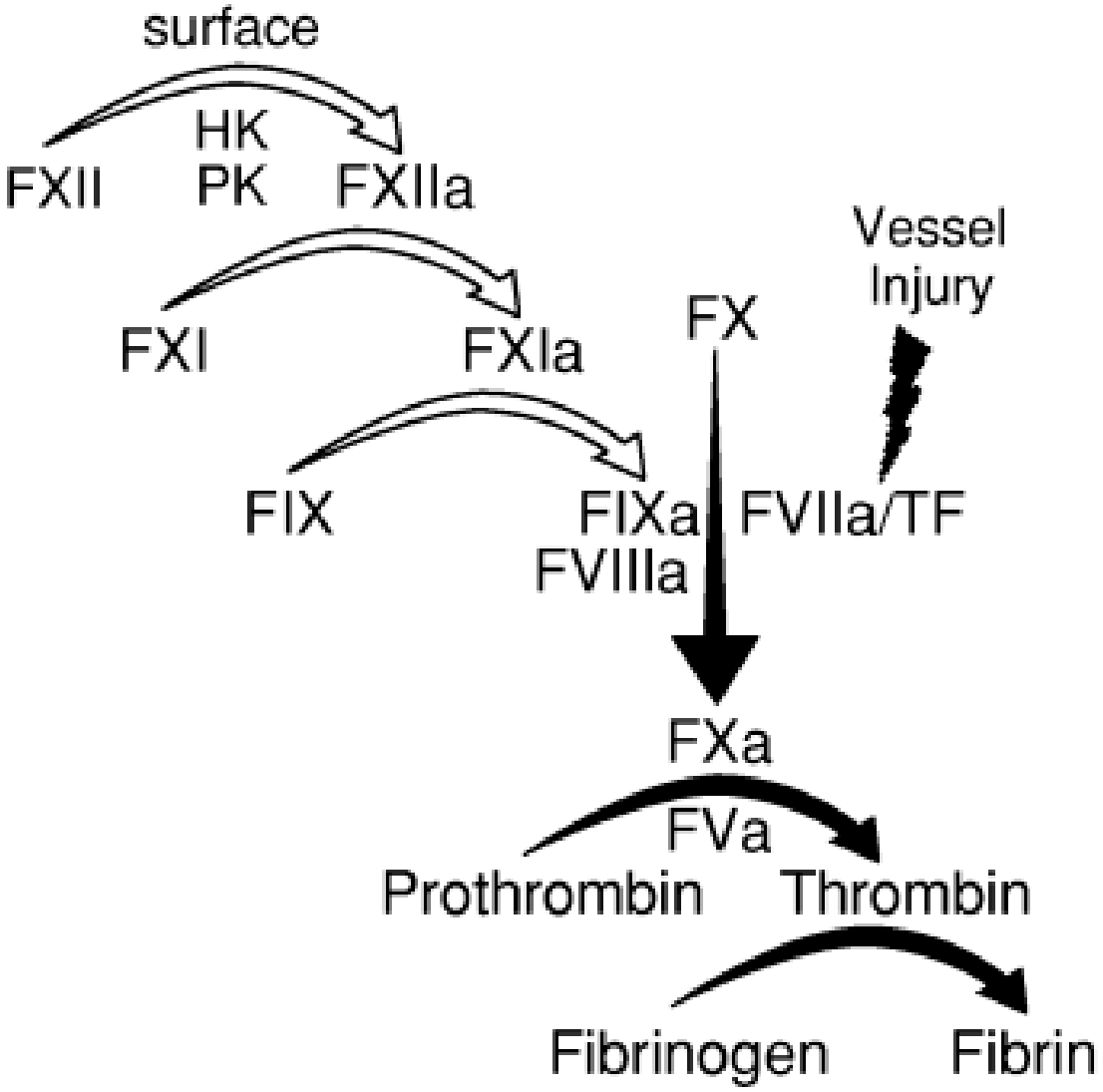

The enzymatic cascades involve the sequential activation of a variety of protease zymogens (inactive enzyme precursors) [154]. Each protease, or clotting factor, in the cascade is labeled with the letter "F" followed by a specific Roman numeral. One cascade is referred to as the contact activation pathway (aka Intrinsic Pathway) and the other is the TF pathway (aka Extrinsic pathway) [154]. Both pathways have a common outcome: the activation of the protein thrombin. Thrombin, a "master regulator" of the clotting cascade, catalyzes the conversion of fibrinogen into fibrin [155], which generates the fibrin clot. The contact activation pathway is initiated upon blood exposure to the negatively charged surfaces of the subendothelia, usually due to superficial wounds in the blood vessel [156]. This cascade is the longer of the two enzymatic clotting cascades, which takes several minutes to activate. The activated partial thromboplastin time (aPTT) clotting test is normally used as a performance indicator of the contact activation pathway. aPTT is measured by exposing platelet poor plasma (PPP) to phospholipids (to mimic platelets), calcium, and a contact activator like the mineral kaolin. The TF pathway is initiated after a deep traumatic blood vessel injury that exposes TF, found in the subendothelia [157]. PT is measured by exposing PPP to phospholipids (to mimic platelets) and a source of tissue factor like rabbit brains. TF is a membrane bound protein that is not found in the lumen of the blood vessel. The prothrombin time (PT) clotting test is the performance indicator for the TF pathway. Exposure of TF to the blood initiates a rapid enzymatic cascade resulting in the activation of thrombin. The TF pathway is considered to be the more physiologically relevant pathway because the contact activation pathway is not required *in vivo* [158].

1.4 Project rationale and general approach

AD is strongly associated with vascular related risk factors. In addition, there is an increasing amount of evidence for the disruption of the cerebrovasculature that accompanies AD disease pathology. Furthermore, disruptions in the BBB can directly lead to interruptions in the cerebral blood flow, which can directly impact brain function. Interruptions in blood flow would suggest an altered hemostatic system may be having an effect during AD. What is not known is the exact cause and effect of the endothelial dysfunction observed in AD patients and various AD mouse models. The amyloid cascade hypothesis suggests that abeta is responsible for the observed cerebrovascular abnormalities. The focus of this thesis was to characterize the brain vasculature, at the molecular level, in AD in comparison to "normal" brains. This thesis had several hypotheses that were tested:

1. BBB dysfunction in AD is caused by abnormal expression of the TJ proteins.
2. BBB TJ dysfunction is directly related to the presence of abeta.
3. Removal of abeta pathology by abeta immunotherapy restores BBB TJ integrity.
4. Abeta induced vascular dysfunction influences the hemostatic system in AD.

Taken together, disruption in the vascular system during AD will have profound effects on the progression of neurodegeneration. Characterizing this pathology could define an early therapeutic intervention point to slow the progression of AD.

Chapter 2: Materials and Methods

2.1 Mice

The Tg2576 AD model mouse expresses the Swedish mutant of the amyloid precursor protein (K670N/M671L) [96, 116], under control of the hamster prion protein promoter (Taconic). Mice were maintained on mixed C57Bl6/SJL background by mating heterozygous Tg2576 males to C57Bl6/SJL F1 females. Wild-type littermates were used as controls. The genotyping protocol were performed as described by [116] by PCR. Briefly, two parallel PCR reactions were performed to distinguish heterozygote from wild-type. The PrP-APP fusion DNA (corresponding to the heterozygote) was amplified using primers 1502 (hamster PrP promoter, 5'-GTGGATAACCCCTCCCCCAGCCTAGACCA-3') and 1503 (human APP, 5'-CTGACCACTCGACCAGGTTCTGGGT-3'). The primer combination 1502 and 1501 (mouse PrP, 5'-AAGCGGCCAAAGCCTGGAGGGTGGAACA-3') was used as a positive control for the reaction. Aged Tg2576 and wild-type mice were at least 18 months of age or older of both genders. Young Tg2576 and wild-type mice were five months old of both genders. Mouse numbers used in the respective Alzheimer's mice experiments are noted in the figure legend. Female C57Bl6 mice were purchased from The Jackson Laboratory were used in the EAE related experiments. Mice were fed standard lab chow and water *ad libitum* and kept under a 12 hr light/dark cycle. All animal procedures were conducted with approval by the University of British Columbia Animal ethics committee.

2.2 EAE induction

Experimental autoimmune encephalomyelitis (EAE) was induced using standard protocols and reagents [159, 160]. Briefly, myelin oligodendrocyte glycoprotein 35-55 (MOG35-55) peptide N-MEVGWYRSPFSRVVHLYRNGK-C was synthesized at The UBC Peptide Core Facility (Vancouver, BC). Each recipient received 200 µg of peptide resuspended in 100 µL of PBS, emulsified with 100uL CFA containing 8 mg/mL *Mycobacterium tuberculosis* H37RA (Difco Labs Inc.). Mice were immunized on shaved hind flanks over 3 sites, followed by *i.v.* administration of 200 ng of pertussis toxin (PTX) in PBS at days 0 and 2 post-immunization. Animals were monitored for development of clinical symptoms and scored as follows: 1- loss of tail tone/ weakness, 2- hindlimb weakness, 3- partial paralysis in one or both hind limbs, 4- complete paralysis in both hind limbs, 5- moribund (animals are euthanized). Time-points were selected based on key milestones in the EAE disease course. Mice, 3-4 per time-point, were harvested at days 0 (initiation), 3 (induction, innate immune response), 5 (innate-adaptive transition, antigen presentation), 7 (adaptive immunity), 14 (preclinical), 18 (onset), 21 (peak), and 28 (remission).

2.3 Vaccination protocol

Abeta vaccination was performed as described by [161] using a protocol that was developed by Schenk *et al* [162]. Briefly, two separate vaccination strategies were carried out, therapeutic and preventative. Prior to immunization, mice were bled from the saphenous vein and serum collected. In the preventative approach, mice were vaccinated

beginning at 6 weeks of age and sacrificed at 12 months. Mice used in the therapeutic strategy were vaccinated beginning at 11 months of age and sacrificed at 15 months. Abeta peptide was freshly prepared from lyophilized powder for each set of injections. For immunizations, 2 mg of abeta (human abeta1-40, Bachem) was added to 0.9 mL of deionized water and thoroughly mixed. Then 100 µL of 10X PBS was added to obtain a final 1X PBS concentration. The solution was vortexed and placed at 37 C overnight until use the next day. Abeta1-40 (100 µg antigen per injection) or PBS (control) was mixed 1:1 (v/v) with complete Freund's adjuvant (CFA) for the first immunization. This was followed by a boost with abeta1-40 (100 µg) or PBS mixed 1:1 (v/v) with incomplete Freund's adjuvant (ICFA) at two weeks and monthly thereafter. From the fifth immunization onward, straight PBS or abeta were injected. Injections were performed *i.p.*.

2.4 Measuring antibody titres

Antibody titres were quantified as described by [161]. Antibody titres for anti-abeta antibodies were assayed after the second immunization. Anti-abeta antibody titres were determined by serial dilutions of sera against aggregated abeta, which had been coated in microtitre wells. Detection was done by using goat anti-mouse immunoglobulin conjugated to horseradish peroxidase and ABTS (2'2-AZINO-bis (3-ethylbenzthiazoline-6-sulfonic acid; Sigma) as substrate. The absorbance was measured using a spectrophotometer plate reader (Spectra Max 190; Molecular Devices) at 405nm.

2.5 Tissue preparation

Tissues were prepared by a variety of methods. Mice were terminally anesthetized with either Avertin (0.0 2mL/1g) or ketamine/xylazine (100 mg/kg;10 mg/kg). Mice used in the abeta vaccination study were transcardially perfused via the left cardiac ventricle with 50 mL of PBS. EAE mice were further perfused with 30 mL of 2% paraformaldehyde (PFA). Brains were rapidly excised and the olfactory bulbs removed. Brains were stored in PFA fixative for four days at 4 C prior to being imbedded in paraffin. Spinal cords were recovered from the vertebral canal by either dissection or flushing with PBS using an 18G needle. Spinal tissues were then fixed in 2% PFA for 48 hrs then stored in 70% ethanol until processed for paraffin sectioning. EAE spinal tissues from each animal were longitudinally embedded in paraffin blocks in three segments and sectioned at 7 µm. Brain tissues were paraffin embedded, coronal serial sectioned at 5 µm. Paraffin embedding, sectioning and dewaxing were performed by Wax-it Histology Services Inc., Vancouver.

2.6 Antigen retrieval for paraffin embedded tissue sections

A pressure cooker was used for antigen retrieval of paraffin sections. Briefly, dewaxed sections were placed into a metal rack and submersed in 20 mM Tris with 0.7 mM EDTA buffer (pH 9.0) within a conventional stovetop pressure cooker. The samples were heated to full steam for 2 min. The cooker was allowed to cool to room temperature under running tap water. The cooled sections were removed and placed under running tap water for 5 min before immunostaining.

2.7 Immunostaining

2.7.1 Immunofluorescence

Paraffin sections were immunostained using a similar procedure as described by [163]. Briefly, sections were incubated in blocking buffer (25% normal goat serum; 3% BSA; 0.3% Triton X-100, Sigma) for 1 hr at room temperature. Primary antibody staining, using the respective antibody dilutions **Table 2.1**, was performed overnight at 4 C in staining buffer (10% normal goat serum; 3% BSA; 0.3% Triton X-100).

Table 2.1: Primary antibodies used.

Antigen	Dilution	Company	Species	Catalog #
ZO-1	1:200	Invitrogen	Rabbit	61-7300
ZO-1	1:200	Invitrogen	Mouse	33-9100
Occludin	1:200	Invitrogen	Mouse	33-1500
Occluidin	1:200	Invitrogen	Rabbit	71-1500
Amyloid-beta (17-24) (4G8)	1:500	Covance	Mouse	SIG-39220
Amyloid-beta (1-16) (6E10)	1:2000	Covance	Mouse	SIG-39320
Mouse F4/80	1:10	Serotec	Rat	MCA497G
Iba-1	1:1000	WAKO	Rabbit	019-19741
Mouse albumin	1:1000	Bethyl	Goat	A90-234A
S100β	1:100	Abcam	Mouse	ab7852
Human CD105	1:20	DAKO	Mouse	M3527
Activated caspase-3	1:1000	Imgenex	Rabbit	IMG-5700

Table 2.2: Secondary antibodies and stains.

Antigen	Dilution	Company	Species	Catalog #
Goat IgG Alexa Fluor 488	1:500	Invitrogen	Chicken	A21467
Rabbit IgG Alexa Fluor 568	1:500	Invitrogen	Goat	A11011
Rabbit IgG Alexa Fluor 488	1:500	Invitrogen	Goat	A21071
Mouse IgG Alexa Fluor 555	1:500	Invitrogen	Donkey	A-31570
Mouse IgG Alexa Fluor 488	1:500	Invitrogen	Goat	A11001
Mouse IgG Alexa Fluor 568	1:500	Invitrogen	Goat	A11031
Propidium iodide (DNA)	1:3000	Sigma		P4170
Toto-3 (DNA)	1:10000	Invitrogen		T3604

Normal donkey serum was used when staining with goat primary antibodies. Secondary antibody staining, using the respective fluorescently labeled antibodies dilutions **Table 2.2**, was performed at room temperature for 1 hr in staining buffer. Either propidium iodide (PI) (Sigma) or TOTO-3 (Invitrogen) was used for nuclear counterstaining. Sections were washed in PBS with 0.1% Tween-20 (Sigma) three times for 5min each between staining steps. Stained sections were coverslipped using Fluoromount-G (Southern Biotech) and allowed to air dry in the dark overnight.

2.7.2 Immunohistochemistry

Paraffin embedded brains from immunized mice were immunohistically stained for abeta deposits and microglia. Tg2576 mice used in the abeta immunization study were serial sections were cut at 8 µm, deparaffinized, hydrated, antigens were unmasked using DAKO Target Retrieval Solution (DakoCytomation) then treated with 3% H_2O_2. Slides were rinsed and blocked using the buffers mentioned above. A mouse anti-human abeta antibody (1:500, clone 4G8, Covance) or rat anti-mouse F4/80 antigen for microglia (1:10, Serotec) were used as primary antibodies **Table 2.1** incubated overnight at 4 C. The slides were then washed and incubated with a secondary biotinylated anti-mouse antibody for 4G8 or a biotinylated anti-rat antibody for F4/80 (DakoCytomation) for 25 min, developed using DAB (Vector Laboratories Inc.), counterstained with Meyer's hematoxylin, dehydrated, and mounted. Slides were examined under a Zeiss Axioplan2 upright microscope (Zeiss, Germany) and images were captured using OpenLab software (version 4, Perkin Elmer, USA). The number of plaques per cortical brain section per mouse was counted and analyzed as described by [161]. Briefly, data were collected from

four alternately spaced (10 sections apart) serial sections of the cortex per mouse. The values for all sections from one mouse were averaged to obtain a single sample for statistical analysis.

For the EAE study, representative sections from each animal were stained with standard H&E or H&E/luxol fast blue (LFB). For immunohistochemistry 7 µm formalin-fixed tissue sections were deparaffinized, and antigen retrieval was performed in a pressure cooker using the method described above. Sites of immune activation were detected using a polyclonal antibody to Iba-1 (Wako Chemicals, USA) **Table 2.1**. Sections were incubated in primary antibody overnight at 4 C, and specific antibody–antigen binding sites were detected using an Envision-Peroxidase system with DAB (DAKO) as a substrate.

2.8 Confocal and quantitative analysis of tight junction morphology

Immunofluorescent stained sections were analyzed on two different confocal microscopes. A Zeiss LSM510 Meta (Zeiss, Germany) laser scanning confocal microscope equipped with multi-line Argon, Diode and HeNe continuous wave (CW) lasers was used in the AD mice study. A Leica TCS/NT confocal microscope equipped with a krypton–argon laser was used in the EAE mice study [160]. Confocal images are representative of at least three experiments with at least 3 animals per condition.

Quantitative analysis of tight junction morphology was analyzed according the methodology developed by McQuaid laboratory [143, 144, 160]. Brain and spinal cord sections were analyzed from paraffin blocks from every fifth section. Images were acquired with 16 slices, averaged four times, through the Z-plane using an x40 oil-immersion objective. The composite projected image was imported into Adobe Photoshop, at 600 dpi, and optimized for contrast and brightness. Confocal data sets represented approximately 100 cerebral blood vessels from both young and aged Tg2576 and littermate controls in the frontal cortex and hippocampus. Tissues used in the EAE experiments were imaged and analyzed similar to AD mice tissues. Individual vessels were scored as either normal (1) or abnormal (0) for ZO-1 expression. Normal ZO-1 expression was judged as strong, continuous, intense and linear staining. In contrast, abnormal ZO-1 expression was judged as weak, punctate and/or discontinuous staining. Abnormal ZO-1 blood vessel expression was compared to normal blood vessels found in normal control or in normal vessels in diseased brains. To minimize the recording of incomplete or undulating vessels as abnormal, due to observed “gaps” in ZO-1 staining, evidence of vessel continuity was sought in the images. For example, the presence of stained nuclei (with TOTO-3 or PI) or punctate or diffuse ZO-1 remnants was used to localize the position of abnormal gaps along the vessel tract. The incidence of tight junction disruption was defined as the average percentage of blood vessels in a given region of brain that displayed abnormal tight junction morphology. In the AD mice, the hippocampus and cortex were analyzed for

2.9 Microvessel density quantification

Microvessel density (MVD) was quantified by confocal microscopy using the methods developed by Guo *et al.* [164] with minor modifications. Briefly, microvessels were indirectly immunofluorescently labeled with a mouse anti-human CD105 (1:20, DAKO) **Table 2.1** primary antibody using the methods discussed above. Images of optimal fluorescent intensity were acquired and analyzed using the Zeiss LSM510 Meta software. Areas within the brain section (across the entire brain) containing high density ("hotspots") [165] CD105 staining were imaged using the x20 objective using the confocal imaging parameters mentioned previously. The total fluorescence area (TFA) in μm^2 was integrated above background, by the software, for each hotspot. The average TFA from four different hotspots per mouse was quantified. The TFA was used as a numerical representation of the total microvessels stained by the CD105 antibody. The MVD of the imaged field was expressed as a ratio of the TFA to the total area of the image.

2.10 Mouse tail bleeding time assay

Mouse tail bleeding times were measured as previously described but with minor modifications [166-168]. Mice were anesthetized with ketamine/xylazine (100 mg/kg; 10 mg/kg) then restrained in a 50 mL Falcon tube. Holes were cut into the tip of the Falcon tube and the lid for breathing and the tail, respectively. The tail was transected with a sterile scalpel at a point where the tail diameter was approximately 1 mm wide (2–4 mm from the tip). After transection, the tail was immediately fully immersed in a 50 mL

falcon tube filled with PBS warmed to 37 C. The time it took for bleeding to stop was recorded. No animal was allowed to bleed for more than 30 min. Mice were allowed to recover from anesthesia or euthanized.

2.11 Hematological analysis

Mouse blood was collected in EDTA blood collection tubes via the saphenous vein. Hematology parameters were analyzed using the Bayer Advia 120 Hematology System. Measured parameters include hematocrit (ratio of cellular and liquid volume in blood), mean platelet volume, hemoglobin, mean cell volume, platelet, white and red blood cell counts. Blood was diluted 1:5 in sterile PBS then immediately analyzed. Advia parameters were set to C57Bl6.

2.12 Coagulation assays

Nine parts whole blood was collected in terminally anesthetized (Avertin, 0.02 mL/1g) mice by cardiac puncture into one part (v/v) 3.8% sodium citrate (Sigma). Platelet-poor plasma (PPP) was prepared by centrifuging the citrated blood at 5000xg for 5 min at room temperature. PPP was subsequently stored at -80C until needed. Activated partial thromboplastin time (aPTT) and prothrombin time (PT) assays were performed using a START4 Coagulation Analyzer (Diagnostica Stago). PT times were measured by diluting 30 µL of PPP with 30 µL of clotting buffer (20 mM Hepes, 150 mM NaCl, 0.1% polyethylene glycol 8000, pH 7.4) and incubating the mixture at 37 C for 3 min. The clotting assay was initiated by adding 30 µL of thromboplastin reagent, warmed to 37 C, in 25 mM $CaCl_2$ (Helena Labs). aPTT times were measured by mixing 30 µL of PPP, 30 µL of clotting buffer and 30 µL of aPTT reagent (Helena Labs). The aPTT mixture was warmed for 5 min at 37 C. The clotting reaction was initiated by adding 30 µL of 25 mM $CaCl_2$ (Sigma) (warmed to 37 C). All measurements were performed in duplicate.

2.13 Statistical analysis

All experiments were performed at least three times in triplicate. Statistical comparisons of data between heterozygous Tg2576 AD mice and wild-type control littermates were performed using Student's *t*-test for unpaired values when appropriate. All statistical analyses wereperformed using Graphpad Prism software (version 5, La Jolla, CA). *p*-values less than 0.05 were considered significant. Values are expressed as mean ± SEM.

Chapter 3: Disrupted Tight Junctions in Tg2576 Mice

3.1 Rationale

Blood-brain barrier (BBB) dysfunction occurs in several neurodegenerative diseases like Alzheimer's and multiple sclerosis (MS). A key component of the pathogenesis of MS is the disruption of the BBB [169], which was later demonstrated to be linked to the breakdown in the tight junctions (TJs) of the barrier [143, 144]. In Alzheimer's disease (AD), BBB dysfunction also occurs, to various degrees, in both AD patients and mouse models of the disease [170-178]. However, how or why BBB dysfunction occurs during AD is not known. According to the amyloid cascade hypothesis, abeta may be directly or indirectly involved in the cerebral endothelial pathology observed during AD. Mechanisms that influence this pathology may include inflammation, angiogenesis and or apoptosis. It is possible that abeta pathology influences AD BBB integrity at the level of the TJs as seen in MS.

The integrity of the BBB has been studied in a limited number of AD mice. Of the mice overexpressing mutant variants of human APP, the Tg2576 [121, 161, 170, 179], TgCRND8 [179], PDAPP [179] and a variant of the bigenic PSAPP (Tg2576 x PS1M146L line 6.2) [121] mice have been shown to have BBB leakiness (the basic descriptions of these mice can be found in **Table 1.1** and **Table 1.2**). These studies have assessed BBB integrity microscopically looking at serum protein leakage and dye extravasation. This suggests that the overexpression of abeta plays a significant role in

the dysfunction of the BBB. Recently, a triple transgenic mouse has been created [108], which overexpresses mutant human variants of APP, PS1 and tau transgenes. The 3xTg mouse was found to have a functionally intact BBB [180] **Table 1.2**. However, underlying vascular abnormalities were present in the 3xTg mice due to thickening of collagen-laden basement membrane of the endothelium surrounding cortical microvessels.

For the current study, the Tg2576 AD mouse was chosen for the following studies because it has been extensively characterized at the BBB level. Ujiie *et al.* [170] demonstrated using a combination of microscopy and serum dye extravasation that the Tg2576 mouse had a compromised BBB. Furthermore, the breakdown in the BBB was evident as early as four months of age, prior to the documented abeta pathology onset in this mouse (about nine months of age) [96]. BBB disruption and serum protein leakage into the brain parenchyma was later confirmed immunohistochemically in the Tg2576 mouse by Kumar-Singh et al. [121]. Disruption was noted to be present but was noted to be subtle, transient and consistent in older transgenic mice. Actively immunizing Tg2576 with abeta was able to directly modulate the permeability of the BBB [161] strongly suggesting abeta directly influences BBB integrity. Finally, fibrin, a major protein involved in the formation of blood clots, has been shown to accelerate BBB leakiness in several AD mouse models including Tg2576 [179]. This study suggests that multiple factors, including inflammation, may be involved in the microvascular injury associated with abeta pathogenesis. However, the above mentioned studies only demonstrate BBB disruption occurs and hint at potential mechanisms for this specific type of tissue injury.

The objective of this chapter was to characterize the relationship between abeta and BBB integrity through TJ morphology. The effect of abeta on the expression of TJs in AD *in vivo*, especially in AD model mice, has not been explored. These studies will help clarify how and where BBB leakage occurs at the molecular level. The working hypothesis for this chapter is that amyloid-related pathology results in TJ disruption ultimately leading to the loss BBB integrity in the Tg2576 AD mouse model. TJ disruption will be assessed through morphology by confocal microscopy. BBB disruption due to TJ pathology should be regarded as a significant form of tissue injury in AD, alongside the classical neuropathologies of AD. Amyloid associated TJ pathology will help to establish a link between AD and cerebrovascular diseases, which may provide new therapeutic targets for BBB repair in AD that could useful for treating both AD and stroke.

3.2 Results

3.2.1 Tg2576 mice exhibit abnormal cerebrovascular tight junction morphology

TJ morphology was characterized in several brain structures including the cortex, hippocampus and choroid plexus of wild-type and Tg2576 mice. Nearly all the observed blood vessels were sectioned longitudinally. Transverse blood vessels were rare. Strong, continuous and linear staining patterns of occludin and ZO-1 within the cerebrovasculature were considered normal, which was indistinguishable in either the cortex or hippocampus regardless of age or genotype. Longitudinal blood vessels had long interwinding thread-like expression of occludin or ZO-1, which was indicative of

normal TJ expression **Figure 3.1a, b, c and d**. Rare but normal transversely sectioned blood vessels had short generally parallel **Figure 3.1e** or radial (not shown) arms of TJ expression. Of the sections examined, the larger blood vessels appeared to contain normal TJ expression **Figure 3.1e**. The choroid plexus, an anatomical region of the brain where the cerebral spinal fluid is produced containing epithelial cells, of wild-type and transgenic, both young and aged, mice had normal TJ patterns for both occludin and ZO-1 **Figure 3.1f and g**. Abnormal TJ expression displayed weak or reduced clarity **Figure 3.1h (white solid arrows)**, punctate **Figure 3.1h and i (white arrowheads)** and/or discontinuous **Figure 3.1j and k (white outlined arrows)** staining for both occludin and ZO-1. The faint outlining of the vessel track, enhanced by nuclear counterstaining, allowed junctional abnormalities to be easily spotted. An example of this is seen in the punctate staining of ZO-1 in **Figure 3.1i**. In affected blood vessels, abnormalities were organized into focal points, surrounded by normal junctions in various proportions. The microvessels displayed the bulk of the TJ abnormalities and the expression patterns of abnormal TJ were indistinguishable between the cortex and hippocampus regardless of age or genotype.

Figure 3.1: Tg2576 AD mice have cerebral tight junction pathology as assessed by confocal microscopy.
Representative confocal micrographs of cerebral blood vessels from aged Tg2576 and wild-type mice immunolabeled for either occludin or ZO-1 (red) and counterstained for DNA (blue) with TOTO-3. Strong, continuous and linear occludin or ZO-1 expression was considered normal in blood vessels. Normal longitudinal sectioned blood vessels in the cortex of (a) wild-type and (b) Tg2576 stained for occludin and ZO-1, respectively. Normal blood vessels in the hippocampus of (c) wild-type and (d) Tg2576 stained for occludin and ZO-1, respectively. Normal tight junction expression in (e) transversely sectioned vessels, stained for ZO-1 in this case, produced linear near-parallel lines in Tg2576. The choroid plexus displayed normal (f) occludin (wild-type) and (g) ZO-1 (Tg2576) expression. Blood vessels displaying punctuate, reduced clarity, discontinuous or interrupted staining TJ staining was considered abnormal. Examples of punctate (white arrow heads) staining in blood vessels in the cortex of (h) wild-type and (i) Tg2576 stained with occludin or ZO-1, respectively. Weak or reduced clarity (solid white arrows) of junctional bands is also depicted in (h). Examples of discontinuous or interrupted (white outlined arrows) staining in the hippocampus of (j) wild-type and (k) Tg2576 stained for occludin or ZO-1, respectively. Results are representative from three mice per group from three seperate experiments. Scale bar represents 20 µm.

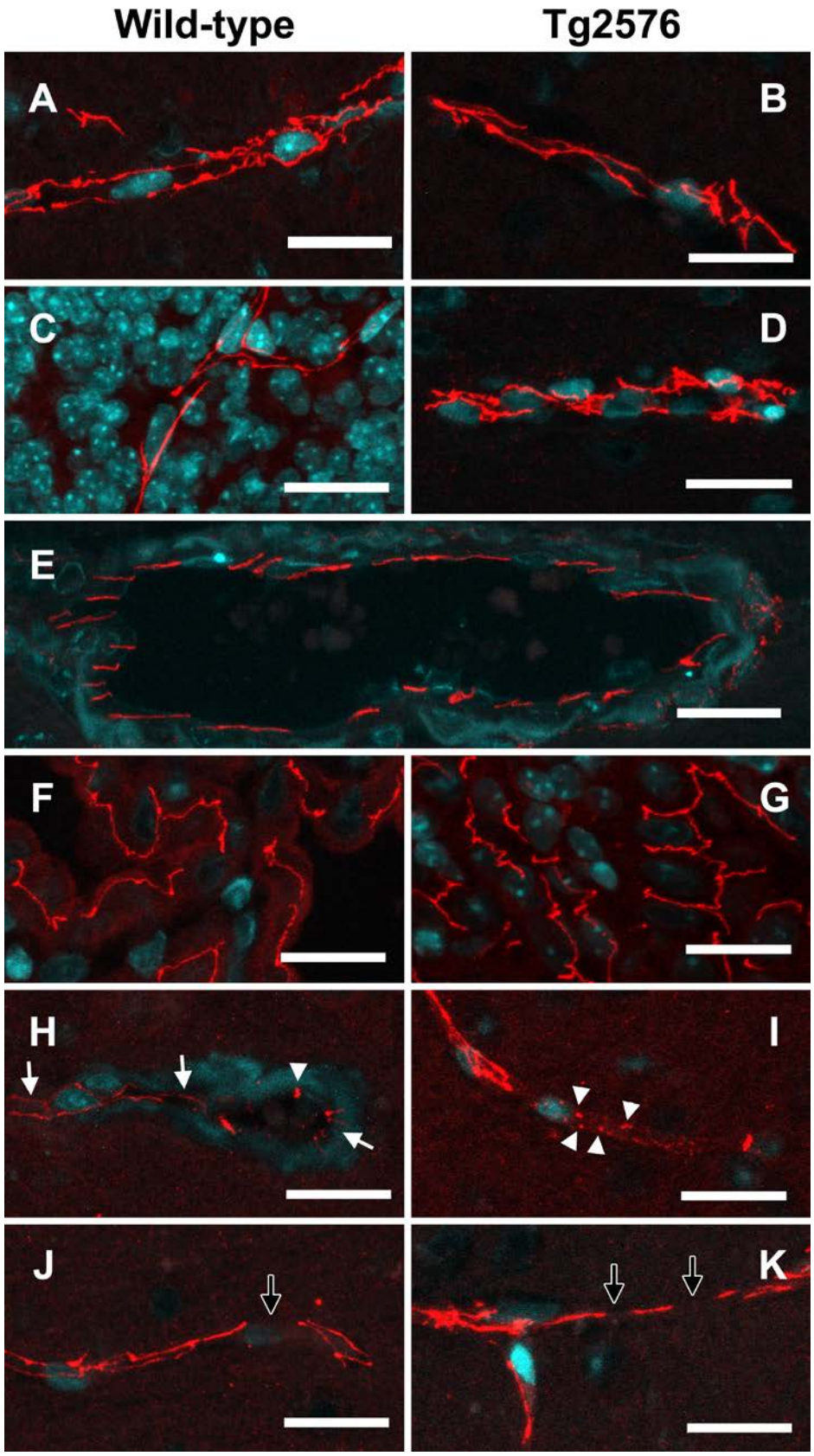
Wild-type
Tg2576
A
B
C
D
E
F
G
H
I
J
K

3.2.2 Quantitative assessment of cerebrovascular tight junction pathology in young and aged mice

The incidence of TJ pathology in the cortex and hippocampus of young and aged Tg2576 mice were quantitatively assessed by confocal microscopy. The incidence of TJ pathology was defined as the average percentage of blood vessels that displayed abnormal TJ morphology. In the cortex of aged, 18 months or older, Tg2576 mice showed a significant increase in TJ disruption (30.50 ± 1.94%; **$p < 0.05$, t-test) compared to age-matched wild-type littermates (which averaged 10%) **Figure 3.2a**. There was also a significant difference in the incidence of TJ disruption between aged Tg2576 and young, five month old, Tg2576 mice (*$p < 0.05$, t-test) **Figure 3.2a**.

Similar results were seen in the hippocampus. Aged Tg2576 mice (24.75 ± 2.32%; ****$p < 0.05$, t-test) showed a significant increase in the incidence of TJ disruption compared to aged matched wild-type mice (averaging 10%) **Figure 3.2b**. A significant increase in the incidence of TJ disruption was seen in the comparison of aged Tg2576 mice with that of young Tg2576 mice (***$p < 0.05$, t-test) **Figure 3.2b**. The amount of TJ disruption in young mice, in both the cortex and hippocampus, of both genotypes averaged approximately 10% and was not significantly different between wild-type and transgenic.

Figure 3.2: Aged Tg2576 mice have a greater incidence of tight junction abnormality.
The incidence of tight junction abnormality between wild-type (+/+) and Tg2576 (Tg/+) in (a) cortex and (b) hippocampus of young and aged mice were compared quantitatively. Graphs represent the percentage of cerebral blood vessels expressing TJ abnormality, by ZO-1 expression patterns. In the (a) cortex, aged Tg/+ mice had a significantly higher incidence of TJ disruption compared to age-matched +/+ (**$p<0.05$). The incidence of TJ disruption was also significantly higher in aged Tg/+ mice compared to young Tg/+ (*$p<0.05$). In the (b) hippocampus, aged Tg/+ mice had a significantly higher incidence of TJ disruption compared to age-matched +/+ (****$p<0.05$). The incidence of TJ disruption was also significantly higher in aged Tg/+ mice compared to young Tg/+ (***$p<0.05$). Values represent mean ± SEM. Young +/+, n = 4; Young Tg/+, n = 3; aged +/+, n = 5; aged Tg/+, n = 4.

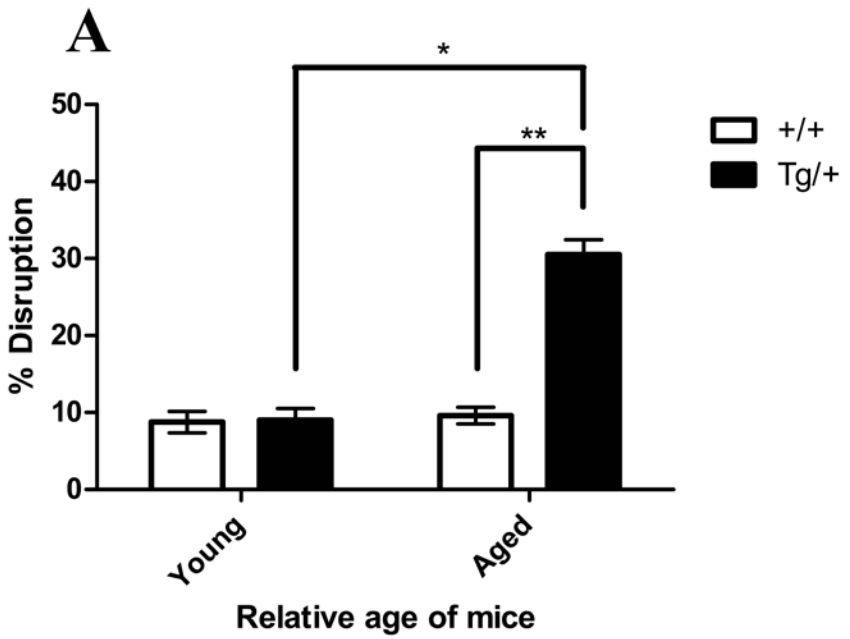
A
*
**
50
40
30
20
10
0
% Disruption
+/+
Tg/+
Young
Aged
Relative age of mice

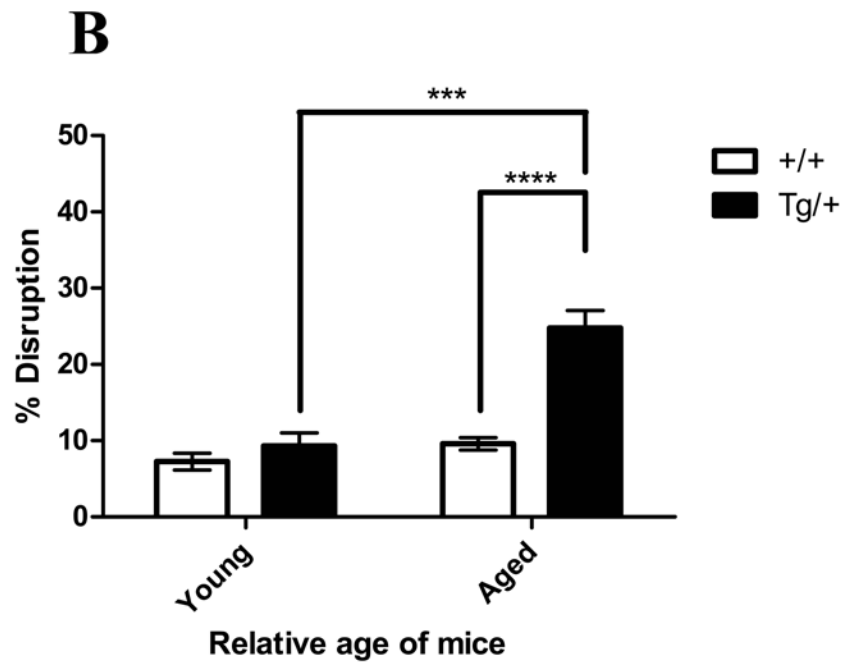
B
***
****
50
40
30
20
10
0
% Disruption
+/+
Tg/+
Young
Aged
Relative age of mice

3.2.3 Aged Tg2576 mice have a typical albumin stained microvessels

Aged and young Tg2576 mice were characterized for the presence of cerebrovascular leakage associated with TJ abnormalities by confocal microscopy. Endogenous mouse albumin was used as a marker for serum vascular leakage into the brain. Mouse albumin was generally found to label all vessels regardless of age or genotype. Vessels that displayed normal vesicular TJ expression had relatively uniform deposition of albumin within the vessel and no apparent evidence of leakage **Figure 3.3a** that was consistent across all mice examined. Uniform staining of albumin was seen in wild-type, young and aged, and young Tg2576 mice. Vessels that displayed abnormal TJ expression did not show any obvious vascular leakage patterns in any of the mice examined regardless of age or genotype **Figure 3.3b-e**. The staining pattern of vascular leakage was expected to be diffuse gradient staining of albumin emanating away from the site of TJ abnormality. However, several different albumin staining patterns were noted in vessels that contained abnormal TJs (both occludin and ZO-1) in the aged Tg2576 mice only. For example, continuous albumin staining throughout the entire vessel regardless of the presence of TJ abnormality was seen **Figure 3.3d**. Partial or fragmented albumin staining was seen in some vessels that displayed abnormal TJs across the entire length of the vessel **Figure 3.3c**. Other vessels had only albumin staining on areas of TJ abnormality, while areas of normal TJ were devoid of albumin staining **Figure 3.3b**. Other vessels had a combination of both normal and abnormal TJs exhibited partially stained albumin regions across the entire vessel **Figure 3.3e**.

Figure 3.3: Aged Tg2576mice have atypical albumin stained microvessels.
Representative confocal micrographs of cerebral blood vessels from aged wild-type and Tg2576 mice immunolabeled with ZO-1 (red) and serum mouse albumin (green). Aged wild-type mice (a) had normal vascular TJ morphology with continuous albumin staining. Aged Tg2576 displayed several types of vascular albumin staining patterns that contained TJ abnormalities (white arrowheads) that did not correspond to cerebrovascular leakage. (b) Vessels displaying albumin staining on regions of TJ abnormality, where as regions of normal TJ morphology was devoid of albumin. (c) Vessels displaying TJ abnormality across the entire length of the vessel had partial or fragmented albumin staining. (d) Continuous albumin staining regardless of the presence of TJ abnormality. (e) Vessels that contained both normal and abnormal TJ morphology had partially stained albumin regions across the entire vessel. Results are representative of three separate experiments of three mice per group of brain tissues examined. Scale bar represents 20 μm.

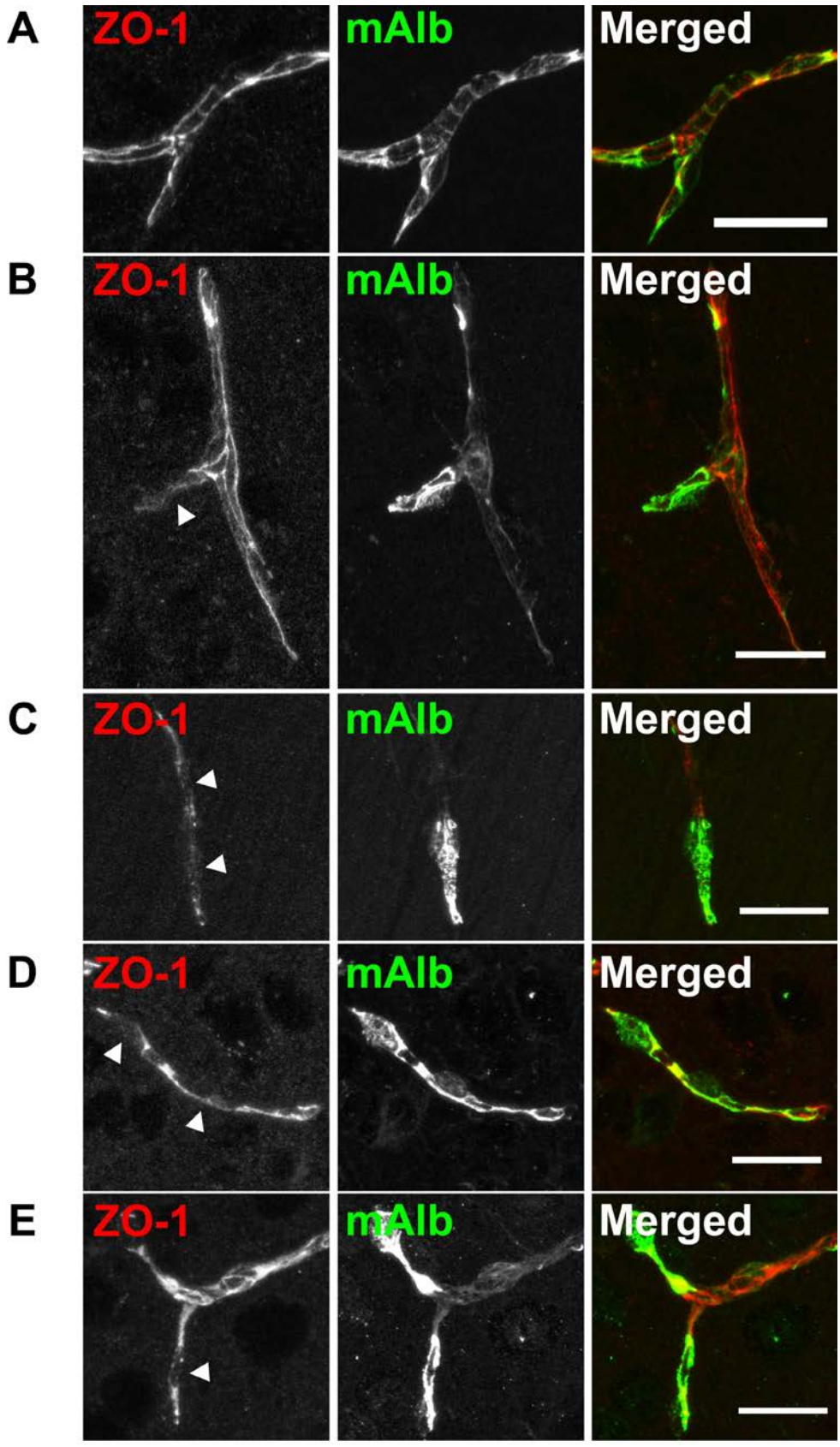
A
ZO-1
mAlb
Merged
B
ZO-1
mAlb
Merged
C
ZO-1
mAlb
Merged
D
ZO-1
mAlb
Merged
E
ZO-1
mAlb
Merged

3.2.4 Angiogenesis and apoptosis in Tg2576 brains

Angiogenesis and apoptosis were explored as possible mechanisms to explain the observed brain vascular TJ abnormalities in the aged Tg2576 mice. CD105 was used as an angiogenic endothelial marker. CD105 stained all vessels uniformly, regardless of age and genotype. Locations of normal and abnormal TJ expression indistinguishable with CD105 stained vasculature with either occludin **Figure 3.4a (white arrowhead)** or ZO-1 **Figure 3.4b (white arrowhead)**. However, a higher proportion of blood vessels were stained with CD105 in aged Tg2576 compared to age-matched wild-type littermates and young mice of both genotypes. Activated caspase-3 was used as a marker of apoptosis **Figure 3.4c-e**. In all examined sections, activated caspase-3 did not directly stain endothelial cells. Positive activated caspase-3 staining bodies were noted in other cell types, presumably neurons, because of the filamentous-like presentation. In young and aged wild-type mice, there was very limited activated caspase-3 staining within the cortex **Figure 3.4c**. Blood vessels in the cortex and hippocampus that exhibited normal TJ (occludin and ZO-1) morphology had neuronal-like activated caspase-3 within the vicinity, similar to what was observed in **Figure 3.4c**. Blood vessels in the cortex and hippocampus that did exhibit TJ abnormalities, **Figure 3.4d**, had neuronal-like staining that was directly adjacent to or overlapped with blood vessels **Figure 3.4d (white arrows)**. Activated caspase-3 did not specifically stain vessels that contained TJ (neither occludin nor ZO-1) abnormalities **Figure 3.4d (white arrowhead)**. All mice had hippocampal staining of activated caspase-3 in the CA1, CA2, CA3 and DG regions to various degrees. Young Tg2576 and wild-type (both young and aged) had significantly higher activated caspase-3 staining densities within the hippocampus compared the cortex.

The overall density of caspase-3 hippocampal staining in young Tg2576 and wild-type (all ages) mice was noted to be lower then aged Tg2576 mice. However, aged Tg2576 mice had significant activated caspase-3 staining within the both the cortex and hippocampus that tended to center around probably plaque locations, denoted by ZO-1 “halos”, (**Figure 3.4e**).

Figure 3.4: Angiogenesis and apoptotic signals were noted in aged Tg2576 mice.
Representative confocal micrographs of TJs (either occludin or ZO-1), and related pathologies, double stained for markers of angiogenesis or apoptosis in aged wild-type and Tg2576 mice. Results are representative of three separate experiments of three mice per group of brain tissues examined. All vessels stained for CD105 regardless of the TJ expression pattern. White arrowheads point to regions of TJ abnormality in the vasculature. (a) Double staining of blood vessels with both normal and abnormal occludin (red) expression with CD105 (green) in wild-type. (b) Uniform CD105 (green) in blood vessels containing ZO-1 (red) abnormality in Tg2576. (c) sporadic activated caspase-3 (green) staining within the cortex of an aged wild-type mouse that never associated with tight junction (ZO-1, red) staining. (d) Double staining of a blood vessel with abnormal occludin (red) expression with activated caspase-3 (green) in the hippocampus of an aged Tg2576 mouse. White arrows point to various presumed neuronal-like filamentous activated caspase-3 staining that was associated with but never costained directly with a vessel. (e) Double staining of a typical dense-core plaque ZO-1 halo (red) with activated caspase-3 (green) staining in the Tg2576 mouse. The filamentous neuronal-like caspase staining surrounded each plaque but did not directly costain with ZO-1 halos. Results are representative of three separate experiments of three mice per group of brain tissues examined. Scale bar represents 20 μm.

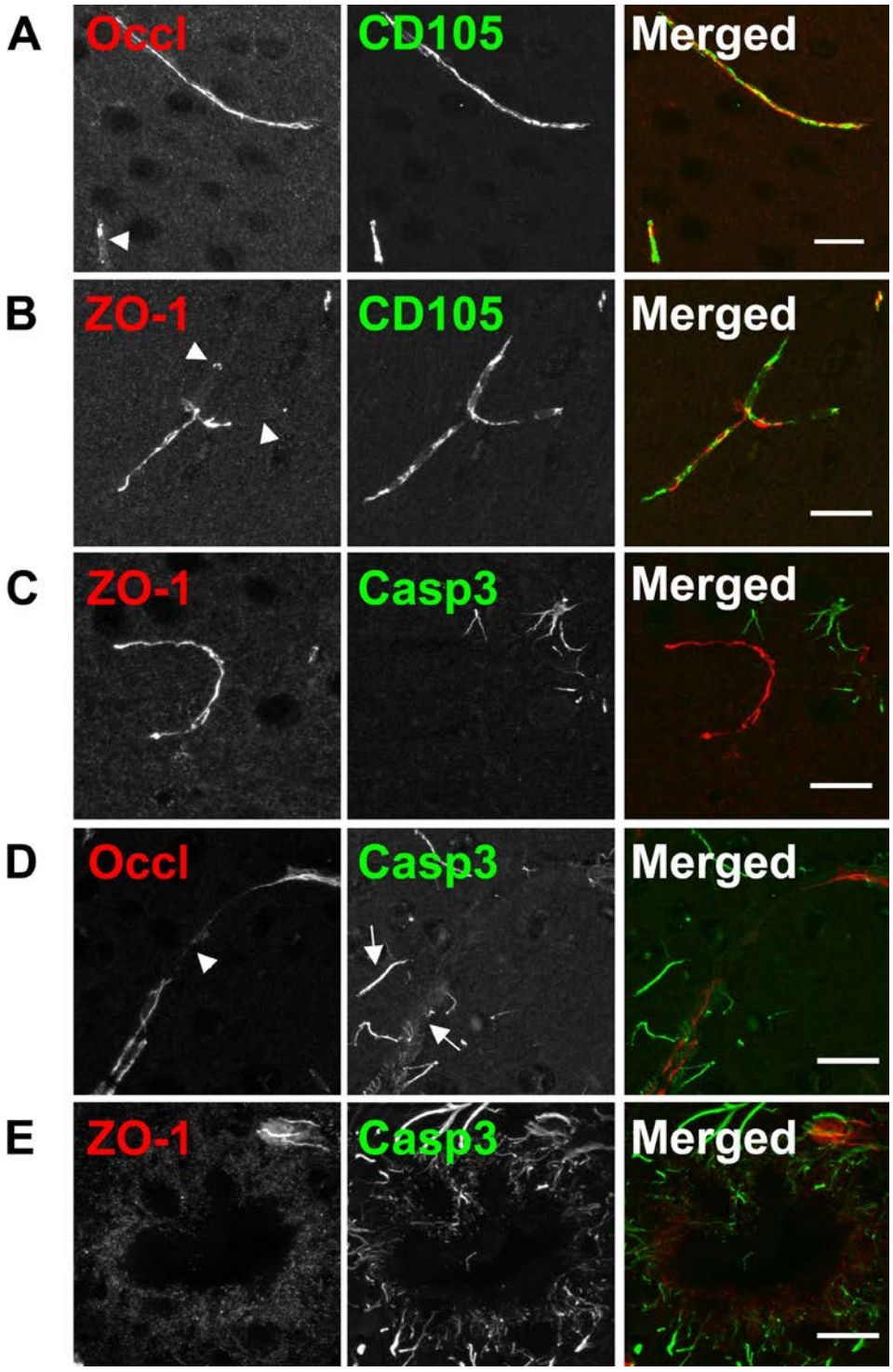
A
Occl
CD105
Merged
B
ZO-1
CD105
Merged
C
ZO-1
Casp3
Merged
D
Occl
Casp3
Merged
E
ZO-1
Casp3
Merged

3.2.5 Quantification of microvascular density in aged and young Tg2576 mice

It was noted earlier that a higher proportion of blood vessels were stained with CD105 in aged Tg2576mice. The microvascular density (MVD) was quantified in the brains of young and aged Tg2576 mice and age-matched wild-type littermates by CD105 staining. The MVD was defined as a ratio of the TFA to the total area of an imaged field and was used as a surrogate measure of angiogenesis. Aged Tg2576 mice, 20 months or older, had a significantly higher MVD compared to wild-type. The average MVD in aged Tg2576 mice (0.4453 ± 0.0146; * $p < 0.0001$, t-test) was over double to that of wild-type (0.1882 ± 0.0010) **Figure 3.5**. When compared to young Tg2576 mice, the MVD in aged Tg2576 was over 1.5 times (** $p = 0.0005$). Young 5 months old Tg2576 mice had a trend towards a higher average MVD (0.2674 ± 0.0161) but the differences were not significantly different compared to wild-type (0.2321 ± 0.0110) **Figure 3.5**.

Figure 3.5: Aged Tg2576 have a higher microvascular density compared to wild-type.
The MVD in the cerebrovasculature of aged and young Tg2576 (Tg/+) and wild-type (+/+) mice was quantified by CD105 staining. Aged Tg/+ mice had a significantly higher MVD compared to +/+ (* $p < 0.0001$, t-test). Aged Tg+/ were had a significantly higher MVD compared to young Tg/+ (** $p = 0.0005$). Although not significant, young Tg/+ mice trended to a higher average MVD compared to +/+. Values represent mean ± SEM. Aged +/+, n = 5; aged Tg/+, n = 4; young +/+, n = 4; young Tg/+, n = 3.

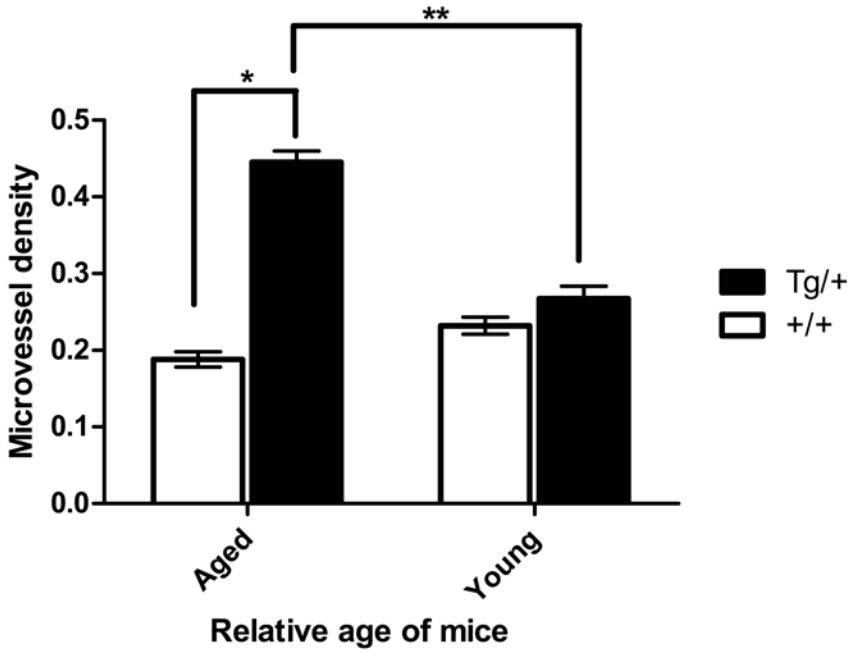

3.2.6 Atypical nonvascular ZO-1 expression

Atypical nonvascular ZO-1 staining pattern was observed in aged abeta plaque bearing Tg2576 mice but absent in the aged wild-type and young mice of both genotypes. This altered ZO-1 expression pattern was visualized as distinct foci of faint and diffuse "halo"-like structures **Figure 3.6a**. The ZO-1 halo-like structures of varying size were found in both the cortex and hippocampus but were generally circular in shape. The center of each foci faintly stained for DNA **Figure 3.6a**. It was hypothesized that these foci could be the location of abeta plaques. Double staining of ZO-1 with abeta (6E10 antibody) demonstrated that all observed ZO-1 halos associated with amyloid plaques **Figure 3.6b**. The presence of DNA at the center of each plaque foci signified that the halos were dense-core plaques. Diffuse amyloid plaques **Figure 3.6c (white arrows)** did not associate with the ZO-1 halos. The diffuse plaques were also separate from typical ZO-1 blood vessel expression **Figure 3.6c**. Neither normal nor abnormal vascular associated ZO-1 expression **Figure 3.6c (white arrowheads)** directly costained with diffuse plaques. However, nearly all blood vessels had some degree of abeta deposition within the vessel **Figure 3.6c (hollow white arrow)**. Double staining of ZO-1 for microglia **Figure 3.6d** or astrocytes **Figure 3.6e** was performed to identify the potential cell type of the ZO-1 halo. Microglia did surround the dense-core plaques but did not directly overlap the ZO-1 halos. Double staining of ZO-1 with the S100β astrocyte marker did produce a high degree of overlap with the halos but no colocalization. Like the diffuse staining of ZO-1, the S100β overlap tended to be diffuse. Prototypical astrocytic morphology was not observed within the overlapping region of the halo. However, prototypical astrocytic morphology was observed in the periphery surrounding the dense-core plaques.

Figure 3.6: Diffuse "halos" of ZO-1 expression is consistent with dense-core plaques in aged Tg2576 mice.

Representative confocal micrographs of ZO-1 "halo" expression double stained for various other antigens in aged Tg2576 mice. (a) Double staining depicting typical diffuse "halo" of ZO-1 (red) with a TOTO-3 nuclear counter stain (blue). The center of the halos consistently stained for DNA. (b) Double staining of a ZO-1 halo (red) with abeta (green) of a dense-core plaque. All observed ZO-1 halos were localized to dense-core plaques. (c) Double staining of abnormal (white arrowhead) and normal ZO-1 (red) expression in a blood vessel with abeta (green) of a diffuse plaques. Diffuse abeta plaques (white arrows) did not associate with ZO-1 halos. Amyloid deposition can be seen inside of vessels (hollow white arrow). (d) Double staining of a dense-core plaque ZO-1 halo (red) with microglia labeled with iba1 (green). Although microglia surrounded dense-core plaques, they did not directly costain with ZO-1 halos. (e) Double staining of a dense-core plaque ZO-1 halo (red) with astrocytic labeling with S100β (green). Astrocytic staining seemed to directly costain with ZO-1 halos. S100β staining of halos was typically diffuse. Actual astrocyte-like morphology was normally seen surrounding the halo as opposed to directly costaining the halo. Results are representative of three separate experiments of three mice per group of brain tissues examined. Scale bar represents 20 μm.

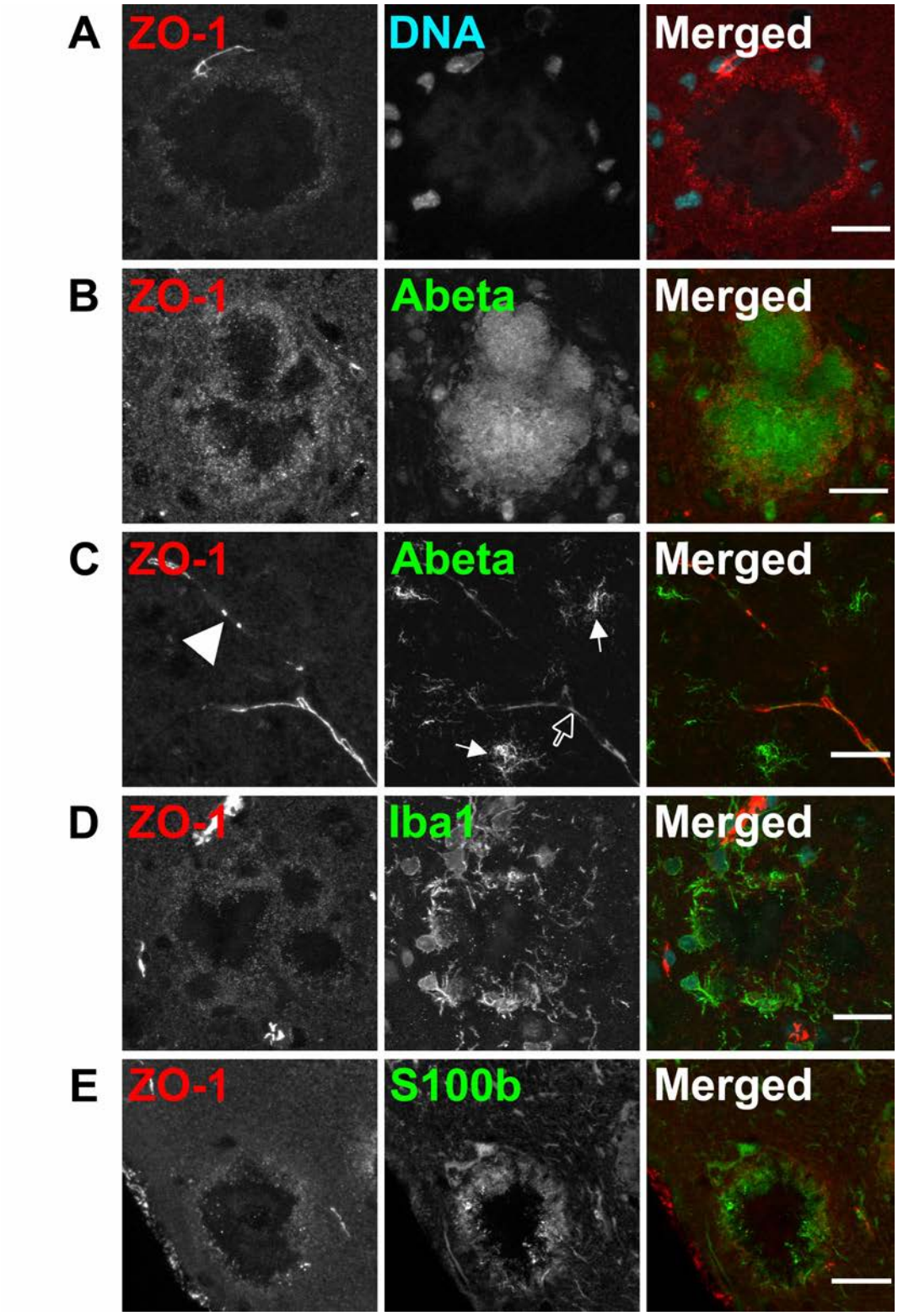
A
ZO-1
DNA
Merged
B
ZO-1
Abeta
Merged
C
ZO-1
Abeta
Merged
D
ZO-1
Iba1
Merged
E
ZO-1
S100b
Merged

3.2.7 Atypical nonvascular occludin expression

Similar to ZO-1, atypical nonvascular staining patterns were also observed for occludin in aged plaque bearing Tg2576 mice but absent in the aged wild-type **Figure 3.7a** and young mice of both genotypes. Rare, faint but distinct staining of a cell type was observed in both the cortex and hippocampus **Figure 3.7b (white arrows)**. The atypical occludin expression was independent of vascular TJ staining **Figure 3.7b (white arrowhead)**. The majority of the atypical occludin expression did surround the periphery of dense-core plaques **Figure 3.7c**, but not always. Double labelling with S100β **Figure 3.7d (white hollow arrow)** identified colocalization **Figure 3.7d (yellow in the merged image)** of this astrocyte marker with the observed atypical occludin expression **Figure 3.7d (white arrow)**. The S100β/occludin colocalization was independent of occludin labelled TJs inblood vessels **Figure 3.7d (white arrowhead)**. The morphology of the S100β labelled cells that did or did not colocalize with the atypical nonvascular occludin expression were very similar. These cells resembled the star-like shape that is characteristic astrocytes. The S100β labelling clearly demonstrated two separate populations of astrocyte-like cells: a rare percentage that appeared to express occludin and the vast majority that does not. Due to the incompatibility of the relevant antibodies and antigen retrieval mechanisms, double staining of the occludin with a microglial marker could not be performed.

Figure 3.7: Rare atypical nonvascular occludin staining colocalizes with S100β stained astroctye-like cells in aged Tg2576 mice.
Representative confocal micrographs of atypical nonvascular occludin expression double stained for various other antigens in aged wild-type and Tg2576 mice. In wild-type mice (a), occludin (red) localized to the vasculature only and did not costain or colocalize with S100β-positive (green) astrocytes. (b) Double staining depicting a rare, faint but distinct atypical nonvascular occludin (red) expression with TOTO-3 nuclear counter stain (blue). Occludin labelled blood vessels, white arrowheads, are independent of the atypical nonvascular occludin expression, white arrow. (c) Double staining of an atypical occludin expression (red) was usually located around abeta (green) of a dense-core plaque. (d) Colocalization of an atypical occludin staining (red, white arrow) with an S100β (green) astrocyte-like cell (white hollow arrow) is represented as yellow in the merged image. The white arrowhead points to a typical occludin blood vessel that is independent of the colocalization. In wild-type mice (a), the atypical occludin-S100β staining is absent. Results are representative of four separate experiments of four mice per group of brain tissues examined. Scale bar represents 20 μm.

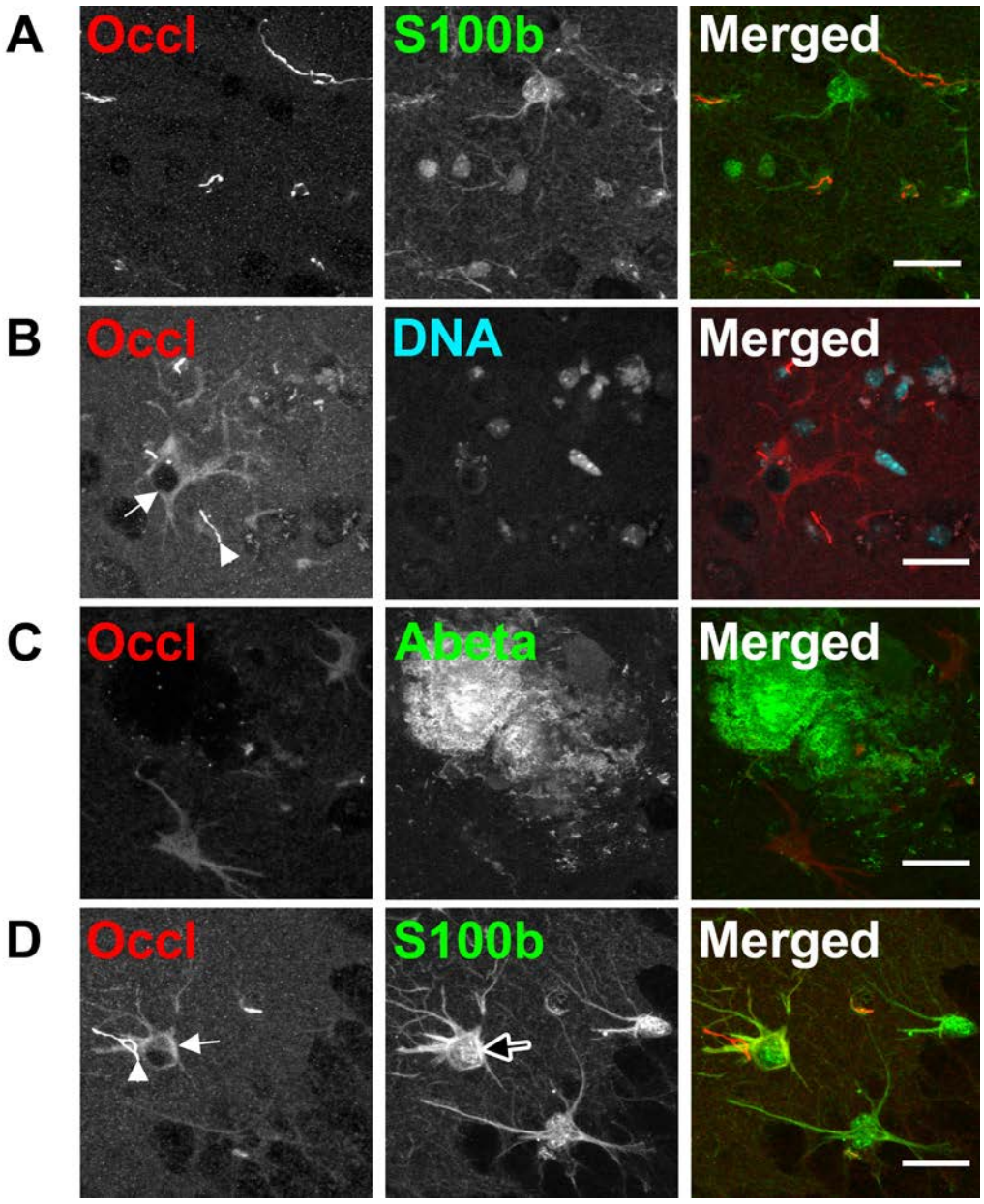
A
Occl
S100b
Merged
B
Occl
DNA
Merged
C
Occl
Abeta
Merged
D
Occl
S100b
Merged

3.3 Discussion

The classically defined BBB is formed by cerebral capillary endothelial cells. The barrier function of the BBB is largely due to the existence of inter-endothelial cell TJs [181, 182], which are composed of linked trans-membrane molecules [182]. Endothelial cell function and integrity are further influenced by the surrounding cells such as neurons, astrocytes and pericytes [183]. The intercellular communication between all of the listed cell types is what creates the neurovascular unit. A loss of one is a loss of all.

The goal of this study was to characterize the integrity of the BBB by examining TJ morphology in the Tg2576 AD mouse in two separate age groups: five months old (prior to disease onset) and aged 18+ months old (well after disease onset). This mouse model was chosen because BBB dysfunction has been previously described [161, 170]. This study is believed to be the first comprehensive examination of TJ related BBB dysfunction in AD.

Normal and abnormal TJ expression in the Tg2576 mice was judged based on the displayed morphology as previously described by Plumb *et al*. [144]. Normal TJ morphology was interpreted as strong and relatively linear staining. Abnormal TJ morphology was interpreted as punctuate, faint and or discontinuous. Both occludin and ZO-1 staining had identical normal and abnormal patterns. The incidence of TJ pathology was then quantified in the young and aged Tg2576 mice. Aged Tg2576 mice had over double the incidence of TJ pathology in the cortex and hippocampus as compared to aged-matched wild-type. However, young mice of both genotypes displayed slight TJ

abnormality. The incidence of abnormal vascular TJ pathology appears to be related to the relative levels of abeta deposition in the Tg2576 mouse. Young mice prior to disease onset, which have no abeta plaques, have minimal TJ pathology. Aged mice well-after disease onset, which have heavy plaque burden, have extensive TJ pathology. This is the first time these observations have been noted and is important in the characterization of pathology of AD brain.

The staining protocol used did not reveal vascular leakage as imaged by endogenous mouse serum albumin. This is in contrast to several previous findings that have found serum leakage in the Tg2576 mice [121, 161, 170, 179]. The ages of Tg2576 mice used in the previous studies ranged from four to 24 months. Staining differences could be attributed to the different antigen retrieval mechanisms and or antibodies used. Furthermore, increased staining sensitivity was achieved in the previous studies using tertiary level staining using immunohistochemistry. Despite a lack of observed vascular leakeage, potential evidence of capillary occlusions was noted with some of the vessels that contained TJ abnormalities of the aged Tg2576 mice. The cause of the occlusions wasn't investigated but recent evidence in the TgCRND8 AD mouse suggested that the association of fibrinogen with abeta could be an explanation [184]. Abeta is known to create abnormal fibrin clots that are resistant to clot lysis in the TgCRND8 mouse. The resistant clots have been observed to create cerebral vascular occlusions in vivo [184]. This finding seems to be consistent with previous studies examining vascular amyloid burden in the APP23 AD mouse model [185], which is known to exhibit cerebral amyloid angiopathy (CAA). The Tg2576 mouse is also known to exhibit CAA-like characteristics

[96, 117]. Occluded vessels would suggest disturbances in cerebral blood flow, ischemia and hypoxia in the Tg2576 mouse. As of current, the incidence or the effects of cerebral blood flow, ischemia or hypoxia has never been directly examined *in vivo* in Tg2576 mice. Neuronal cultures from Tg2576 mice have been examined under the effects of hypoxic and ischemic conditions, *ex vivo* [186]. These conditions resulted in the increase in abeta production by influencing APP metabolism. Thus, neuropathology in Tg2576 mice and by extension in humans [187] could be exacerbated by ischemic and hypoxic conditions.

The large aggregated extracellular abeta plaques, a hallmark of AD pathology, are not believed to cause the neurodegenerative effects in AD; however, the smaller, more toxic, soluble abeta oligomers are (reviewed by [48]). A specific highly toxic dodecameric 56kDa abeta oligomer has been directly implicated in memory loss in Tg2576 mice, referred to as “abeta*56” [51]. This oligomer emerges at about six months of age (when memory deficits in Tg2576 first become apparent) but is absent in younger mice. In the present study, five month old mice had a trend towards increased abnormal vascular TJs. However, Tg2576 mice begin showing a loss of BBB integrity as early as four months of age [170]. During this time, a build up of smaller less toxic oligomers could begin negatively influencing BBB integrity in this mouse. By six months of age, it is hypothesised that the toxic presence of abeta*56 initiates a cascade of the pathological events associated with the Tg2576 mouse. Although, Tg2576 mice between the ages of six to 13 months the relative levels of abeta*56 remains constant [51]. During this time the eventual accumulation of plaques and dystrophic neurons is enough to cause further

pathological loss in this mouse. This could explain the dramatic presence of abnormal cerebral vascular TJ expression in the aged Tg2576 mice.

The presence of these toxic oligomers could influence endothelial survival and TJ expression. Several lines of *in vitro* evidence have explored endothelial dysfunction by abeta. Marco *et al.* [188] demonstrated that abeta1-42 stimulated endothelial cultures induced aberrant expression of TJ proteins including claudins, occludins and ZO-1. Gonzalez *et al.* [189] demonstrated that smaller abeta1-40 aggregates induced endothelial cell permeability and the relocalization of ZO-1 to the cytoplasm. Abeta induced reactive oxygen species (ROS) was ruled out as a potential cause of BBB leakiness because the presence of ROS detoxifying enzymes did not influence abeta induced damage [190]. However, the reorganization of cytoskeletal proteins was believed to directly influence BBB integrity [190]. Although involvement of abeta related ROS is debatable, ROS from other sources (microglial activation and serum leakage) could still have an effect [191].

Apoptosis was examined as a possible mechanism of abeta induced TJ disruption in the BBB. In the context of AD, apoptosis and the gradual loss and death of neurons is normally discussed as the proposed mechanism of neurodegeneration. Whether apoptosis has a direct role in neuronal loss is still controversial [192, 193]. Nevertheless, the apoptotic process involves a complex internal signaling and an enzymatic cascade (involving caspases) that results in the programmed cell death by fragmenting DNA, blebbing of the membrane and creating apoptotic bodies, reviewed by [194]. A key enzyme is caspase-3. When cleaved into its active form, caspase-3 can proteolytically

cleave a variety of cellular proteins resulting in cell death [194]. Numerous stimuli have been found to provoke apoptosis in AD including abeta and ROS [195]. Furthermore, several different caspases have been implicated in generating abeta, being activated by abeta and cleaving tau, leading to the generation of neurofibrillary tangles (NFT) [196, 197]. Thus, a direct link has been proposed between abeta pathology, apoptosis, NFT and neuronal death from NFTs [198].

In this study, an anti-active caspase-3 antibody failed to detect endothelial apoptotic events but what was presumed to be neurons were visualized. Young Tg2576 and wild-type (young and aged) mice had active caspase-3 neuronal-like staining within the hippocampus. This finding is consistent with a recent paper examining neuronal loss in Tg2576 mouse [199]. Hippocampal neuronal apoptosis in the wild-type mice maybe a product of long-term memory generation [200]. Aged Tg2576 mice were found to have extensive neuron-presumed active caspase-3 staining both in the cortex and hippocampus. Higher density caspase-3 staining did appear to coincide with dense-core plaques. This suggests that abeta plaque burden influences caspase-3 activity in neurons. In contrast to these findings, several studies have noted little to no active caspase-3 staining in the Tg2576 mouse [122, 201]. These difference could be attributed to the antibodies and staining techniques used. Although, apoptotic endothelial cells were not seen, *in vitro* evidence does suggest that abeta can induce apoptosis in cultured endothelial cells [202-204].

Angiogenesis was also examined as another potential mechanism for TJ disruption in

cerebrovascular endothelium. There are several lines of evidence that suggest angiogenesis occurs during AD. First, neuroinflammation is a pathological feature of AD [205] and is associated with the increase in cytokines that are capable of inducing angiogenesis [206, 207]. The pro-angiogenic growth factor VEGF is also induced by these cytokines [208] and is elevated in AD patients [209]. VEGF directly stimulates endothelial proliferation [210]. Abeta peptides themselves have also been shown to have angiogenic properties [211]. Demonstrating that signals for angiogenesis are present is one thing. Proving that a specific endothelial cell is actively undergoing angiogenesis is a different matter. There are several markers for angiogenic vessels including the integrin αV-β3 [212] and CD105 (endoglin) [213].

Angiogenesis in the Tg2576 mice were characterized by CD105 staining because it is known to stain the BBB [214, 215]. In mice examined, CD105 was found to stain all cerebral blood vessels labeled with TJ marker. The antibody staining was not able to distinguish vessels with TJ abnormalities from those without. However, different CD105 antibodies have been shown to stain brain vasculature to different degrees [216]. The apparent pan endothelial staining of CD105 allowed for the quantitation of the density of CD105 staining, the microvascular density (MVD), in the entire brain. The MVD was used as a surrogate marker for the amount of angiogenesis present within a given area of tissue section. The greater the vascular density the more angiogenesis is believed to have occurred. Measuring the MVD is not without limitations including a lack of standardization and relying on the operator to minimize bias leading to the loss of objectiveness [217]. Despite the disadvantages, the MVD is a popular prognostic marker

of tumor angiogenesis and by extension angiogenesis in general. Aged Tg2576 (18 months or older) mice had nearly double the MVD compared to age-matched wild-type mice. Young Tg2576 mice had a slight increase in MVD compared to the control but this did not reach significance. Angiogenesis in the Tg2576 mouse is controversial. The present study demonstrated that CD105 related MVD did not directly correlate TJ abnormalities with angiogenesis. However, an increased CD105-related MVD does indirectly demonstrate that angiogenesis and TJ abnormalities are related in the Tg2576 mouse. Elevated VEGF in 20 month old Tg2576 mice [218] further supports the hypothesis that angiogenesis occurs in this AD model. However, a conflicting study by Paris *et al* [219] noted the Tg2576 mouse to have limited angiogenesis. The pan endothelial marker PECAM was used to quantify angiogenesis in mice up to 17 months of age. PECAM is not favoured as an angiogenic marker as compared to CD105 [220-223]. Finally, confirmation of increased angiogenic cerebral vasculature has been observed in human AD brains [224] (integrin αV-β3 expression) and in the APP23 AD mouse model [208] (beta3-integrin subunit). These studies demonstrated that number of angiogenic vessels increases in AD and correlates with abeta load.

TJs are normally exclusively associated with endothelial cells. Rare atypical nonvascular TJ staining patterns were noted in the aged abeta plaque bearing Tg2576 mice only. These patterns included dense-core plaque (which positively stain for DNA [225]) associated ZO-1 “halos” and altered occludin expression on a subset of S100β-positive astrocytes. The ZO-1 halos did not directly colocalize with astrocytes but there was high degree of overlapping expression. These atypical TJ expression anomalies were not

associated with blood vessels. Mice lacking abeta plaque pathology were devoid of the TJ anomalies suggesting abeta could influence the altered expression of TJ. These TJ anomalies have never been described in any AD mouse model. Non-typical TJ expression has been observed *in vitro* where ZO-1 [226] and occludin [227] have been localized to astrocytes. Recently, non-typical TJ (occludin and claudin) staining has been noted in human AD tissues [228, 229]. In the human studies, occludin and claudin expression was increased in neurons, astrocytes and oligodendrocytes. Explanations and significance of the *in vitro* and human AD staining of non-typical TJ expression on astrocytes have been vague and highly speculative including hypoxia and abberant angiogenesis. Another novel explanation is the brain's failed attempt to create a neuroprotective glial scar. This structure is normally associated with physical injury and diseases like MS where activated astroctes attempt to compartmentalize damaged CNS tissues by creating scar-like structure [230]. During this process, it has been suggested that activated astrocytes create a physical barrier by expressing TJs [231]. Glial scars are not associated with AD; however they are associated with neuroinflammation [230, 232], which is present during AD. Although the function of the non-typical TJ expression patterns is unclear, there are several potential inducers including hypoxia, inflammation and direct stimulation by abeta. These mechanisms have not directly been shown to modulate TJ expression in astrocytes but have in endothelial cells. Altered protein expression in one cell type could be mirrored in another.

Strong links between vascular abnormalities and AD have suggested hypoxia (oxygen starvation) as a major pathologically condition in the brain, reviewed by [187]. BBB

dysfunction, increased production of abeta and reduced abeta clearance has been implicated in AD related hypoxia. Hypoxia-induced gene regulation [233] could influence downstream TJ expression in non-endothelial cells. Neuroinflammation is the third major hallmark of AD (after abeta plaques and NFT) that is believed to result from oxidative stress, vascular pathology and or abeta [63], the effects of which can directly disrupt the BBB [183]. The atypical nonvascaular TJ expression were seen to be associated with a subset of S100β-positive astrocytes. S100β is a calcium binding protein that has numerous and complex autocrine, paracrine and endocrine effects (for an extensive review see [234]). In the context of AD, S100β has been shown to exacerbate inflammation, AD-like pathology and relating brain damage [235]. Although the TJ anomalies were not found on all S100β-positive astrocytes, they did associate mainly with astrocytes in the vicinity of abeta plaques. It could be speculated that inflammatory conditions present in plaque burden regions of the AD mouse brain could be responsible for the altered TJ expression. Abeta peptides themselves may potentially induce or alter TJ expression directly in astrocytes [236]. Although, abeta induced TJ expression has yet to be demonstrated directly in astrocytes.

Chapter 4: Disrupted Tight Junctions in Immunized Tg2576 Mice

4.1 Rationale

Alzheimer's disease (AD) is currently unpreventable and incurable. Drugs currently available on the market (reviewed by [237]), are marginally effective and only treat symptoms of the disease. There have been several approaches in the development of disease modifying treatments of AD (reviewed by [8]). The majority of these therapeutic strategies have focused on different aspects of amyloid-beta (abeta) metabolism including modifying production, preventing aggregation, enhancing elimination and increasing degradation. One strategy that has received considerable attention is abeta immunotherapy.

It was noted *in vitro* that monoclonal antibodies towards abeta could prevent and inhibit fibrillation of the peptide and its toxic effects [238, 239]. The *in vitro* data spurred an *in vivo* immunization study using the PDAPP AD mouse model [162] (a brief description of the mouse is given in **Table 1.1)**. One of the early AD mice developed, the PDAPP mouse over expresses human APP with the so-called Indiana mutation and develops plaque pathology by six to nine months of age [94]. Mice were actively immunized with fibrillated abeta1-42 using two different strategies: preventative (prior to disease onset) or therapeutic (well after disease onset). For the preventative strategy, six week old mice were immunized with abeta for an entire year, whereas in the therapeutic strategy 11 month old mice were immunized with abeta for a four month period until 15 months of

age. AD-like neuropathologies in PDAPP immunized mice, using both strategies, were significantly reduced. This strongly suggested that at least the familial form of AD is potentially treatable. The PDAPP immunization study has been replicated in variety of other AD mouse models using both active **Table 4.1** and passive **Table 4.2** and **Table 4.3** immunization.

Table 4.1: Active abeta vaccination in AD mice models.
Significant reduction in abeta plaque burdens (+++); moderate reduction abeta plaque burdens (++); no effect on abeta plaque burdens (=). CNS & Neurological Disorders Drug Targets, 2009, with permission [240].

Ref	Animal Model	Immunogen	Efficacy of Vaccination (Depending on Pre-Existing Plaque Burdens)			Behavior Outcomes/Comments
			Pre-	Mild-Moderate	High	
[162]	PDAPP	Aggregated Abeta1-42	+++	++		First demonstration that abeta immunization could reduce abeta plaque burdens in the brain.
[241]	TgCRND8	Aggregated Abeta1-42	+++			Improvement in behavioral outcomes.
[242]	Tg2576 Tg2576-PS1	Aggregated Abeta1-42	+++			Improvement in behavioral outcomes
[243]	PDAPP-	Nasal administration of Abeta1-40	+++			Novel route of immunization
[244]	Tg2576	Aggregated Abeta1-42	+++	++	=	Efficacy decrease with increased abeta loads at initiation of Rx
[161]	Tg2576	Aggregated Abeta1-40	+++	++		Restored BBB integrity
[245]	Tg2576 Tg2576- PS1	Aggregated Abeta1-42				Behavioral protection is task specific, preservation of hippocampal-associated working memory
[246]	PDAPP	Abeta1-5, 3-9, or 5-11 + T-cell epitope of ovalbumin		++		First demonstration that a subunit vaccine is effective
		Abeta15-24 + T-cell epitope of ovalbumin		=		
[247]	Tg2576	Aggregated Abeta1-42		++		Fc-receptor-mediated effects are not required for efficacy.
	Tg2576 x FcRgamma -/-	Aggregated Abeta1-42		++		
[248]	Tg2576- PS1	Aggregated Abeta1-42				Vaccination in older mice does not improve cognitive deficits/abeta not assessed
[249]	Caribbean Vervet Monkeys	Abeta1–40: Abeta1–42 3:1 molar ratio		++		Age-related abeta deposition in the vervet monkey and lowering of cerebral abeta by abeta vaccination in a non-human primate
[250]	J20	Nasal administration of a tandem repeat of Abeta1-15 peptides.	+++			Modest improvements in Morris water maze performance
[251, 252]	3xTG-AD	Aggregated Abeta1-42		++		Reduced soluble abeta levels and tau levels. Improved T-maze and passive avoidance behavior. Decreased intracellular abeta
[253]	J20/TGF-beta	Aggregated Abeta1-42				Increased T-cell infiltration into CNS following vaccination.
[254]	PDAPP	Aggregated Abeta1-42	+++	++		Did not improve Morris water maze performance in mice with higher levels of preexisting abeta.
[255]	APP/PSEN1dE9	Transcutaneous administration of Aggregated Abeta1-42		++		Different route of administration
[256]	Tg-SwDI	Aggregated Abeta1-42, Abeta40-DI Abeta1–11 fusion with PADRE	=	=		Impaired transcytosis of abeta correlated with lack of efficacy with respect to antibody-mediated reduction of Abeta.
[257]	Tg2576	Mannan-Abeta28	+++		++	Elevated levels of CAA. Increased microhemorrhages in older mice

Table 4.2: Passive abeta vaccination in AD mice models.
Significant reduction in abeta plaque burdens (+++); moderate reduction abeta plaque burdens (++); no effect on abeta plaque burdens (=). CNS & Neurological Disorders Drug Targets, 2009, with permission [240].

Ref	Animal Model	Anti-Abeta mAbs	Efficacy of Vaccination (Depending on Pre-Existing Plaque Burdens)			Behavior Outcomes/Comments
			Pre-	Mild-Moderate	High	
[258]	PDAPP	10D5 (N-terminal)		++		First demonstration that passive immunization could reduce abeta plaque burdens in the brain
		3D6 (N-terminal)		++		
		21F12 (C-terminal)		=		
		16C11 (C-terminal)		=		
[259]	PDAPP	m266 (mid-domain)	+++			Supports "Peripheral Sink" as a mechanism of antibody-mediated clearance of abeta from the brain.
[260]	PDAPP	m266 (mid-domain)			=	Improvement in behavioural deficits. These alterations occur rapidly, without abeta plaque reductions.
[261]	Tg2576	BAM-10 (N-terminal)		=		Improvement in behavioral outcomes. Suggest that behavioral effects occur rapidly, without abeta; plaque reductions.
[262]	APP23	β1(N-terminal)			++	First report to raise concerns about increases in brain microhemorrhages.
[246]	PDAPP	6 N-terminal abeta; mAbs (various IgG subclasses)		++		Suggest that antibody isotype and affinity for abeta; amyloid may be important in reducing neuritic dystrophy.
[263, 264]	Tg2576	2286(A.28-40)			++	Improved behavior on the Y maze. Fully reversed radial arm water maze deficits. Increased micro-hemorrhages.
[265]	Tg2576	F(ab')2 fragments or intact IIA2 mAb (N-terminal)		++		Suggest that Fc-receptor-mediated effects may not be required for efficacy.
[266]	PDAPP	10D5 (N-terminal)			=	Improved spatial learning in the Morris water maze. LTP rescued in hippocampal slice cultures.
[267]	PDAPP	m266 (mid-domain) 3D6 (N-terminal)				Increased microhemorrhages in 3D6 treated mice but not m266 treated mice.
[268]	Tg2576	BC-05 (C-terminal x-42)	+++			C-terminal mAb effective in primary prevention
[269]	Tg2576	NAB61 (Oligomeric selective)			=	Antibody treatment improved Morris water maze performance.
[270]	Tg2576, BRI2-Abeta1-42	Ab9 (N-terminal)	=			No effect on steady state total brain abeta levels prior to deposition

Table 4.3: Continued passive abeta vaccination in AD mice models.
Significant reduction in abeta plaque burdens (+++); moderate reduction abeta plaque burdens (++); no effect on abeta plaque burdens (=). CNS & Neurological Disorders Drug Targets, 2009, with permission [240].

Ref	Animal Model	Anti-Abeta mAbs	Efficacy of Vaccination (Depending on Pre-Existing Plaque Burdens)			Behavior Outcomes/Comments
			Pre-	Mild-Moderate	High	
[271]	Tg2576, TgCRND8	Ab2 (N-terminal)	+++	++		C-terminal mABs do not recognize abeta amyloid but recognize monomeric abeta Though they are effective in a true prevention study, C-terminal anti-abeta mAbs are not beneficial in mice with pre-existing abeta plaque loads.
		Ab3 (N-terminal)	+++	++		
		Ab5 (N-terminal)	+++	++		
		Ab9 (N-terminal)	+++	++		
		Ab42.2 (C-terminal x-42)	+++	=		
		Ab40.1 (C-terminal x-40)	+++	=		
[272]	Tg2576	2H6, Deglycosylated 2H6			++	Both mAbs improved radial arm water maze performance. Deglycosylated mAb treatment reduced CAA/ microhemmorhage.
[273]	PDAPP	m266 (mid-domain)			= CAA	3D6 treatment reduced CAA whereas m266 did not affect CAA. Parenchymal abeta not reported
		3D6 (N-terminal)			+++ CAA	
[274]	PDAPP	m266 (mid-domain)	=	=		Efficacy is achieved with anti-abeta mAbs that bind abeta plaques.
		3D6 (N-terminal)	+++	+++		

The overall positive effects of the preclinical abeta immunization of AD mice encouraged a Phase I clinical human trial by Elan/Wyeth in late 1999 [275]. Patients were actively immunized with a vaccine consisting of fibrillated abeta1-42, designated as AN1792, and showed no initial ill effects. A larger Phase IIa clinical trial using AN1792 was initiated but was prematurely stopped when 6% of the patients developed meningoencephalitis and died [276, 277]. However, when examined post-mortem, patients involved in the study had reduced plaque pathology but taupathies still remained [117, 240, 278-280]. A limited follow-up study suggested that immunotherapy also failed to improve cognitive function in participating patients [281]. Furthermore, a consistent feature found in these patients was increased abeta deposition on the vasculature [279, 282-284], *ie.* cerebral amyloid angiopathy (CAA). Immunohistochemical studies also showed increased CAA and its associated microhemorrhages in immunized patients [284, 285]. Thus, increased CAA and microhemorrhages are important caveats to consider for future success of abeta immunization therapy.

The vascular pathology seen in the human abeta immunization trails was also observed in AD mice. Both passive [262, 264, 267] and active [257, 286, 287] immunization in a variety of AD mouse studies resulted in microhemorrhaging and varying degrees of CAA on the vasculature. The mechanism of microhemorrhaging on the cerebralvasculature is unknown. An attempt was made to characterize the integrity of the blood-brain barrier (BBB) post-abeta immunization in the Tg2576 AD mouse model [161]. Mice were actively immunized either preventatively or therapeutically, similar to what was

originally described by Schenk *et al.* [162]. Both immunization strategies demonstrated that the BBB was restored.

The Dickstein *et al*. [161] study examined the global integrity of the BBB but did not characterize the molecular details of at the microscopic level. The current study will expand on the previous results by examining the molecular details of the BBB breakdown and restoration as a result of active abeta immunization. As discussed in the previous chapter, Tg2576 mice have extensive BBB tight junction (TJ) abnormalities. How do the TJs in the BBB of abeta immunized Tg2576 mice compare? An assessment of the TJs in the BBB of immunized mice has never been described. The objective of this chapter is to characterize the relationship between abeta and TJ morphology in an abeta immunization AD mouse model. The incidence of TJ disruption in the Tg2576 immunized mice was compared to the experimental autoimmune encephalomyelitis (EAE) mouse model. MS-like symptoms are mimicked, like neuroinflammation [288] and tight junction loss [145-147], upon induction by immunization in the EAE model [289]. The comparison of the two models examined the effects on TJ integrity from several different aspects including immunization strategies and difference between the neurodegenerative models. The hypothesis for this chapter is that abeta immunized Tg2576 have reduced TJ abnormalities at the capillary level. Immunotherapy is the most promising strategy towards treating AD. Understanding the relationship between the vascular side effects associated with abeta immunization has direct clinical relevance in treating AD.

4.2 Results

4.2.1 Anti-abeta antibody titers in immunized animals

Two groups, therapeutic and preventative, of Tg2576 mice and aged-matched wild-type controls were used for the vaccination protocol. The therapeutic group was immunized with fibrillated abeta peptide or PBS beginning at 11 months of age, after disease onset, and immunized for four months (15-month-old mice). The preventative group was immunized with fibrillated abeta beginning at 6 wk of age, well before any pathological disease symptoms, for 11 months (12-month-old mice). Mice immunized with abeta, from both preventative **Figure 4.1a** and therapeutic **Figure 4.1b** groups, produced a high IgG response to abeta1-40. No detectable antibody titers were observed in the Tg2576 and age-matched wild-type mice vaccinated with PBS. Mice vaccinated with abeta, which did not exhibit high anti-abeta antibody titers, were eliminated from the study. These results were originally described by Dickstein [161, 290].

Figure 4.1: Abeta immunized mice have increased serum antibody titers compared to mice immunized with PBS.
Serum antibody titers were measured by ELISA after the second vaccination. In all cases, Tg2576 (Tg/+) and age-matched wild-type (+/+) mice immunized with fibrillar abeta1-40 had a high anti-abeta antibody titer against abeta peptide. No anti-abeta antibodies were detected in mice immunized with PBS. (a) Mice immunized preventatively for one year. PBS +/+, n = 5; PBS Tg/+, n = 7; abeta +/+, n = 6; abeta Tg/+, n = 4. (b) Mice immunized therapeutically for four months. PBS +/+, n = 7; PBS Tg/+, n = 8; abeta +/+, n = 5; abeta Tg/+, n = 6. The mean is indicated in for each group by the horizontal bars. Reprinted from The FASEB Journal, 20(3), Dickstein, D. L., Biron, K. E., Ujiie, M., Pfeifer, C. G., Jeffries, A. R. and Jefferies, W. A., Abeta peptide immunization restores blood-brain barrier integrity in Alzheimer disease, p 426-33, Copyright (2006), with permission from Elsevier [161, 290].

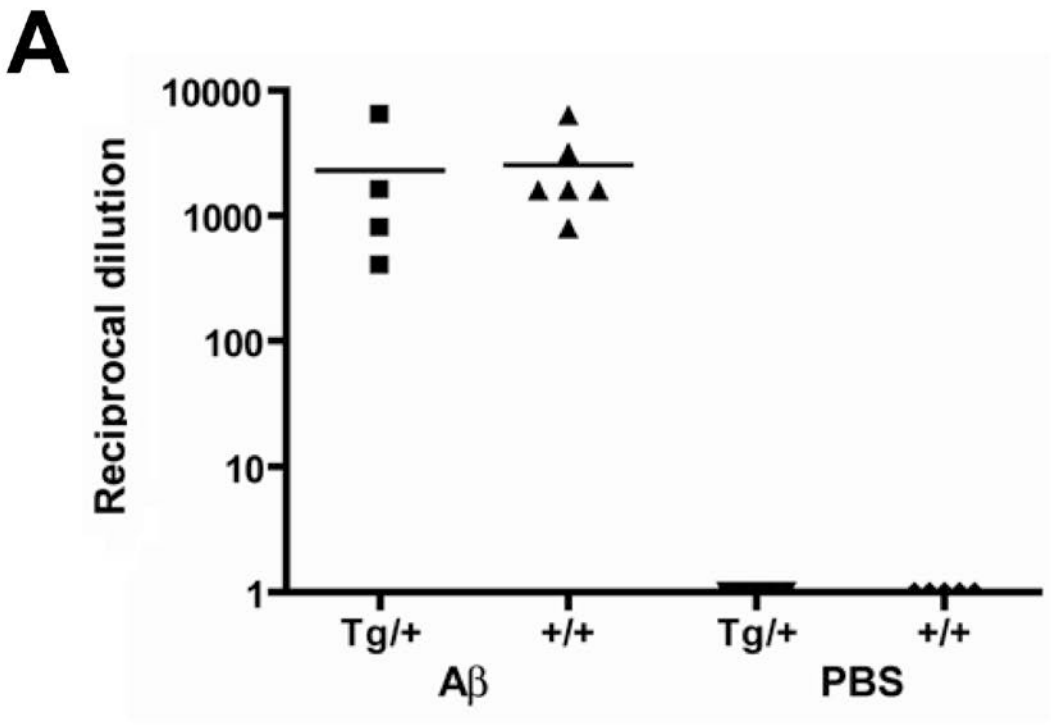
A
10000
1000
100
10
1
Reciprocal dilution
Tg/+
+/+
Tg/+
+/+
Aβ
PBS

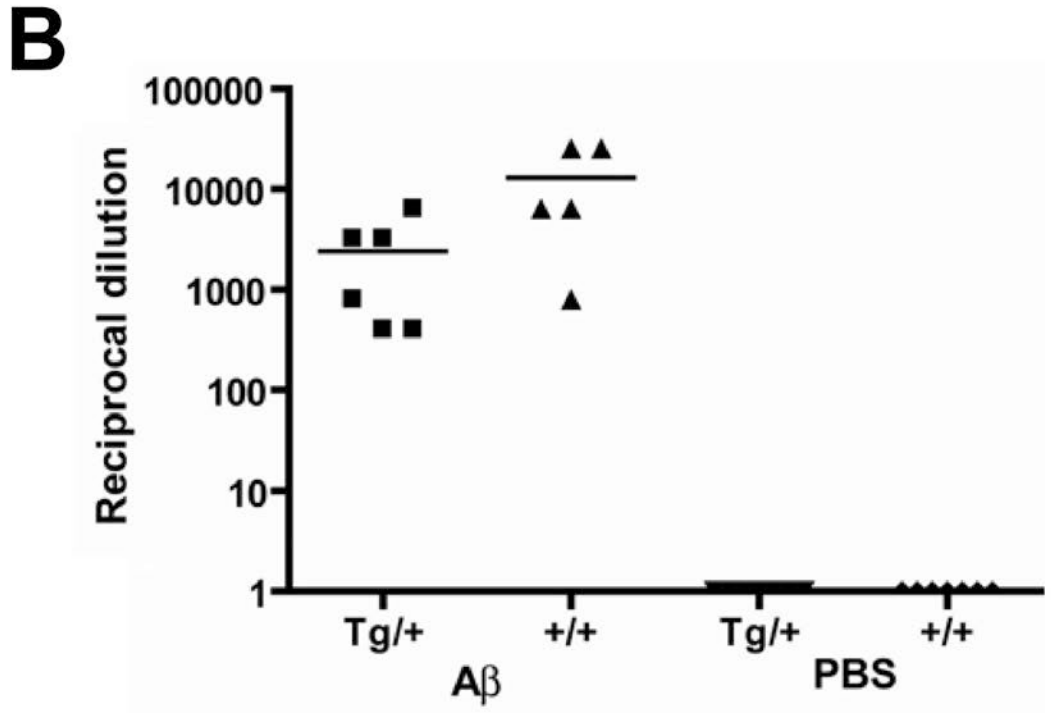
B
100000
10000
1000
100
10
1
Reciprocal dilution
Tg/+
+/+
Tg/+
+/+
Aβ
PBS

4.2.2 Immunohistochemistry of plaque burden in Tg2576 immunized mice

The relative amyloid plaque burden was assessed by immunohistochemistry, using the 4G8 anti-abeta antibody, in Tg2576 and wild-type mice immunized with either abeta or PBS. Overall, there was a significant reduction in the plaque burden in the cortex and hippocampus of transgenic mice immunized with abeta compared to those immunized with PBS.

Mice immunized as part of the therapeutic strategy with abeta had a dramatic decrease in both size and number of abeta plaques but not a total elimination of plaque burden **Figure 4.2b, Figure 4.3a**. Conversely, Tg2576 mice therapeutically immunized with PBS contained numerous amyloid deposits **Figure 4.2a, Figure 4.3a**.

Tg2576 mice immunized as part of the preventative strategy with abeta had an almost complete prevention of abeta deposition **Figure 4.2d, Figure 4.3b**. In abeta immunized transgenic mice, four of six mice had no detectable amyloid deposits. Two mice from the preventative group had a single isolated plaque in the four brain sections examined. Similar to the therapeutic group, PBS-treated Tg2576 mice exhibited numerous amyloid deposits in their cortical and hippocampal regions **Figure 4.2c, Figure 4.3b**. There were no detectable plaques in wild-type controls vaccinated with either abeta or PBS. These results were originally described by Dickstein *et al*. [161].

Figure 4.2: Abeta immunized Tg2576 mice have less amyloid pathology compared to mice immunized with PBS.
Micrographs shown are representative abeta immunohistochemically stained, using the 4G8 anti-abeta antibody, Tg2576 mouse brains (the cortex) from mice immunized with either abeta or PBS. There was a significant reduction in the total number of abeta plaques in Tg2576 mice vaccinated with abeta compared with those vaccinated with PBS in both the preventative and therapeutic treatment groups. (a) Tg2576 mice vaccinated under the thereaputic strategy with PBS. (b) Tg2576 mice vaccinated under the thereaputic strategy with abeta. (c) Tg2576 mice vaccinated under the preventative strategy with PBS. (d) Tg2576 mice vaccinated under the preventative strategy with abeta. No plaques were present in all wild-type mice immunized with either abeta or PBS. Results are representative of three separate experiments of three mice per group of brain tissues examined. Scale bar represents 190 um. Reprinted from The FASEB Journal, 20(3), Dickstein, D. L., Biron, K. E., Ujiie, M., Pfeifer, C. G., Jeffries, A. R. and Jefferies, W. A., Abeta peptide immunization restores blood-brain barrier integrity in Alzheimer disease, p 426-33, Copyright (2006), with permission from Elsevier [161, 290].

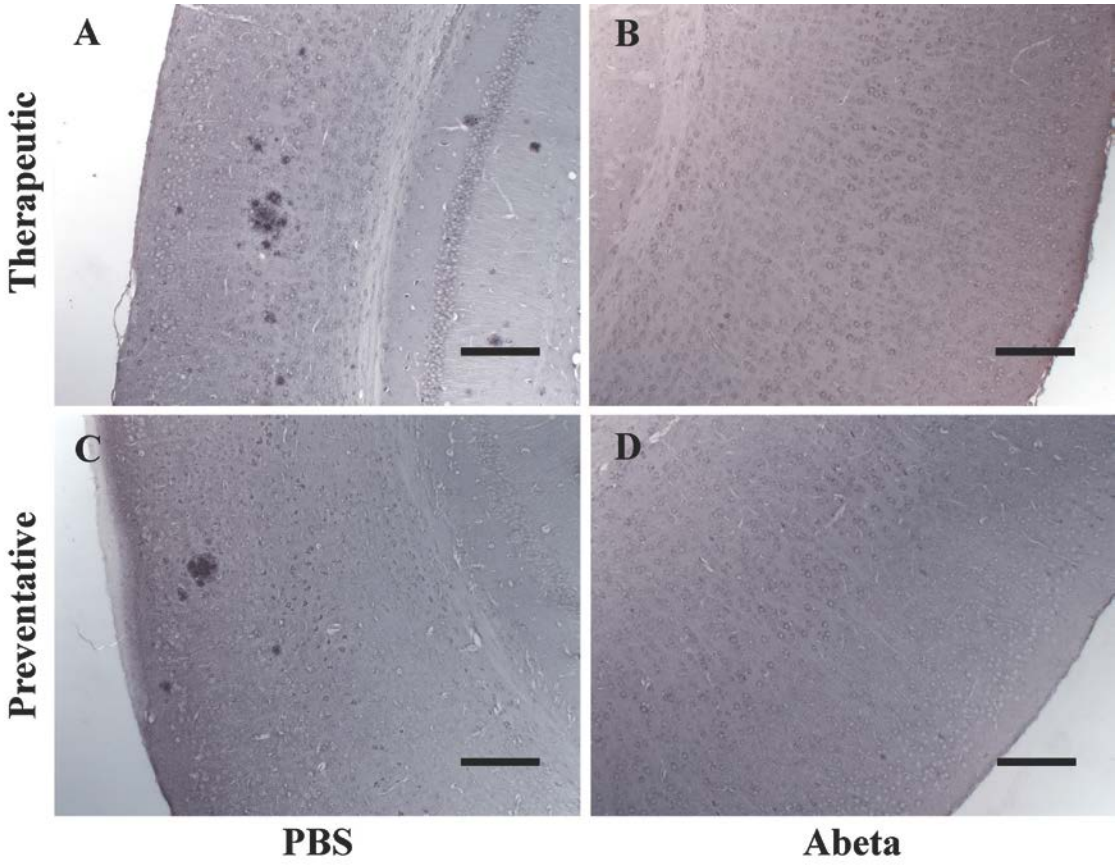

Figure 4.3: Cerebral amyloid levels are reduced in Tg2576 mice after abeta immunization. Abeta plaques were detected using the 4G8 anti-human abeta antibody on serial brain sections. The presence of discrete plaques made it feasible to count the number of plaques in the entire section. Plaques were counted by visual inspection under the microscope for each of 4 sections at equal plane for each cortical mouse brain section. The total averaged number of plaques is presented. There was a significant reduction (*t* test, * $p<0.05$) in the total number of abeta plaques in Tg2576 mice vaccinated with abeta compared with those vaccinated with PBS for both the (a) therapeutic and (b) preventative immunized groups. In the preventative group: PBS Tg/+, n = 7; abeta Tg/+, n = 4. In the therapeutic group: PBS Tg/+, n = 8; abeta Tg/+, n = 6. Values represent mean ± SEM. Reprinted from The FASEB Journal, 20(3), Dickstein, D. L., Biron, K. E., Ujiie, M., Pfeifer, C. G., Jeffries, A. R. and Jefferies, W. A., Abeta peptide immunization restores blood-brain barrier integrity in Alzheimer disease, p 426-33, Copyright (2006), with permission from Elsevier [161, 290].

A

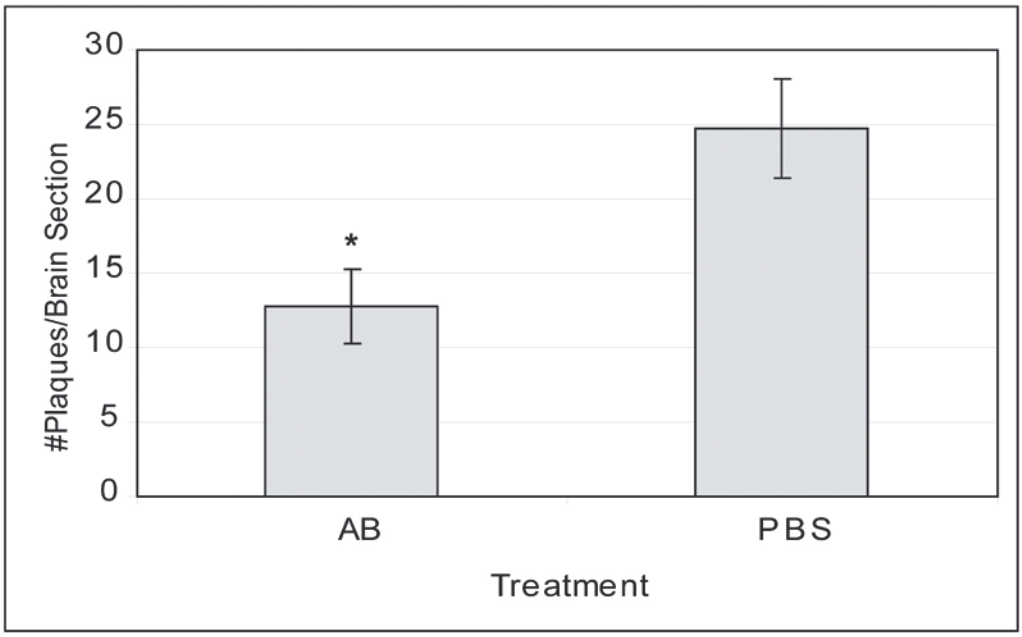
30
25
20
15
10
5
0
#Plaques/Brain Section
*
AB
PBS
Treatment

B

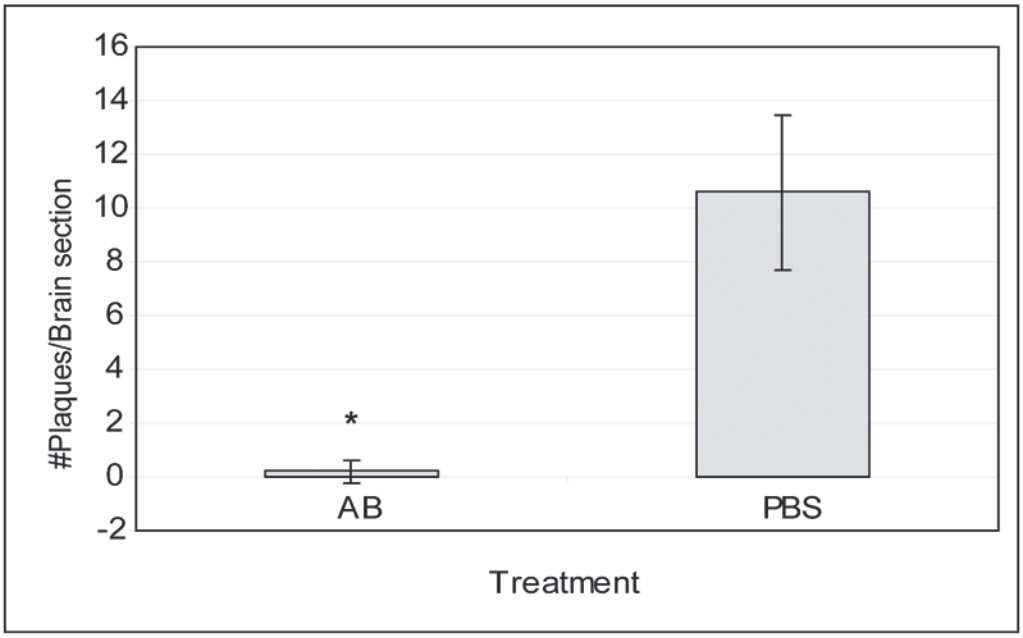
16
14
12
10
8
6
4
2
0
-2
#Plaques/Brain section
*
AB
PBS
Treatment

4.2.3 Microgliosis in immunized Tg2576 mice

The relative microgliosis, referring the accumulation and activation of microglia, in immunized Tg2576 mice was assessed by F4/80 antigen immunohistochemistry and associated cell morphology. Activated microglia exhibited thickened ramified processes and larger cell bodies, which progress to a final amoeboid/phagocytic state. Resting or non-activated microglia exhibited morphology that had small cell bodies with thin highly branched processes. Overall, there appeared to be a reduction in the presence of activated microglia in the brains of abeta immunized mice compared with PBS controls, in both immunization strategies. Therapeutically immunized transgenic mice with PBS had more plaque infiltrating microglia present than those immunized with abeta **Figure 4.4e and g**. There were more densely stained F4/80 positive microglia with swelled cell bodies and thickened processes in PBS-treated transgenic mice compared with mice treated with abeta.

Using the preventative strategy, it was noted that the brains of Tg2576 mice immunized with PBS had more amoeboid shaped and thick ramified microglia, whereas the microglia in the abeta immunized mice had smaller cell bodies and more extensively ramified processes **Figure 4.4f and h**. The microglia present in wild-type mice displayed largely non-activated morphology **Figure 4.4a to d**. These results were originally described by Dickstein *et al*. [161].

Figure 4.4: Abeta immunized Tg2576 mice with abeta have reduced microgliosis compared to mice immunized with PBS.
Micrographs shown are representative F4/80, for microglia in black, immunohistochemically stained Tg2576 mouse brains from mice immunized with either abeta or PBS. Images were taken from cortex and hippocampus. Activated microglia can be distinguished from resting microglia by the presence of ramified processes and condensed cell bodies. Neocortex sections from Tg2576 mice immunized preventatively or therapeutically with abeta showed a reduction of activated, plaque associated microglia. PBS immunized Tg2576 mice, from both immunization strategies, had noticeably higher amounts of activated microglia. Control wild-type mice exhibited no microgliosis. (a) Therapeutically immunized wild-type mice with PBS. (b) Preventatively immunized wild-type mice with PBS. (c) Therapeutically immunized wild-type mice with abeta. (d) Preventatively immunized wild-type mice with abeta. (e) Therapeutically immunized Tg2576 mice with PBS. (f) Preventatively immunized Tg2576 mice with PBS. (g) Therapeutically immunized Tg2576 mice with abeta. (h) Preventatively immunized Tg2576 mice with abeta. Results are representative of three separate experiments of three mice per group of brain tissues examined. Scale bar represents 50 µm. Reprinted from The FASEB Journal, 20(3), Dickstein, D. L., Biron, K. E., Ujiie, M., Pfeifer, C. G., Jeffries, A. R. and Jefferies, W. A., Abeta peptide immunization restores blood-brain barrier integrity in Alzheimer disease, p 426-33, Copyright (2006), with permission from Elsevier [161, 290].

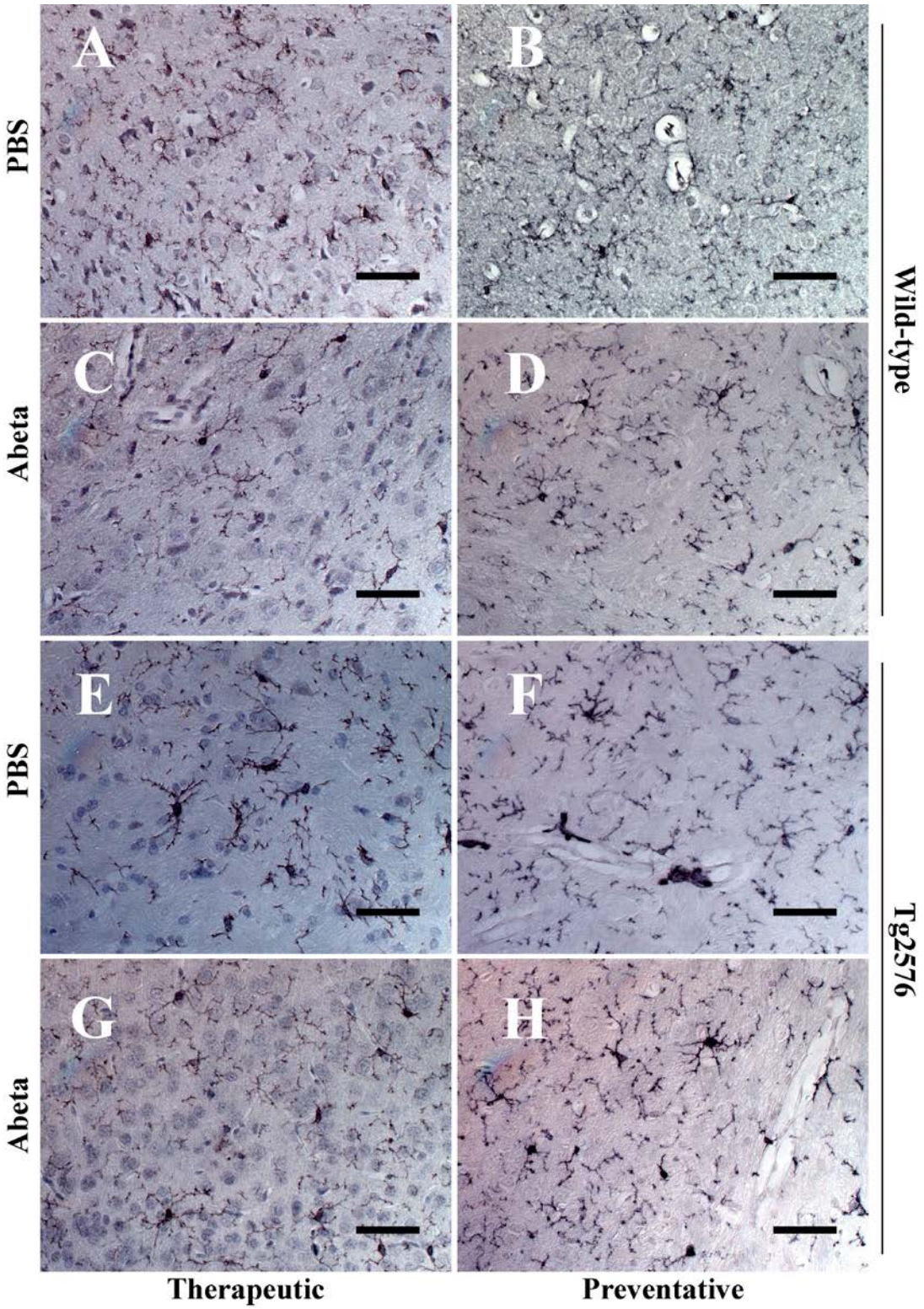
A
B
C
D
E
F
G
H
PBS
Abeta
PBS
Abeta
Therapeutic
Preventative
Wild-type
Tg2576

4.2.4 Immunized Tg2576 mice exhibit reduced cerebrovascular tight junction pathology

Tight junction (TJ) morphology and pathology was characterized in the cortex and hippocampus of Tg2576 and wild-type mice immunized with either abeta or PBS. Strong, continuous and linear staining patterns of occludin and ZO-1 within the cerebrovasculature **Figure 4.5a and b** were considered normal, which was consistent and indistinguishable in either the cortex or hippocampus regardless of genotype, immunizing strategy or agent. Weak, punctate and or discontinuous staining patterns **Figure 4.5c and d (white arrowheads)** for both occludin and ZO-1 on the cerebrovasculature were considered abnormal. Expression of TJ abnormalities was consistent and indistinguishable in the cortex and hippocampus of all mice regardless of genotype, immunizing strategy or agent. Most of the observed microvessels in abeta immunized Tg2576 mice had normal TJs **Figure 4.5a and b**, while vessels displaying TJ abnormalities were rare. However, larger vessels in the Tg2576 mice immunized with abeta, either preventatively or therapeutically, appeared to have a larger proportion of abnormal TJ expression **Figure 4.5e and f (white arrowheads)** compared to the capillaries.

Figure 4.5: Abeta and PBS immunized Tg2576 mice exhibit normal and abnormal TJ expression as assessed by confocal microscopy.
Representative confocal micrographs of cerebral blood vessels from abeta immunized (preventatively or therapeutically) Tg2576 mice immunolabeled for either occludin or ZO-1 (red) and counterstained for DNA (blue) with TOTO-3. Normal tight junction expression had strong, continuous and linear occludin or ZO-1 expression in the blood vessels. (a) Normal occludin expression in the microvessels of the hippocampus of a Tg2576 mouse immunized with abeta therapeutically. (b) Normal ZO-1 expression in the microvessels of the cortex of a Tg2576 mouse immunized with abeta preventatively. Abnormal tight junction expression in blood vessels of the cortex and hippocampus displayed faint, punctate and discontinuous morphology (white arrowheads). (c) Abnormal ZO-1expression in the cortex of a therapeutically immunized Tg2576 mouse. (d) Abnormal occludin expression in the hippocampus of a preventatively immunized Tg2576 mouse. (e) Large transversely sectioned vessels displaying abnormal occludin expression in a thereaputically immunized Tg2576 mouse. (f) Large transversely sectioned vessels displaying abnormal ZO-1 expression in a preventatively immunized Tg2576 mouse. Results are representative from three mice per group from three separate experiments. Scale bar depicts 20 µm.

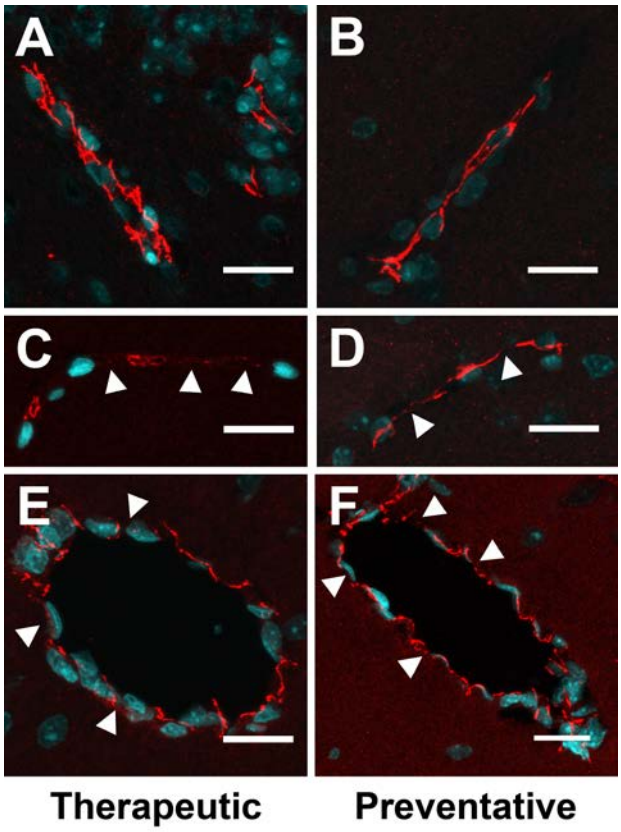

4.2.5 Quantitative assessment of cerebrovascular tight junction pathology in the immunized Tg2576 mice

The incidence of TJ pathology was quantitatively assessed, by confocal microscopy, in Tg2576 mice immunized as part of a therapeutic (starting at 11 months until 15 months of age) or preventative (starting at six weeks of age until one year old) strategy with either abeta or PBS. The incidence of TJ pathology was defined as the average percentage of blood vessels that displayed abnormal TJ morphology. The cortex of preventatively immunized PBS Tg2576 mice displayed a significantly higher percentage (29.00 ± 4.02%; ** p = 0.0080, t-test) of disrupted TJ expression compared to PBS wild-type baseline of about 10% **Figure 4.6a**. Abeta immunized Tg2576 mice displayed a significantly lower percentage of abnormal vascular TJ expression (11.33 ± 2.40%; * p = 0.0188, t-test) compared to the PBS transgenic counterpart in the cortex **Figure 4.6a**. The incidence of TJ disruption in the hippocampus mirrored the cortex for preventatively immunized mice. Tg2576 mice immunized with PBS displayed significantly higher disruption (29.75 ± 1.89%; **** p = 0.0006, t-test) compared to PBS mice baseline of about about 10% **Figure 4.6b**. Hippocampal TJ disruption in abeta immunized Tg2576 mice were significantly lower (11.91 ± 1.73%; *** p = 0.0009, t-test) compared to PBS immunized Tg2576 mice **Figure 4.6b**.

Therapeutically immunized mice displayed similar incidents of disrupted vascular TJs like that of the preventative mice. In the cortex of therapeutic immunized PBS Tg2576 mice displayed a significantly higher percentage of disrupted TJ expression (28.67 ± 4.91%; ** p = 0.0046, t-test) compared to PBS wild-type baseline of about 10% **Figure 4.7a**. Abeta immunized Tg2576 mice displayed a significantly lower percentage of

abnormal vascular TJ expression (10.40 ± 0.81%; * p = 0.0028, t-test) compared to the PBS transgenic counterpart in the cortex **Figure 4.7a**. The incidence of TJ disruption in the hippocampus mirrored that of the cortex for therapeutic immunized mice. Tg2576 mice immunized with PBS displayed significantly higher disruption (27.33 ± 4.06%; **** p = 0.0115, t-test) compared to PBS wild-type mice baseline of about 10% **Figure 4.7b**. Hippocampal TJ disruption in abeta immunized Tg2576 mice were significantly lower (11.00 ± 2.26%; *** p = 0.0083, t-test) compared to PBS immunized Tg2576 mice **Figure 4.7b**.

Figure 4.6: Tg2576 mice immunized preventatively for one year with abeta had reduced tight junction abnormalities as compared to PBS immunized controls.
The incidence of TJ abnormality in the (a) cortex and (b) hippocampus of Tg2576 (Tg/+) and wild-type (+/+) mice preventatively immunized with either PBS or abeta was compared quantitatively. Graphs depict the percentage of blood vessels expressing TJ abnormality, by ZO-1 expression patterns. In the (a) cortex, PBS immunized Tg/+ had significantly higher incidence of TJ disruption compared to PBS +/+ (** $p = 0.0080$). The incidence of TJ disruption was also significantly higher in PBS Tg/+ compared to abeta immunized Tg/+ mice (* $p = 0.0188$). In the (b) hippocampus PBS immunized Tg/+ had significantly higher incidence of TJ disruption compared to PBS +/+ (**** $p = 0.0006$). The incidence of TJ disruption was also significantly higher in PBS Tg/+ compared to abeta immunized Tg/+ mice (*** $p = 0.0009$). Values represent mean ± SEM. PBS +/+, n = 3; PBS Tg/+, n = 4; abeta +/+, n = 3; abeta Tg/+, n = 3.

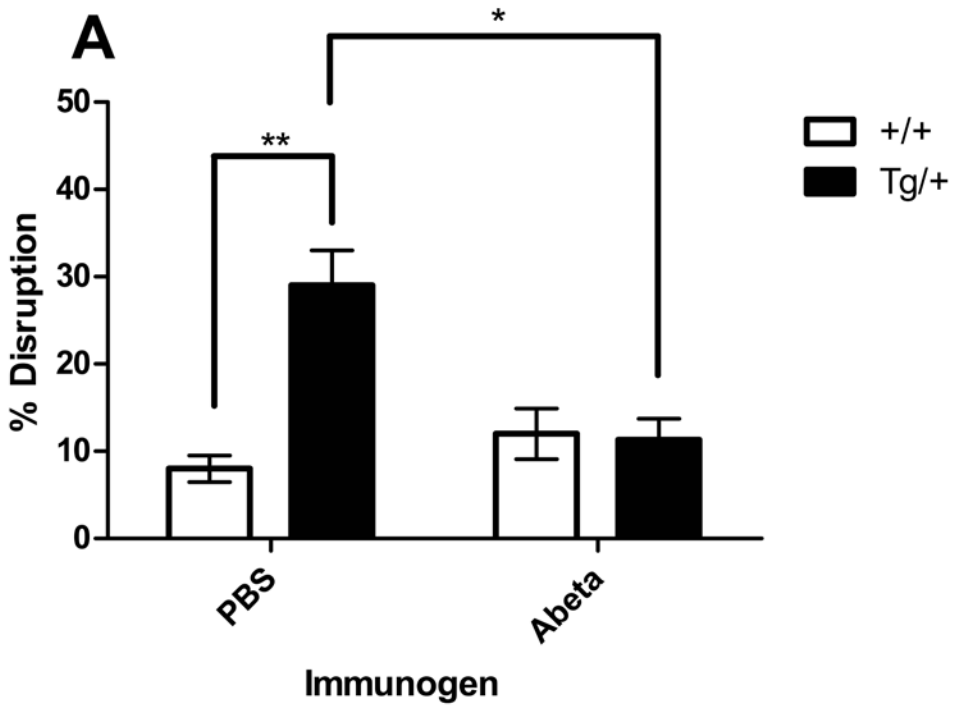
A
*
**
50
40
30
20
10
0
% Disruption
+/+
Tg/+
PBS
Abeta
Immunogen

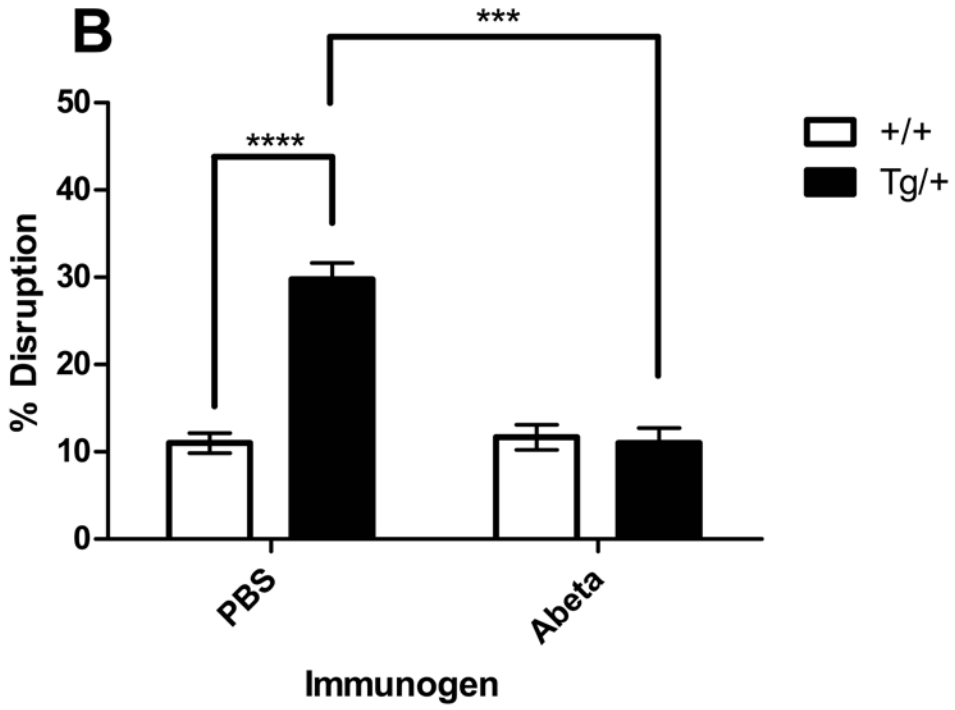
B
***
****
50
40
30
20
10
0
% Disruption
+/+
Tg/+
PBS
Abeta
Immunogen

Figure 4.7: Tg2576 mice immunized therapeutically for four months with abeta had reduced tight junction abnormalities as compared to PBS immunized controls.
The incidence of TJ abnormality in the (a) cortex and (b) hippocampus of Tg2576 (Tg/+) and wild-type (+/+) mice therapeutically immunized with either PBS or abeta was compared quantitatively. Graphs depict the percentage of blood vessels expressing TJ abnormality, by ZO-1 expression patterns. In the (a) cortex, PBS immunized Tg/+ had significantly higher incidence of TJ disruption compared to PBS +/+ (** $p = 0.0046$). The incidence of TJ disruption was also significantly higher in PBS Tg/+ compared to abeta immunized Tg/+ mice (* $p = 0.0028$). In the (b) hippocampus PBS immunized Tg/+ had significantly higher incidence of TJ disruption compared to PBS +/+ (**** $p = 0.0115$). The incidence of TJ disruption was also significantly higher in PBS Tg/+ compared to abeta immunized Tg/+ mice (*** $p = 0.0083$). PBS +/+, n = 4; PBS Tg/+, n = 3; abeta +/+, n = 4; abeta Tg/+, n = 5. Values represent mean ± SEM.

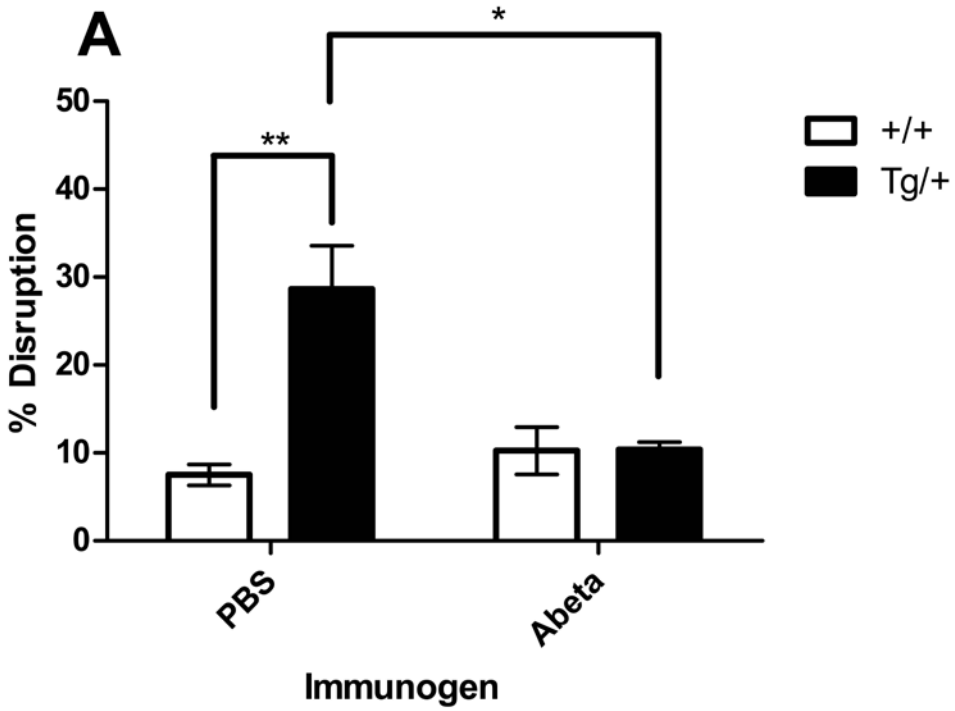
A
*
**
50
40
30
20
10
0
% Disruption
+/+
Tg/+
PBS
Abeta
Immunogen

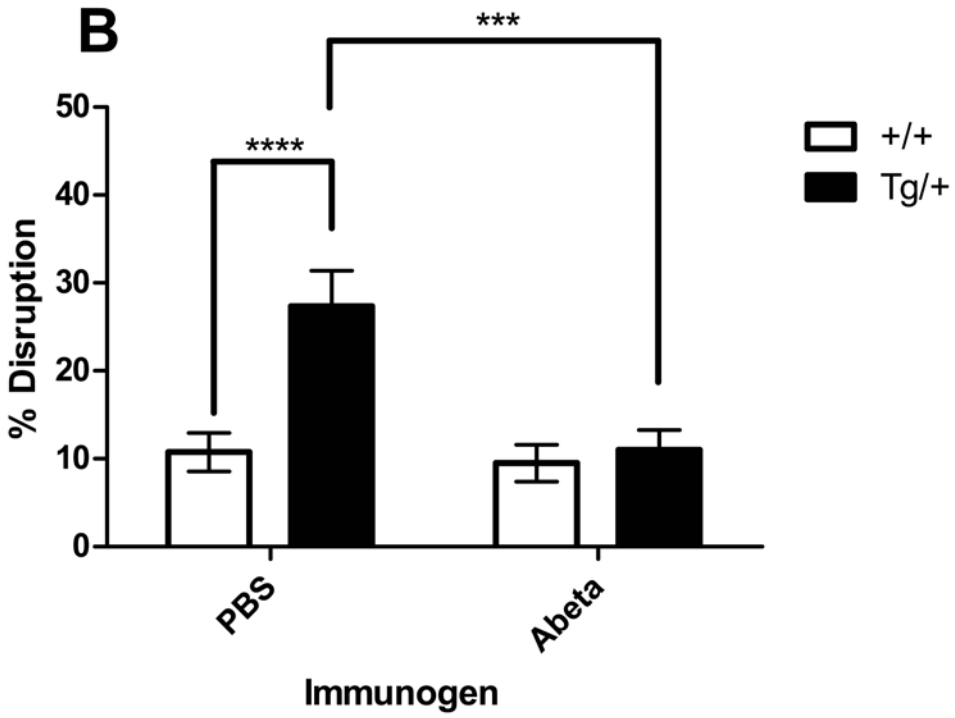
B
***
****
50
40
30
20
10
0
% Disruption
+/+
Tg/+
PBS
Abeta
Immunogen

4.2.6 Abeta immunized Tg2576 have overall reduced cerebrovascular leakage

Tg2576 and wild-type mice immunized, preventatively or therapeutically, with either abeta or PBS were assessed for cerebrovascular leakage and TJ abnormalities by confocal microscopy. Mouse albumin was used as a marker for vascular leakage and was visualized as diffuse gradient staining emanating away from vessels **Figure 4.8b (white arrowhead)**. Regardless of the immunizing strategy or agent, all wild-type mice examined had no vascular leakage and produced staining patterns similar to **Figure 4.8a**. Tg2576 mice immunized with PBS, either preventatively or therapeutically, did not display any notable signs of vascular leakage in neither the cortex nor hippocampus. Vascular leakage in PBS immunized Tg2576 mice was associated with TJ abnormalities (not shown), as determined with staining with both occludin and ZO-1.

Tg2576 mice immunized with abeta had little to no vascular leakage within the microvessels **Figure 4.8a**. However, the larger vessels of abeta immunized Tg2576 mice did have periodic vascular leakage **Figure 4.8b (white arrowhead)**. Abnormal TJ expression, both occludin (not shown) and ZO-1 **Figure 4.8b**, was consistently seen in the larger vessels that had vascular leakage. To assess if the larger vessels from Tg2576 mice immunized with abeta had disrupted TJ pathology was associated with vascular abeta deposits, double staining for TJs and abeta was performed **Figure 4.8c**. Mild vascular abeta deposition was seen in only the larger vessels in both the preventative and therapeutic abeta immunized Tg2576 mice. Large vessels that had vascular deposition of abeta also had TJ, both occludin (not shown) and ZO-1 **Figure 4.8c (hollow white arrows)**, pathology. No abeta deposition was seen in the cerebral capillaries in the abeta

immunized Tg2576 mice. Treated wild-type had no vascular abeta. PBS treated Tg2576 for either one year or four months had very limited vascular abeta.

Figure 4.8: Abeta immunized Tg2576 mice have overall reduced vascular leakage.
Representative confocal micrographs of cerebral blood vessels from preventatively immunized Tg2576 mice with abeta immunolabeled for ZO-1 (red), mouse albumin (mAlb, green) or abeta (green). Microvessels (a) typically had normal ZO-1 expression and did not display albumin leakage. White arrows point to two normal and seperate ZO-1 expressing microvessels. Albumin leakage was typically associated with larger vessels (b), which displayed TJ abnormalities. Leakage (white arrowhead) was represented as diffuse gradient like staining emanating away from vessels. (c) A large vessel with abnormal TJ expression (hollow white arrows) containing vascular deposition of abeta. Results are representative from three mice per group from three separate experiments. Scale bar represents 20 µm.

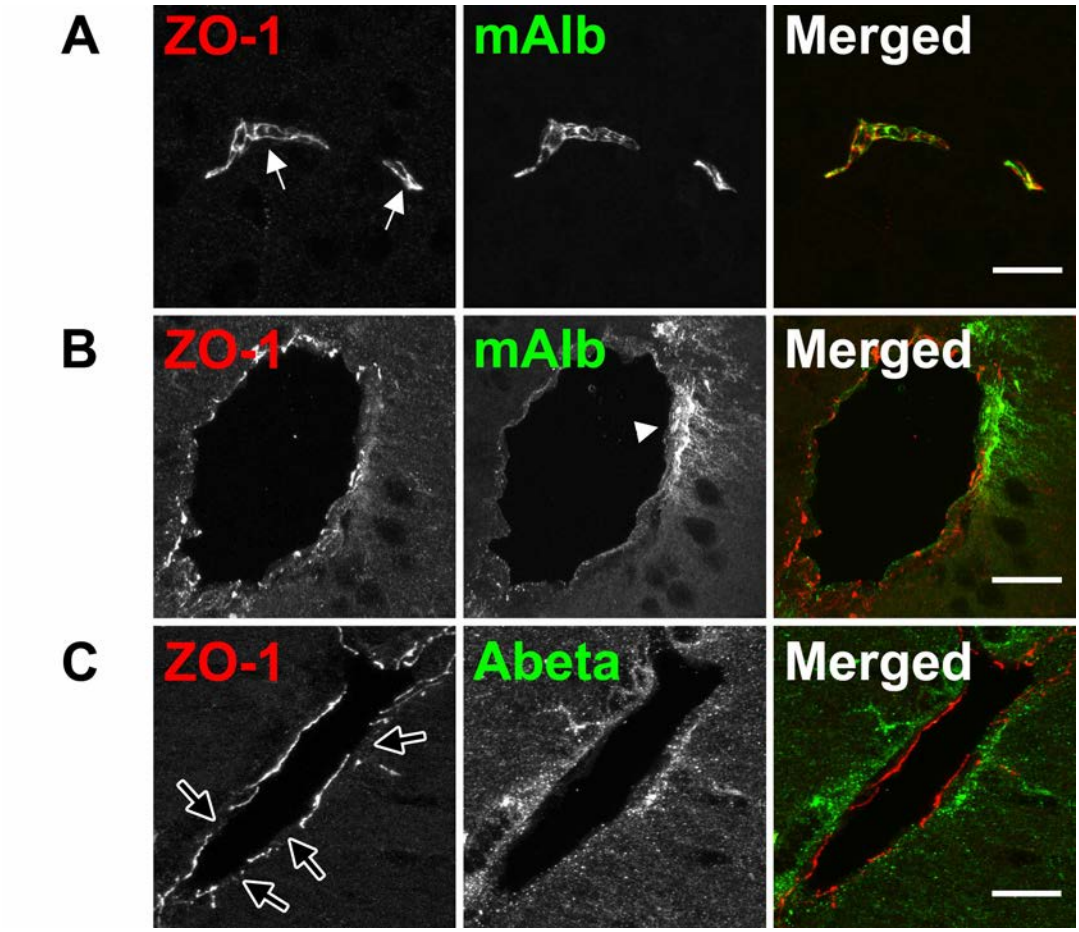

4.2.7 Angiogenesis and apoptosis in immunized Tg2576 brains

Incidence of apoptosis and angiogenesis were examined, by confocal microscopy, in Tg2576 mice immunized preventatively (starting at six weeks of age until one year old) or therapeutically (starting at 11 months until 15 months of age) with either abeta or PBS. An anti-activated caspase-3 antibody was used as a marker of apoptosis **Figure 4.9**. In all examined sections, activated caspase-3 did not directly stain the endothelia. Similar to the staining patterns noted in aged and young Tg2576 mice, activated caspase-3 was seen in filamentous-like cell bodies that were presumed to be neurons. All immunized mice exhibited activated caspase-3 staining in the hippocampus, albeit in various amounts, in the CA1, CA2, CA3 and DG regions. PBS immunized Tg2576 mice, both preventative and therapeutic, had significant activated caspase-3 staining within the **Figure 4.9a** cortex and hippocampus (not shown) that tended to surround probable abeta plaques. Wild-type (abeta and PBS) and abeta immunized Tg2576 mice exhibited hippocampal restricted caspase-3 staining **Figure 4.9b**. The overall density of activated caspase-3 staining in these mice was noted to be lower then the Tg2576 treated with abeta. The cortex of abeta immunized, both preventative and therapeutic, Tg2576 mice had limited caspase-3 staining **Figure 4.9c**. Cortex activated caspase-3 staining appear similar in the abeta immunized Tg2576 to the wild-type varients. These results were consistent across all mice examined.

CD105 staining was used as an angiogenic endothelial marker; however, CD105 staining was seen on all the brain vasculature regardless of the absence or presence of TJ abnormalities. The microvessel density (MVD), by CD105 staining, was quantified by

confocal microscopy in the mice immunized as part of the therapeutic or preventative strategy with either abeta or PBS. The MVD was defined as a ratio of the TFA to the total area of an imaged field and was used as a surrogate measure of angiogenesis. The average MVD in Tg2576 mice immunized with PBS for either preventatively for one year (0.4560 ± 0.0072; * $p < 0.0001$, t-test) was significantly higher compared to the wild-type immunized with PBS (0.1951 ± 0.0123) **Figure 4.10a**. Tg2576 mice immunized preventatively with abeta had a significantly reduced MVD (0.1972 ± 0.0075; ** $p < 0.0001$, t-test) compared to transgenic immunized with PBS **Figure 4.10a**. The MVD in the therapeutically immunized mice was similar to the preventative group. The average MVD in Tg2576 mice immunized with PBS for either therapeutically for four months (0.4939 ± 0.0077; *** $p = 0.0001$, t-test) was significantly higher compared to the wild-type immunized with PBS (0.2044 ± 0.0222) **Figure 4.10b**. Tg2576 mice immunized therapeutically with abeta had a significantly reduced MVD (0.2180 ± 0.0130; **** $p < 0.0001$, t-test) compared to transgenic immunized with PBS **Figure 4.10b**.

Figure 4.9: Abeta immunized Tg2576 mice have reduced activated caspase-3 staining. Representative confocal micrographs (taken at 20x) depict activated caspase-3 staining (casp3, green) with occludin (occlu, red) TJs. (a) Activated caspase-3 staining in the cortex of PBS therapeutically immunized Tg2576 mice surround TJ halos. Filamentous-like structures probably corresponding to neurons can be seen in green that surround a probably plaque location. (b) Activated caspase-3 staining within the hippocampus of a wild-type mouse immunized preventatively with abeta. Filamentous-like structures probably corresponding to neurons can be seen in green. No overlap or costaining was seen with either occludin or ZO-1 labeled blood vessels. (c) Activated caspase-3 staining in the cortex of an abeta therapeutically immunized Tg2576 mouse. Limited caspase-3 staining can be seen in this region of the brain. Results are representative from three mice per group from three separate experiments. Scale bar represents 20 µm.

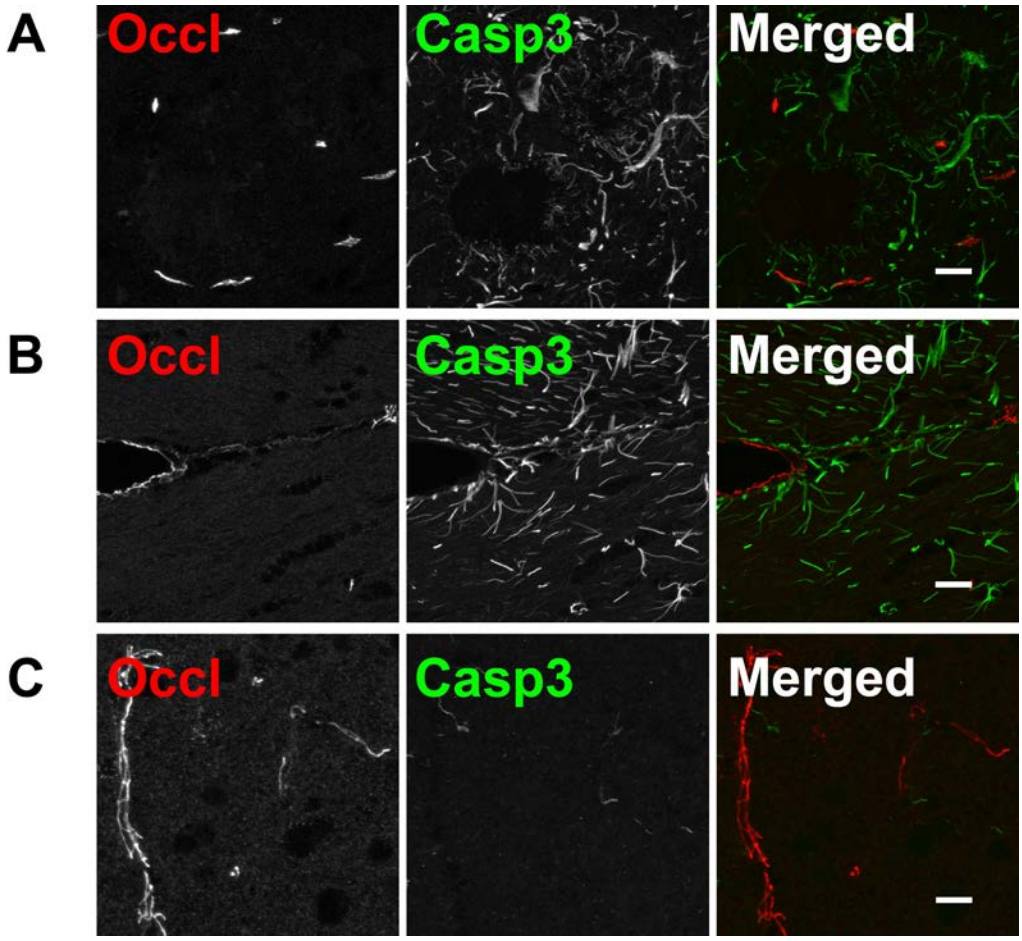

Figure 4.10: Abeta immunized Tg2576 mice have reduced microvascular density compared controls. The MVD in the cerebrovasculature of abeta and PBS immunized, preventatively and therapeutically, Tg2576 (Tg/+) and wild-type (+/+) mice was quantified by CD105 staining. (a) Preventatively immunized Tg/+ mice with PBS had significantly increased MVD compared to the PBS immunized +/+ (* $p < 0.0001$, t-test). Abeta immunized Tg/+ had a significantly reduced MVD compared to the Tg/+ immunized with PBS (** $p < 0.0001$, t-test). PBS +/+, n = 4; PBS Tg/+, n = 4; abeta +/+, n = 4; abeta Tg/+, n = 4. (b) Therapeutically, immunized Tg/+ with PBS had significantly increased MVD compared to the PBS immunized +/+ (*** $p = 0.0001$, t-test).). Abeta immunized Tg/+ had a significantly reduced MVD compared to the Tg/+ immunized with PBS (**** $p < 0.0001$, t-test). PBS +/+, n = 5; PBS Tg/+, n = 4; abeta +/+, n = 4; abeta Tg/+, n = 3. Values represent mean ± SEM.

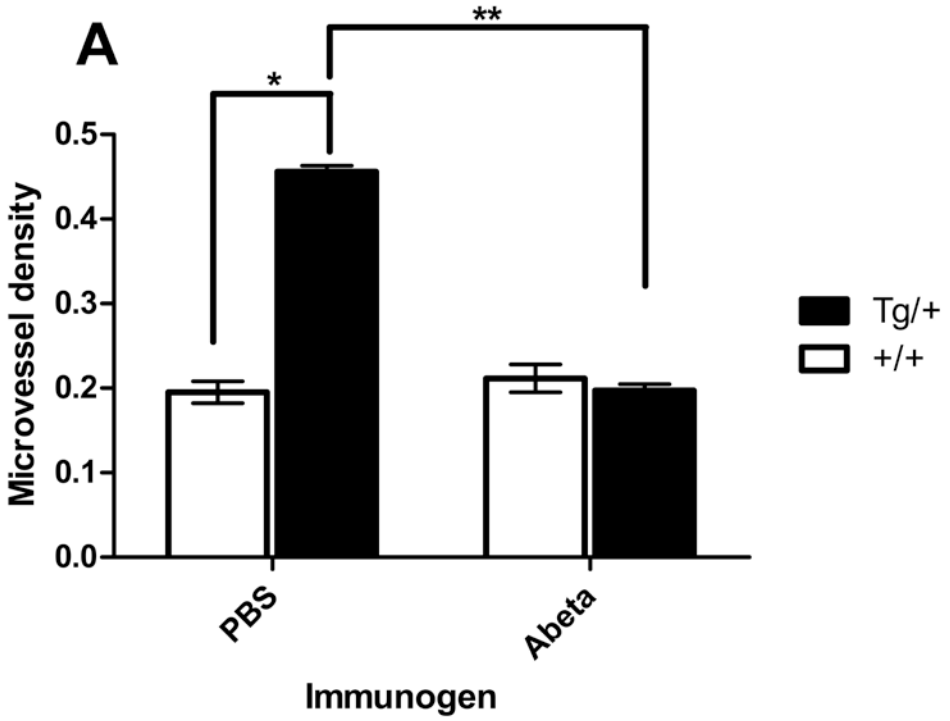
A
**
*
0.5
0.4
0.3
0.2
0.1
0.0
Microvessel density
Tg/+
+/+
PBS
Abeta
Immunogen

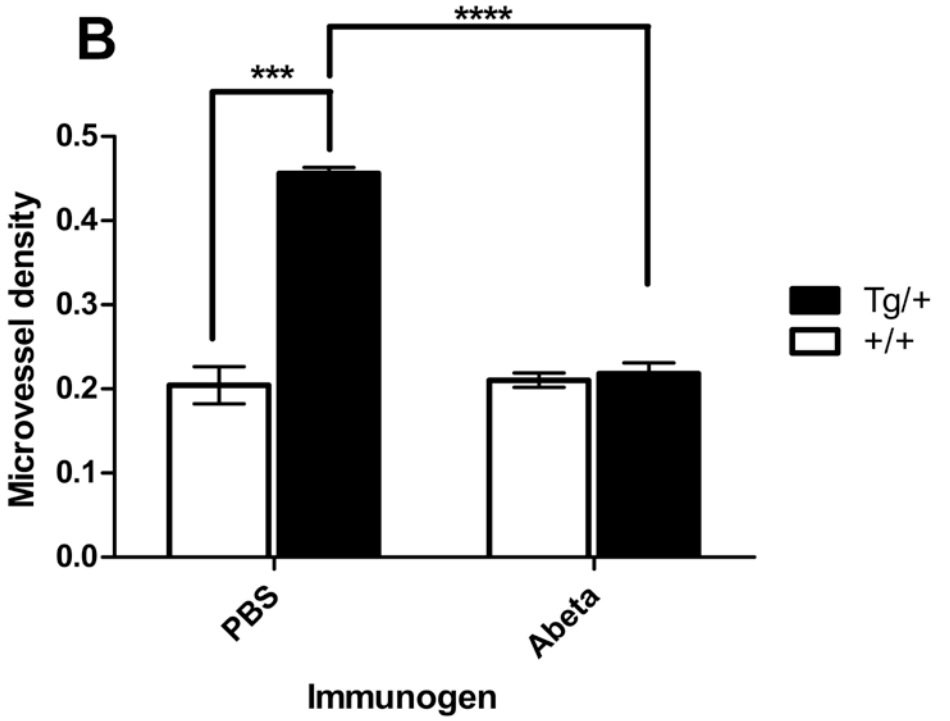
B
****
***
0.5
0.4
0.3
0.2
0.1
0.0
Microvessel density
Tg/+
+/+
PBS
Abeta
Immunogen

4.2.8 Atypical non-vascular TJ expression in immunized Tg2576 mice

In the previous chapter, atypical non-vascular TJ staining patterns were observed in plaque bearing Tg2576 mice. For example, ZO-1 “halos” were found to be associated with dense-core plaques. The halos also appeared to have overlapping staining with astrocytes. Rare atypical non-vascular occludin expression was also found to be expressed on a subpopulation of astrocytes. These rare S100β-positive astrocytes expressing occludin tended to also associate with abeta plaques. The incidence of these atypical nonvascular TJ staining patterns were examined in the abeta and PBS immunized Tg2576 and wild-type mice.

All immunized wild-type mice, both preventative and therapeutic strategies, were devoid of either atypical non-vascular TJ staining patterns of either ZO-1 or occludin. TJ expression was only localized to vasculature in these mice. Tg2576 mice immunized with PBS did express the atypical non-vascular TJ staining patterns seen with ZO-1 **Figure 4.11a** and occludin **Figure 4.11b**. The atypical TJ expression patterns were indistinguishable in both the preventative and therapeutic immunization strategies. Abeta immunized Tg2576, either preventatively or therapeutically, were devoid of the atypical TJs. Occludin (not shown) and ZO-1 **Figure 4.11c**, and S100β astrocytic expression patterns were indistinguishable from the wild-type mice.

Figure 4.11: Abeta immunized Tg2576 mice have typical tight junction protein expression patterns. Representative confocal micrographs of typical and non-typical TJ (occludin and ZO-1, red) expression in PBS or abeta immunized Tg2576 mice with associated astrocytes (S100β, green). (a) PBS immunized Tg2576 preventatively had abeta associated ZO-1 halos. S100β-positive astrocytes staining seemed to directly costain with ZO-1 halos. (b) PBS immunized Tg2576 therapeutically had astrocytes colocalized with occludin represented as yellow in the merged image. (c) Abeta immunized Tg2576 therapeutically had normal vascular associated expression of occludin. Typical S100β labeled astrocytes associate near and with blood vessels. Results are representative from three mice per group from three separate experiments. Scale bar represents 20 µm.

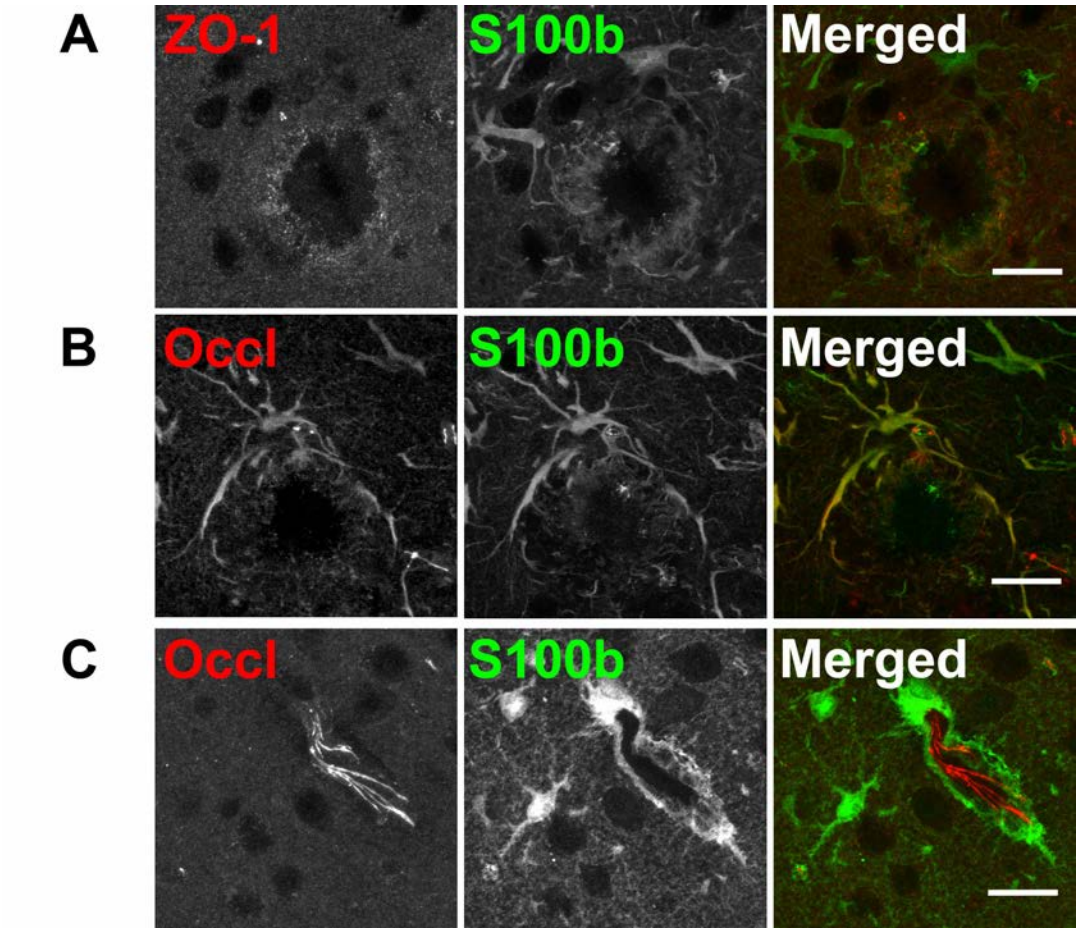

4.2.9 White matter lesions and focal mononuclear infiltrate are readily identified with Luxol Fast Blue and Iba-1 staining in EAE

MOG-induced EAE in C57Bl/6 mice was used to investigate regulation of the TJ protein ZO-1 over the course of clinical disease, to identify the stage of initial BBB disruption. Three histological methods were used for identification of focal lesion sites in the CNS tissue of EAE-induced animals. First, H&E histology marked areas of mononuclear infiltration. Second, LFB staining identified both infiltrates and areas of demyelination **Figure 4.12a, d, and g**. Third, Iba-1 immunohistochemical labeling of microglia and infiltrating monocytes, can discriminate lesion locations and identify smaller foci of activity at earlier time points of disease. Microscopic examination of sections from naïve control spinal cord tissues, immunostained with antibody to Iba-1, revealed the presence of small numbers of resting microglia cells **Figure 4.12b, e** . An increase in cell numbers and changes in morphology of microglia were present in treated animals that reached the highest level at the peak of clinical disease **Figure 4.12f and h** with very heavy clustering of Iba-1-positive microglia in focal areas of the lumbar spinal cord **Figure 4.12i**. The amplified degree of demyelination and appearance of inflammatory infiltrates during clinical disease compared to all preclinical and control groups was readily observed, correlating with Iba-1 expression levels. Thus, LFB and Iba-1 distribution provide a measure for assessment of lesion-area formation in EAE. These results were originally described by Bennett *et al.* [160].

Figure 4.12: White matter lesion sites and focal mononuclear infiltrate identified with LFB and Iba-1 staining in EAE spinal cord.
Representative immunohistochemical staining of focal lesion sites in the CNS tissue of EAE-induced animals at various clinical stages. White matter lesion sites and focal mononuclear infiltrate identified with LFB and Iba-1 (black) staining in EAE spinal cord. H&E/LFB (a, d and g) and Iba-1 staining (b, c, e, f, h and i) were used to identify lesion sites indicated by activated microglia and mononuclear infiltrate in the mouse spinal cord tissue. In the MOG-induced EAE tissue, progressive pathology is evident as mononuclear cell infiltration, myelin loss, and intensity and distribution of Iba-1 staining increase with disease development. (a and b) naïve (7 days after initiation of experiment in same environment), (c) 5 days post-immunization; (d and E) 14 days post-immunization; (f) 7 ays post-immunization; and (g, h, and i) 21 days post-immunization (peak of disease). Images are representative of at least three experiments with at least 3 animals per condition. Reprinted from Journal of Neuroimmunology, Bennett, J., Basivireddy, J., Kollar, A., Biron, K. E., Reickmann, P., Jefferies, W. A. and McQuaid, S., Blood-brain barrier disruption and enhanced vascular permeability in the multiple sclerosis model EAE, Copyright (2010), with permission from Elsevier [160].

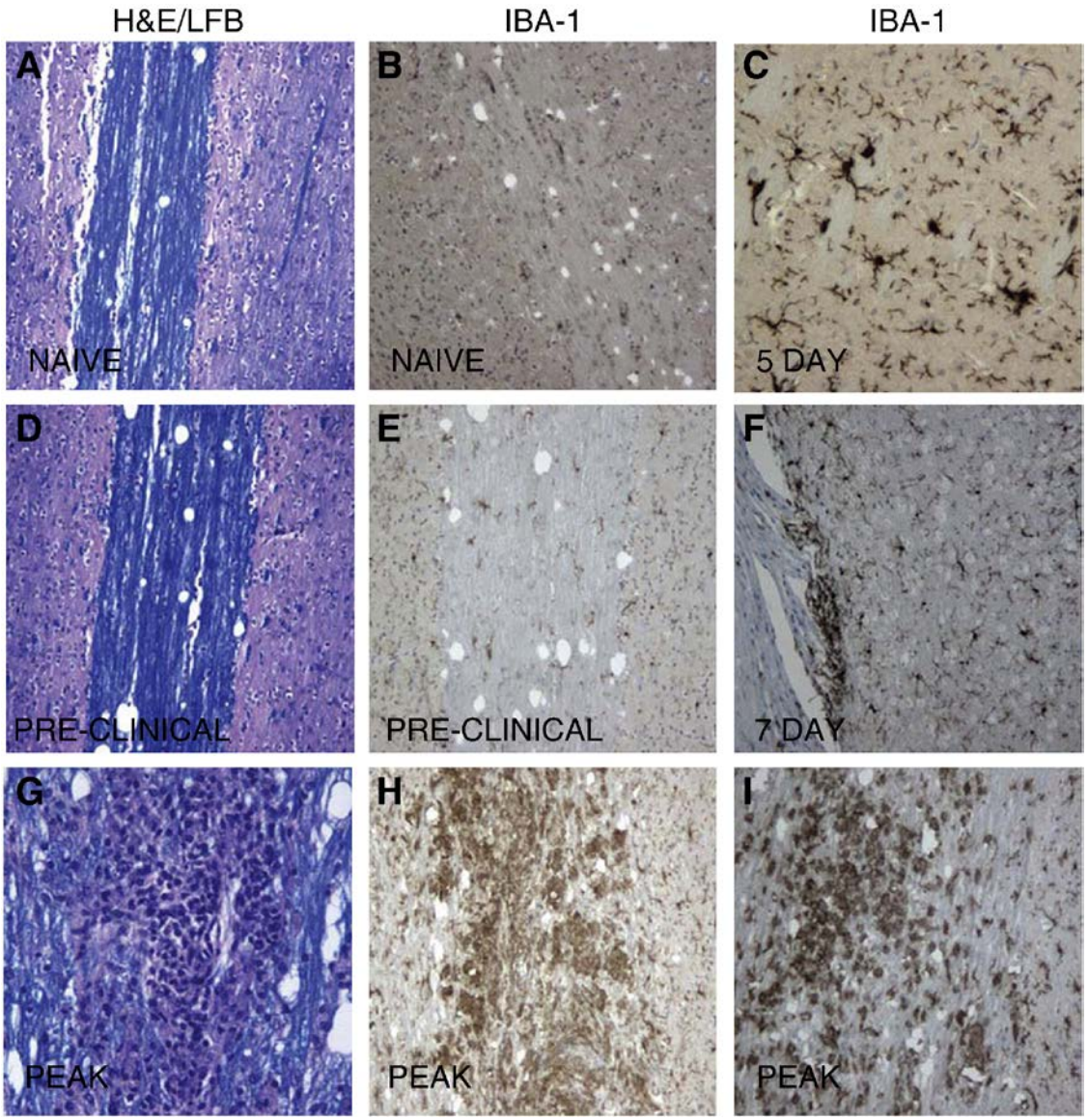
H&E/LFB
IBA-1
IBA-1
A
NAIVE
B
NAIVE
C
5 DAY
D
PRE-CLINICAL
E
PRE-CLINICAL
F
7 DAY
G
PEAK
H
PEAK
I
PEAK

4.2.10 Disruption of ZO-1 in spinal cord vessels correlates with MS-like lesions and mononuclear infiltrate.

The endothelial TJ abnormalities of CNS tissues from control and EAE animals were examined by immunofluorescence staining **Figure 4.13**. In transversely sectioned vessels ZO-1 staining revealed short, radial or near radial fluorescent bands **Figure 4.13a and f**. In longitudinal view, fluorescent staining of tight junctions (ZO-1) in vessels was predominantly linear **Figure 4.13b and e**. Normal vessels demonstrate a narrow, regular, single-layer pattern around a vessel opening. In the normal appearing white matter (NAWM) of spinal cord and brain, endothelial cells are orientated in a flat smooth layer facing the vessel lumen **Figure 4.13a, b, e and f**. In spinal cord lesions, ZO-1 staining was disorganized, with loss of regular orientation around the lumen and infiltrating cells interspersed within the ragged appearing ZO-1 staining **Figure 4.13c, d, g and h**. A close association of abnormal vascular TJ integrity, indicated by ZO-1 disorganization, with focal lesions in the white matter (WM) was observed. Normal TJ integrity was seen in the CNS regions not involved in inflammatory processes like the choroid plexus or the periventricular zone of the white matter **Figure 4.13i and j**. The uniform expression of melanotransferrin, a pan endothelial marker, on all spinal cord and brain blood vessels examined **Figure 4.13k** at various stages of disease suggests that overt loss of the endothelial architecture is not the cause of ZO-1 redistribution. These results were originally described by Bennett *et al.* [160].

Figure 4.13: EAE induced mice have abnormal CNS TJ expression as assessed by confocal microscopy.
Representative confocal micrographs of CNS blood vessels from EAE induced mice immunolabeled for ZO-1 (green) and counterstained for DNA (red) with propidium iodide in various CNS regions. Normal distribution of ZO-1 in naive animals is observed in staining of spinal cord (a and b) and brain tissue (e and f). At the peak of MOG-induced EAE disease, disrupted expression of ZO-1 is present in longitudinally and transverse aspects of vessels (c, d, g, and h). In the arrowed vessels in the spinal cord, there is disruption of tight junctions associated with perivascular inflammation (g). (h) In blood vessel labeled with *** there is almost total dissociation of tight junction integrity in a vessel where there is definite inflammatory response/infiltrate. The ZO-1 expression pattern from EAE mice showed definite interruptions reflecting an opening of the vessel barrier with discontinuous and diffuse ZO-1 localization, supporting a role for tight junction loss in the lesions. Normal ZO-1 expression was seen in distinct areas of the CNS during EAE including the choroid plexus (i) and the periventricular zone (j). Uniform melanotransferrin expression (k, green) in a blood vessel demonstrates normal blood vessel integrity from an EAE spinal cord tissue at the peak of acute disease, suggesting that overt loss of the endothelial architecture is not the cause of ZO-1 redistribution. Images are representative of at least three experiments with at least 3 animals per condition. Reprinted from Journal of Neuroimmunology, Bennett, J., Basivireddy, J., Kollar, A., Biron, K. E., Reickmann, P., Jefferies, W. A. and McQuaid, S., Blood-brain barrier disruption and enhanced vascular permeability in the multiple sclerosis model EAE, Copyright (2010), with permission from Elsevier [160].

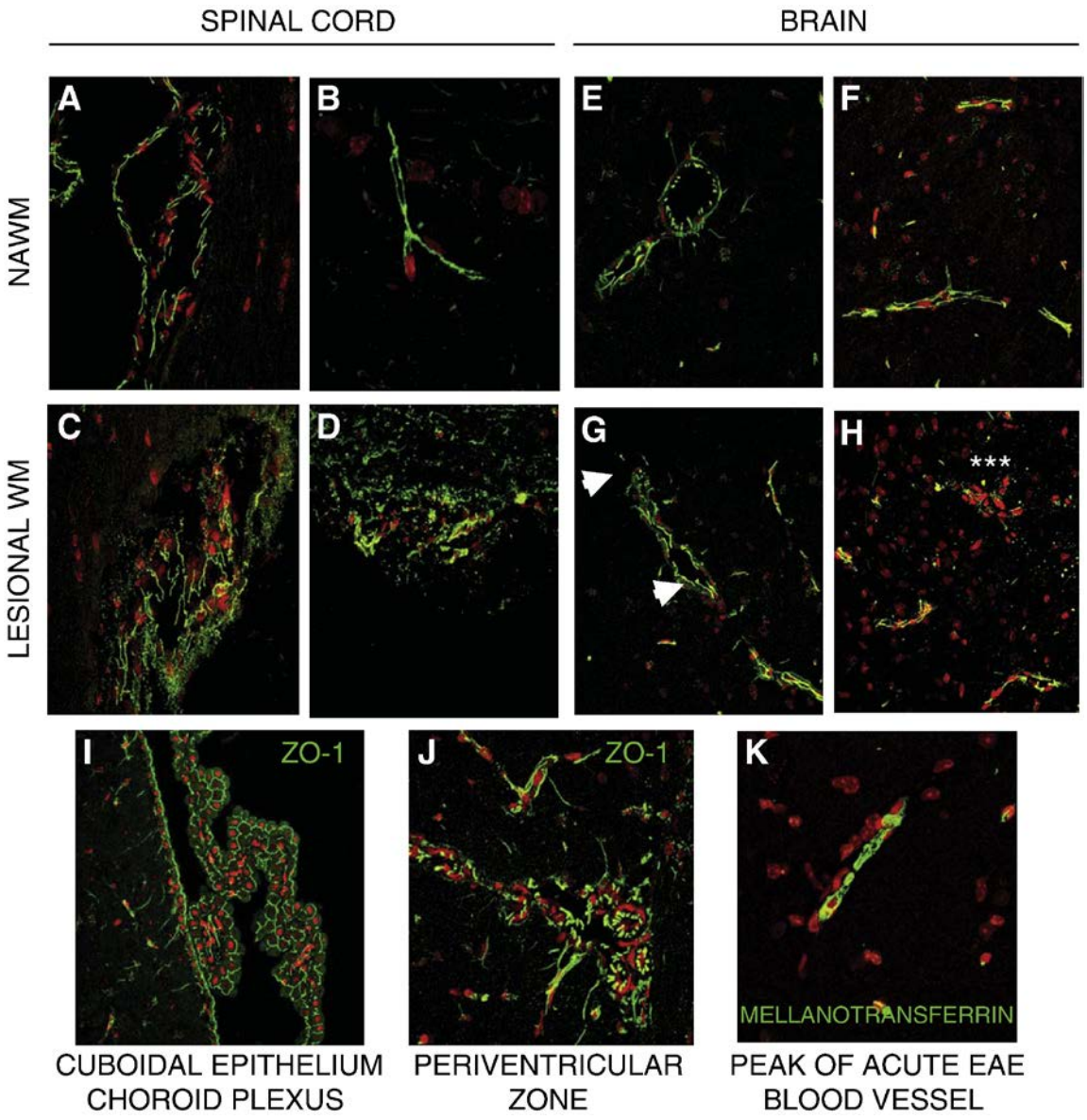
SPINAL CORD
BRAIN
NAWM
LESIONAL WM
A
B
E
F
C
D
G
H
***
I
ZO-1
J
ZO-1
K
MELLANOTRANSFERRIN
CUBOIDAL EPITHELIUM
CHOROID PLEXUS
PERIVENTRICULAR
ZONE
PEAK OF ACUTE EAE
BLOOD VESSEL

4.2.11 Disruption of ZO-1 in spinal cord vessels correlates with clinical and pathological EAE disease progression.

The incidence of vessel ZO-1 tight junction disruption was quantitated, by confocal microscopy, to correlate disruption with the clinical symptoms during the course of the EAE disease model. CNS tissues from EAE induced mice were harvested at the indicated time points after induction **Figure 4.14g**. Representative images of normal ZO-1 TJ expression in spinal cord white matter **Figure 4.14a, b and c** and lesional areas **Figure 4.14d, e and f** are shown. Abnormalities included interruption or beading, absence along the whole or part of the vessel, or reduced clarity of TJ bands with a tendency towards more diffuse intra-cytoplasmic staining. The average percentages ZO-1 disrupted blood vessels correlating with the EAE clinical stages **Figure 4.14g** and total vessels assessed **Figure 4.14h** are shown. To rule out the induction protocol directly affecting vascular TJ abnormality, control mice received no treatment (Naive), MOG35-55 peptide alone in IFCA (Peptide), CFA, or PTX alone. Naive tissues had a consistent low level ZO-1 disruptive staining in normal appearing, non-lesional tissue **Figure 4.14g (gray bars)**. Focal lesion formation was not observed after treatment with MOG35-55 peptide, CFA, or PTX alone. The controls had consistent baseline levels of ZO-1 disruption similar to the naive mice. In contrast, animals receiving the full EAE induction regimen began to form acute focal lesions by day 7 post-immunization, substantially earlier than overt clinical symptoms. Lesion site volume increased over time in parallel with clinical symptoms of disease from day 7 onward **Figure 4.14g (black bars)**. Normal and abnormal ZO-1 expression on vessels could be identified in the same focal lesion areas of tissue. However, a substantial increase in the percentage of vessels demonstrating TJ abnormality in lesion areas during clinical disease was seen. The percentage of abnormal

vessels associated with lesions peaked at an average of about 40%. At the peak of acute disease, when lesion sites and abnormal vessel TJs were most apparent, there was an increase in the percentage of abnormal vessels in non-lesion area tissue. Past the peak of disease, fewer vessels with abnormal ZO-1 expression in animals were noted. These results were originally described by Bennett *et al.* [160].

Figure 4.14: Disruption of ZO-1 in spinal cord vessels correlates with clinical and pathological EAE disease progression.
The incidence of ZO-1 tight junction abnormality in the vessels of EAE induced mice were compared quantitatively at various time points during disease progression. Confocal micrographs are representative of spinal cord blood vessels from EAE induced mice immunolabeled for ZO-1 (green) and counterstained for DNA (red) with propidium iodide. Images of normal ZO-1 expression in white matter (a, b and c) and lesion areas (d, e and f) are shown. Graph (g) depicts the percentage of tight junction abnormality, by ZO-1 expression patterns, in spinal cord blood vessels. Abnormal ZO-1 expression was quantified in normal appearing white matter (non-lesion areas, gray bars) and lesion area white matter (lesion areas, black bars) in each condition. The total numbers of vessels and mice examined in the data represented in the graph are also shown (h). Images are representative of at least three experiments with at least 3 animals per condition. Reprinted from Journal of Neuroimmunology, Bennett, J., Basivireddy, J., Kollar, A., Biron, K. E., Reickmann, P., Jefferies, W. A. and McQuaid, S., Blood-brain barrier disruption and enhanced vascular permeability in the multiple sclerosis model EAE, Copyright (2010), with permission from Elsevier [160].

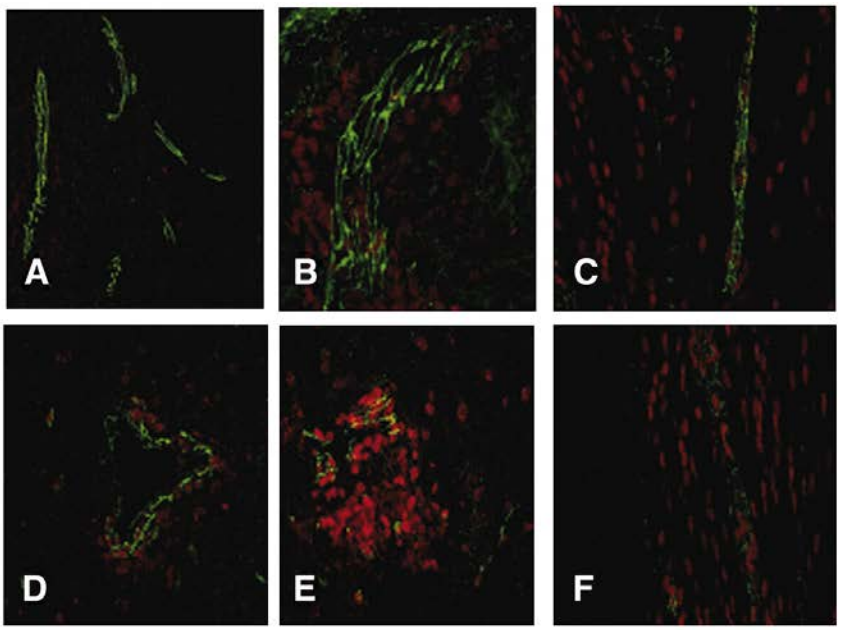

G

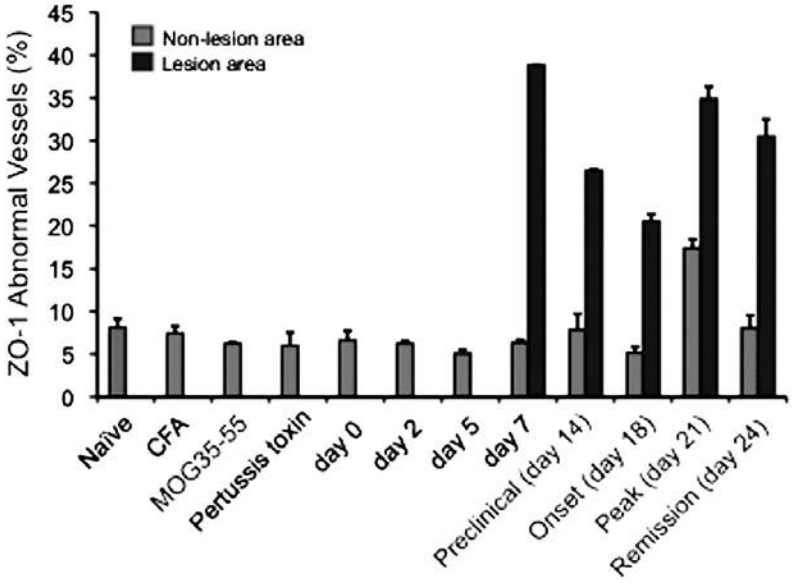

H

	Vessels examined	n
Naïve	86	2
CFA	149	3
Peptide	96	2
PTX	85	2
Day 0	106	2
Day 2	223	4
Day 5	215	4
Day 7	205	4
Pre-clinical	177	4
Onset	236	4
Peak	182	4
Remission	62	2

4.3 Discussion

Mice immunized with abeta, either preventatively and therapeutically, elicited an immune response to the peptide as measured through an increase in anti-abeta antibody titres [161]. Pathologically, these abeta immunized Tg2576 mice had significantly reduced plaque burdens and microgliosis [161]. These findings were consistent with previously published results using similar AD mice models and immunotherapy methods.

It was previously shown that the global integrity of the BBB improves significantly in post-abeta immunized Tg2576 mice [161]. The question addressed in this study was whether the improved BBB extend down to the level of the TJs. Abeta immunized Tg2576 mice were shown to have a markedly reduced TJ pathology in the microvasculature. The reduction in TJ pathology was seen in both the cortex and hippocampus, which are normally heavily affected during AD [96, 291]. Serum mouse albumin leakage from the microvessels of abeta immunized Tg2576 mice was minimal. However, increased mouse albumin leakage was noted in the larger vessels, which displayed TJ abnormalities and mild vascular deposition of abeta. Although mild vascular abeta deposition and serum leakage was qualitatively noted in this study, Wilcock *et al.* [264] (see **Table 4.2** for details) described significant increases in CAA and CAA-related microhemorrhaging in the passive immunization of the same AD mouse strain. This difference is most likely attributed to the age of the mice used in the respective vaccination studies. In the current study, mice immunized preventatively were sacrificed at one year. Mice immunized therapeutically were sacrificed at 15 months. Vascular deposition in the Tg2576 mouse is known to be fairly “intermediate” at 15 months [117].

The Tg2576 immunized mice in the Wilcock *et al.* [264] study were vaccinated beginning at 23 months of age, when CAA is known to be "widespread" [117]. Taken together, cerebrovasculature TJ disruption is directly related to the presence of abeta, whereby preventing the accumulation of abeta allows the microvasculature to repair any damage.

Several hypotheses have been proposed to explain the mechanism(s) of abeta immunotherapy. Briefly, the most popular mechanisms are microglial removal of abeta plaques, catalytic dissolution and the peripheral sink hypothesis. The mechanism of microglial removal of abeta has been summarized [292]. Briefly, peripheral circulating anti-abeta antibodies enter the brain and opsonize plaques. Microglia, the resident brain macrophages, removes plaques via Fc-receptor mediated phagocytosis. Catalytic dissolution involves peripheral circulating anti-abeta antibodies binding to and disrupting abeta aggregation by disrupting tertiary structure of the plaque [238]. The final mechanism is the peripheral sink hypothesis [259]. In this mechanism, circulating anti-abeta antibodies bind and sequester plasma abeta, which disrupts the equilibrium of abeta efflux-influx through the BBB. The net result is the removal of abeta from the brain. This mechanism has gained favour recently due to increased incidence of CAA and related microhemorrhages in human trials of abeta immunotherapy [279, 282-284]. CAA is an independent disease where abeta is deposited on vasculature resulting in the thickening of cerebral arteries and is described as a protein-elimination-failure arteriopathy [91]. Abeta that is removed from the brain as a result of immunotherapy is deposited in the arteries and thus exacerbates the observed immunotherapy related CAA [91]. It is debatable as to

which if any of these mechanisms plays a prominent role in abeta reduction or clearance. However, a combination of all three of the mechanisms is likely.

A side effect observed in the failed clinical abeta immunization trial was CAA-associated cerebral microhemorrhaging [285]. Several studies have noted microhemorrhaging in a variety of AD mouse models on the brain vasculature after active [257, 286, 287] and passive [262, 264, 267] immunization. Disruption of the cerebrovasculture TJs does explain this side effect in relation to the peripheral sink hypothesis. The following abeta removal model is proposed. Pre-immunization, the abundance of abeta influences the integrity of the BBB endothelia resulting in the disruption of the TJs. Microvascular leakage ensues. During immunization, various abeta clearance mechanisms are activated including microglia removal and antibody dissaggregation. As the abeta plaques are dissolved, solubilized abeta is removed from the brain parenchyma along perivascular drainage routes [91]. For unknown reasons, the perivascular drainage of abeta is halted and becomes deposited in the cerebral arteries, resulting in CAA. The primary abeta species found deposited in the CAA-affected vasculature is more soluble abeta1-40, believed to be of neuronal origin [293]. The deposition of abeta damages the surrounding endothelial TJs creating the observed microhemorrhages that could be mediated abeta induced ROS derived from NADPH-oxidase [294]. This model appears to be echoed in the failed human AD abeta immunization trial [285].

As of current, there are no published studies examining the effects of abeta immunotherapy on apoptosis in the brain. This study would be the first to characterize

apoptosis post-abeta immunization. Endothelial apoptosis, as measured by activated caspase-3 staining, was never visualized in any of the mice, via activated caspase-3 staining. All immunized mice, wild-type and Tg2576, had extensive activated caspse-3 staining in the hippocampus, which appeared to be neuronal-like. The presence of hippocampal activated caspase-3 in both wild-type and Tg2576 mice is consistent with a previous study [199]. However, PBS immunized Tg2576 had extensive neuronal-like activated caspase-3 throughout the cortex and hippocampus. Much of the caspase staining was centered on plaque associated TJ (specifically ZO-1) halos. Abeta immunized Tg2576, lacking plaque pathology, had caspase-3 staining within the hippocampus only. Although the exact nature of cell death that occurs during AD is still controversial, apoptosis is believed to play a significant role [193]. Furthermore, the Tg2576 mouse is not known to exhibit neuronal loss [122]. The presence of cortex activated caspse-3 in control treated Tg2576 mice suggests that increased signals for apoptosis are present, likely due to abeta. Once abeta is removed, it is presumed the apoptotic signals are reduced. However, whether activated caspase-3 expressing cells are actively undergoing apoptosis remains to be demonstrated [193].

Abeta immunization also appeared to modulate angiogenic signals in treated mice. Angiogenesis can be quantified through the average microvesicular staining densities of CD105 in the brain [214, 215]. The relative amount of angiogenesis was quantified by the MVD of CD105 staining. PBS treated Tg2576 mice, both preventatively and therapeutically, had significantly higher vascular densities compared to wild-type mice and abeta treated Tg2576 mice. This implies that angiogenic signals are reduced when

abeta is removed. It is presumed that neuroinflammation is reduced as a result of amyloid immunotherapy. As noted in this study microgliosis is reduced after active abeta immunotherapy. Microglia are believed to a significant source of neuroinflammation in neurodegenerative disease [295]. A reduction in both neuroinflammation and abeta may directly or indirectly reduce angiogenic signals associated with both [206, 207, 211]. Contrary to the current study, a passive immunization study using APP+PS1 mice examined neurogenesis related angiogenesis [296]. After passive immunization in the transgenic AD mice, angiogenesis was found to be increased in the hippocampus, by BrdU staining, which can label cells undergoing DNA repair [297] as opposed to angiogenic (replicating) vessels. One of the drawbacks of the current study was MVD was quantified globally in the mouse brain. It is possible that specific regions of brain could have higher incidents of angiogenesis.

Finally, atypical non-vascular TJ expression were found to be eliminated in abeta immunized Tg2576 mice. The atypical expression included dense-core plaque associated ZO-1 halos and occludin expression on a subset of astrocytes. Wild-type immunized mice lack abeta deposits and were devoid of the atypical TJ expression. Tg2576 mice receiving PBS injections did display the anomalies, which are mirrored in humans [228]. However, abeta immunized Tg2576 mice did not display the atypical TJ expression. The elimination abeta pathology appears to be directly connected to the presence of the atypical TJ expression in the brain. The observed astrocyte associated TJ expression correlated with S100β expression. The astrocyte marker S100β is a calcium binding protein that has numerous and complex autocrine, paracrine and endocrine effects [234].

In the context of AD, S100β has been shown to exacerbate inflammation, AD-like pathology and relating brain damage [235]. Although the TJ anomalies were not found on all S100β-positive astrocytes, they did associate mainly with astrocytes in the vicinity of abeta plaques. It could be speculated that inflammatory conditions present in plaque burden regions of the AD mouse brain could be responsible for the observed atypical non-vascular TJ expression.

Abeta immunotherapy is the most promising treatment option for AD. The unexpected negative vascular side effects seen in the early human clinical trials of the human AD vaccine demonstrate that our knowledge of abeta and AD pathogenesis is incomplete. This study demonstrated that in an active abeta immunization AD mouse model BBB TJ integrity is related to the presence of abeta. Removing abeta from the brain parenchyma eliminates the microvascular related TJ pathology. Furthermore, the observed CAA related microhemorrhaging in the human immunization trials can be explained by the loss of the TJs in the affected blood vessels. Clarifying the connection between the cerebrovasculature and AD will lead to improved therapeutic options for AD patients.

BBB pathology has been demonstrated in several diseases of the central nervous system (CNS). In order to address whether BBB pathology is evident as a common feature in other models of neurodegeneration a Multiple sclerosis (MS) [125] model was examined. Chronic inflammation of the CNS is a hallmark of MS that results in the demyelination of the nerves of the brain and spinal cord, reviewed by [142]. During the course of MS, BBB disruption leads to the leakage of T-cells, which may exacerbate neuroinflammation.

The T-cells destroy the cells that create myelin sheaths that wrap neurons. Oligodendrocytes are the cells that create myelin, a fatty substance that acts as electrically insulator when wrapped around neurons. Myelin sheaths help to increase the speed of the electrical impulses of neurons. Symptomatically, MS is complex and variable but are all related to the loss of function of the CNS nerve cells. The cause of MS is unknown and there is no cure. Experimental autoimmune encephalomyelitis (EAE) is an inducible rodent model of inflammation and MS [298]. Mice are immunized with a cocktail of mouse myelin proteins, adjuvant and pertussis toxin (to allow cell entry into the CNS). EAE afflicted mice develop characteristics of MS-like paralysis, inflammation, BBB disruption and T-cell infiltration into the brain.

Disruptions in the BBB have long been thought to be a key initiating factor in MS and EAE. ZO-1 TJ abnormalities in the CNS were examined in EAE mice in order to determine if inflammation influences MS disease pathology. Mice afflicted with EAE developed ZO-1 TJ disruption with similar pathology seen in the Tg2576 mice. TJ disruptions were closely associated with MS-like lesions in the EAE mice. The incidence of ZO-1 disruption in the EAE mice was quantified and correlated with the clinical symptoms during the course of EAE. TJ pathology was present several days prior to clinical symptoms onset and was significantly increased throughout the disease course. These data suggest that TJ pathology precedes clinical disease and correlates with symptomatic clinical signs in EAE. The data presented in this study demonstrate that lesion associated TJ pathology occurs in EAE to a similar degree as that seen in MS patients [143, 144, 299]. Although the cause of MS is unknown, this study supports the

role for pathogen-associated factors (in this case pertussis toxin) initiating and/or amplify neuroinflammation and BBB breakdown. Neuroinflammation is believed to influence BBB leakiness by directly acting on TJ organization through phosphorylatin or TJ degradation [300]. *In vitro*, TNFα and IFNγ, secreted by activated lymphocytes in MS, act in concert to decrease occludin promoter activity and mRNA expression in epithelial cells [301]. Taken together, the EAE model share MS-like BBB dysfunction allowing this model to be an ideal tool for future evaluation of TJ breakdown and repair in MS-like pathology. For example, Zamboni *et al.* [302] recently reported that chronic cerebrospinal insufficiency appears in all 65 clinically defined MS patients examined but is absent in 235 controls (including healthy patients and those with other neurological disorders). It was suggested that part of the disease process includes the jugular vein and the azygous vein blood vessels near the brain or spine becoming blocked, resulting in reflux and restricted blood flow. Distended blood vessels were also reported, suggesting the potential for greater vascular leakage. The Zamboni report has initiated widespread excitement, discussion and controversy among researchers, clinicians and patients, placing vascular aspects of disease directly in the spotlight of the MS community. The EAE model can provide for directly testing the relationship between blood flow, vascular permeability, TJ pathology and disease progression.

The data presented here demonstrates that TJ pathology is associated with two well studied models of neurodegeneration, AD and MS. Both of these debilitating diseases have dramatically different pathologies but do have neuroinflammation as commonality. The exact mechanism of TJ disruption resulting in BBB breakdown in the Tg2576 and

EAE mice remains to be clarified. Although the mechanisms of BBB breakdown are likely to be very different in both models the influence of neuroinflammation cannot ignored. Establishing a link between cerebrovascular abnormalities in both MS and AD will help to provide new therapeutic targets for BBB repair in both diseases.

Chapter 5: Blood Clotting and AD Mice

5.1 Rationale

A direct link between Alzheimer's disease (AD) and clotting abnormalities has never been shown; however, circumstantial evidence linking AD and clotting exists. Amyloid precursor protein (APP) has been shown to participate directly in blood coagulation cascade. Isoforms of APP contain a Kunitz protease inhibitor (KPI) domain [303]. This domain is a powerful inhibitor of several enzymes that induce the coagulation cascade [25-28]. APP isoforms expressing the KPI domain are known to have to cerebral anticoagulant properties *in vivo* [304, 305]. Outside of the brain, platelets are known to harbour the largest peripheral source of APP [306] and can process APP to produce abeta fragments [307]. The abeta peptide has been proposed to be a vascular sealant [308], from an observation that abeta plaques have been directly co-localized to sites of microhemorrhage within the blood-brain barrier (BBB) [309]. Removal of abeta by immunotherapy results in increased microhemorrhage [285]. *In vitro*, abeta has been shown to alter fibrin clot structures creating clots that are denser and more resistant to clot lysis [310]. Similar altered clot structure have also been reported in TgCRND8 AD mouse [184]. Furthermore, the *in vivo* studies reported lessened cerebral amyloid angiopathy (CAA) pathology and cognative decline in the mice when fibrinogen is depleted. Thus, a direct link is suggested between vascular abnormalities, blood hemostasis and AD.

As discussed in the previous chapters, vascular pathologies and diseases have been strongly linked to AD [311, 312]. Many of these vascular diseases have been additionally linked to increases in serum clotting factors and dementia [313]. Several patient studies have attempted to clarify if serum clotting and inflammatory factors are associated with AD and related dementias [314-316]. For example, tissue plasminogen activator (tPA), an enzyme involved in the breakdown of blood clots, has reduced activity [317]. Fibrinogen, which is converted into fibrin that makes up an actual blood clot, is elevated in human AD [318]. AD mouse models mirror the reduced tPA activity [319] and increased fibrinogen [179]. This suggests a potential hypercoagulable state in AD that could potentially influence cerebral blood and affect brain function. These studies support the hypothesis that abnormalities in hemostasis affect vascular-related dementias including AD. What has yet to be established is whether the abnormalities have any direct effect on the clotting mechanisms in AD. In the first step to clarify the relationship between clotting and AD, Tg2576 mice were characterized for potential defects in hematology and basic blood clotting mechanisms. The hypothesis for this study was the Tg2576 AD mouse model have an inherent blood clotting anomaly. Understanding the role that clotting mechanisms play in AD progression will broaden our limited understanding of the relationship between vascular abnormalities and AD.

5.2 Results

5.2.1 Hematologic analysis of Tg2576 mice

Aged, 12 months or older, Tg2576 mice were analyzed for various hematological parameters and compared to age-matched wild-type littermates. Summarized in **Figure 5.1**, the hematocrit, platelet counts, mean platelet volume, hemoglobin, mean cell volume, white and red blood cell counts in the Tg2576 mice were not statistically different from that of the wild-type.

Figure 5.1: Aged Tg2576 mice have normal hematology parameters.
Whole blood from aged, 12 months or older, Tg2576 (Tg/+) and age-matched wild-type (+/+) littermates were analyzed for various hematological parameters including (a) hemoglobin (gram per litre), (b) hematocrit (litres per litre), (c) mean cell volume (femtolitres), (d) mean platelet volume (femtolitres), (e) average platelet count, average (f) red blood cell and (g) white blood cell counts. +/+, n= 6; Tg/+, n = 7. Values represent mean ± SEM.

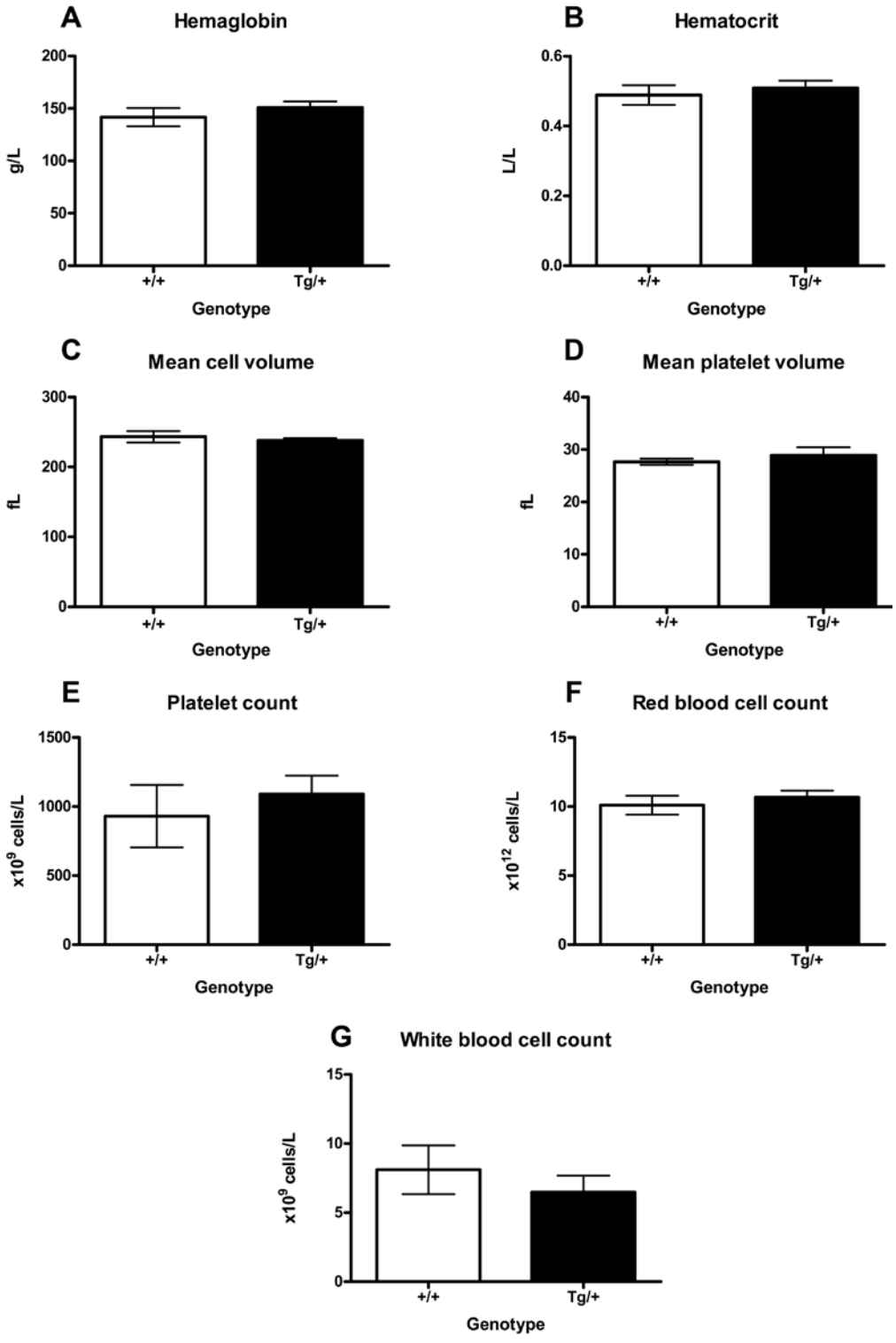
A
Hemaglobin
g/L
200
150
100
50
0
+/+
Tg/+
Genotype
B
Hematocrit
L/L
0.6
0.4
0.2
0.0
+/+
Tg/+
Genotype
C
Mean cell volume
fL
300
200
100
0
+/+
Tg/+
Genotype
D
Mean platelet volume
fL
40
30
20
10
0
+/+
Tg/+
Genotype
E
Platelet count
x10^9 cells/L
1500
1000
500
0
+/+
Tg/+
Genotype
F
Red blood cell count
x10^12 cells/L
15
10
5
0
+/+
Tg/+
Genotype
G
White blood cell count
x10^9 cells/L
15
10
5
0
+/+
Tg/+
Genotype

5.2.2 Clotting assays and Tg2576 mice

A tail bleed assay was performed to gauge the relative clotting status of aged Tg2576 mice, 12 months or older. The average whole blood clotting time of the Tg2576 mice (51.64 ± 3.95s; *p = 0.0067, t-test) was nearly a third faster then age matched wild-type (77.25 ± 4.11s) **Figure 5.2**. aPTT and PT clotting times are used to gauge the relative performance of the contact activation and the tissue factor clotting pathways, respectively. The aPTT **Figure 5.3a** and PT **Figure 5.3b** clotting times of the aged Tg2576 mice (averaging about 30s and 12s, respectively) was not significantly different to that of the wild-type.

Figure 5.2: Whole blood clotting times in aged Tg2576 mice clot faster than age-matched wild-type. A whole blood bleeding assay was performed by clipping tails from immobilized mice and measuring the time until the cessation of blood flow. Transgenic Tg2576 (Tg/+) mice had significantly faster (*p = 0.0067, t-test) clotting time compared to age-matched wild-type (+/+) littermates. Tg/+, n= 8; +/+, n = 11. Values represent mean ± SEM.

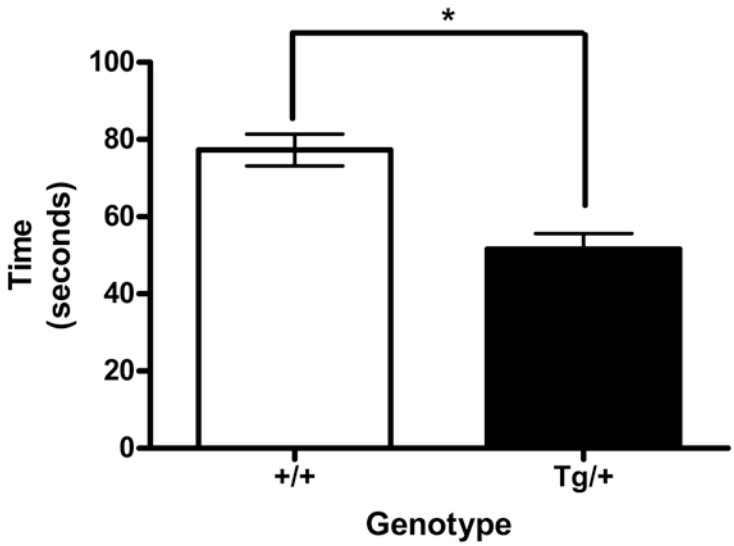

Figure 5.3: aPTT and PT clotting times in aged Tg2576 and age-matched wild-type mice appear to be normal.
aPTT and PT clotting times were measured on an automated coagulation analyzer from aged Tg2576 (Tg/+) and age-matched wild-type (+/+) mice. (a) aPTT (activated partial thromboplastin time) and (b) PT (prothrombin time) clotting times were not significantly different between transgenic and wild-type mice. Tg/+, n = 12; +/+, n = 12. Values represent mean ± SEM.

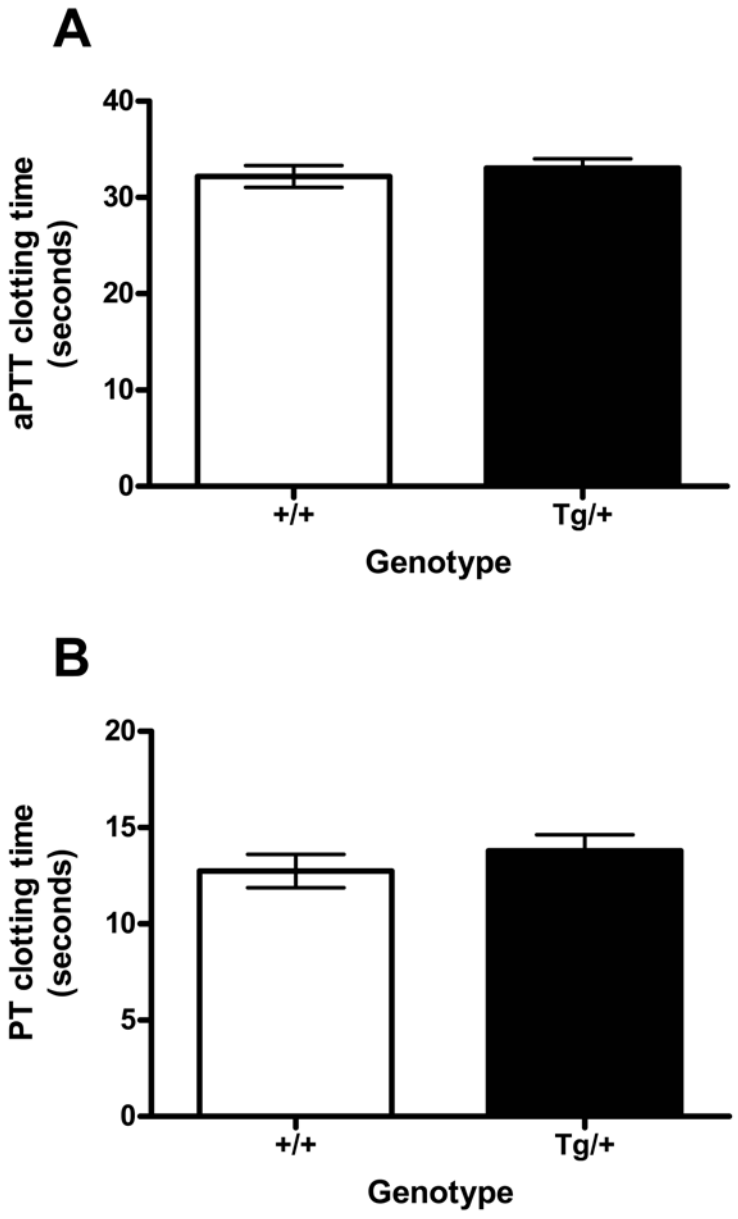

5.3 Discussion

It is believed that this is the first characterization of the hematology and blood clotting of the Tg2576 mouse. The hematology in aged Tg2576 mice was normal compared to age-matched wild-type littermates. Unexpectedly, aged Tg2576 mice were found to have a significantly faster whole blood clotting times compared to the control. This indicated that some form of a clotting abnormality does exist in this mouse. aPTT and PT clotting tests were used to narrow down the location of the abnormality in the coagulation cascade. aPTT and PT clotting times were found to be insignificant between the aged Tg2576 mouse and the wild-type. The aPTT and PT tests are overall performance indicators of the contact activation and tissue factor clotting pathways. The contact activation pathway is initiated when blood comes into contact with the negatively charged surfaces of the subendothelium. The tissue factor pathway is initiated when the blood is exposed to the cells expressing tissue factor in the subendothelium. Normal clotting times implies an overall normal performance of both pathways and hence entire coagulation cascade.

Although Tg2576 were seen to have a normal coagulation cascade, aberrant APP695 platelet expression or platelet-abeta interactions could explain the rapid whole blood clotting times. However, the Tg2576 mouse is unlikely to have a direct abnormality relating to APP on circulating platelets. The AD mouse overexpresses a mutant human variant of APP695 driven by a hamster prion promoter [96, 116]. There are three major isoforms of APP of varying lengths: 695, 751 and 770 amino acids long. APP695 is predominantly expressed in the brain [18] and does not have a KPI domain. APP751 and 770 are mainly found on platelets [22, 23]. Although hamster prion protein is strongly

expressed in the brain [320], other peripheral tissues have been noted [321, 322]. The overexpressed APP695 is unlikely to be expressed on mouse platelets as normal hamster prion expression was not localized to platelets [323, 324]. The observed clotting times are, therefore, most likely not explained by platelet APP expression.

Soluble plasma abeta is capable of inducing platelet aggregation and adhesion *in vitro* [325]. Abeta can activate and enhance platelet aggregation in a concentration dependent manner [326]. The Tg2576 mouse also has circulating soluble abeta [322], albeit at low levels as abeta is deposited within the brain. It is plausible that the Tg2576 mouse could have enhanced platelet activation and aggregation due to circulating abeta. To date there have been no studies that have examined abeta peptide and platelet function in any AD mouse model. Soluble abeta is also capable of interacting directly with fibrin and alter blood clot structure [184, 310]. The abeta-fibrin association has been shown to lead to inefficient clot lysis in the TgCRND8 AD mouse [184] which leads to occluded blood vessels. Furthermore, the abeta strengthen fibrin clot has been shown to clot faster in these mice. This was determined by quantifying the time taken to occlude the cerebral vasculature in the AD mice. Fibrinogen is elevated in the Tg2576 mouse [179] and therefore an altered abeta-fibrin interaction affecting blood clotting could be in effect here.

In a contradicting view to the involvement of abeta in clotting, a study examined the gain and loss of function of APP in cerebral thrombosis [327]. Engineered mice overexpressing APP770 (containing the KPI domain) in platelets were found to clot

slower than wild-type. These mice also had a severe incidence of cerebral hemorrhaging. These results can be readily explained by the APP KPI domain inhibiting clotting mechanism *in vivo*. In the loss of function experiment, APP knockout mice clotted faster than wild-type and had drastically reduced cerebral hemorrhaging. Homozygous APP knockout mice are viable and have no obvious phenotype [291]. Although it is entirely conjecture at this point, the involvement of abeta in clotting could be concentration dependent. Further study will yield important additional data linking clotting to AD pathology.

Chapter 6: Conclusions and Future Directions

AD is the most common form of dementia. According to the amyloid cascade hypothesis, abeta is central to the pathology of the disease. However, the exact mechanisms that link abeta to the various pathologies associated with AD are yet to be clarified. A strong relationship between the cerebral vasculature and AD neuropathology exists. The vascular link to AD has been shown to extend to the level of BBB where vascular dysfunction has been noted in both humans and various AD mouse models.

The overall goal of this thesis was to characterize the cause of the observed BBB dysfunction in AD using the Tg2576 mouse model. This was achieved by examining the morphology of the TJs in the brain vasculature of this mouse. Aged Tg2576 mice were noted to have TJ-related vascular pathologies, which were absent in the aged-matched controls and young mice. The observed brain vascular pathologies appeared to be linked to the presence of abeta. This argument was further strengthened by the fact that Tg2576 mice treated with abeta immunotherapy have reduced brain abeta levels [162, 258, 283]. Tg2576 mice actively immunized with abeta had normal TJ morphology in the capillary cerebral vasculature. However, the larger vessels in the abeta immunized Tg2576 mice displayed TJ pathology that appeared to be associated with vascular deposition of abeta. This unique pathology has never been extensively characterized *in vivo*.

The mechanism(s) for abeta immunotherapy are still debated. The work presented here suggests that the peripheral sink hypothesis is an important mechanism in the active abeta

immunization of Tg2576 mice. Active abeta immunization refers to the direct stimulation of host's immune system to produce antibodies by administered abeta. In contrast, passive abeta immunization refers to the administration of anti-abeta antibodies into the host, which bypasses the host's immune response to the antigen in question. Under normal physiological conditions, abeta is thought to be cleared from the brain by several mechanisms **Figure 6.1**. Abeta can be effluxed out of the brain parenchyma through the BBB into the blood by receptor-mediated transport [125]. In the brain parenchyma, abeta can be degraded by various catabolic enzymes [328]. Finally, perivascular lymphatic drainage mechanisms have been proposed to remove abeta out of the brain [91]. Drainage of the brain's interstitial fluid (containing solutes like abeta) occurs along the thin basement membrane structure found on the walls of capillaries that make up the BBB. The fluid eventually drains along the basement membrane of the connecting arteries and collects within the cervical lymph nodes of the neck. In AD, the drainage mechanisms have been suggested to be impaired [91] with age but for unknown reasons. During abeta immunotherapy, anti-abeta antibodies are thought to bind and sequester serum abeta, which is the key step in the peripheral sink hypothesis. The sequestration of abeta might reactivate impaired abeta catabolic and transport mechanisms, allowing for more efficient solubilization and removal of abeta. However, the perivascular drainage mechanisms are still impaired. As the concentration of soluble abeta increases, the drainage mechanisms become further clogged in the larger vessels. This would cause the observed increased incidence of CAA, and related microhemorrhages, in the human trials of abeta immunotherapy [279, 282-284].

Figure 6.1: Elimination of abeta from the brain.
Abeta is (i) produced by neurons and other cells in the brain and then (ii) diffuses with interstitial fluid and other solutes through the narrow extracellular spaces (ECS) of the brain to (iii) the bulk flow lymphatic drainage pathways in the basement membranes of capillaries and in the tunica media of artery walls and (iv) out of the brain to the cervical lymph nodes. Smooth muscle cells and perivascular macrophages take up abeta and are part of the elimination pathway. Degradation of abeta occurs in the brain parenchyma, by a variety of catabolic enzymes and abeta is absorbed into the blood by specific receptor-mediated transport proteins in capillary endothelia. These mechanisms for the elimination of abeta from the brain tend to fail with age and in AD. Alzheimer's Research and Therapy, 2009, with permission [91].

Elimination of Aβ from the brain

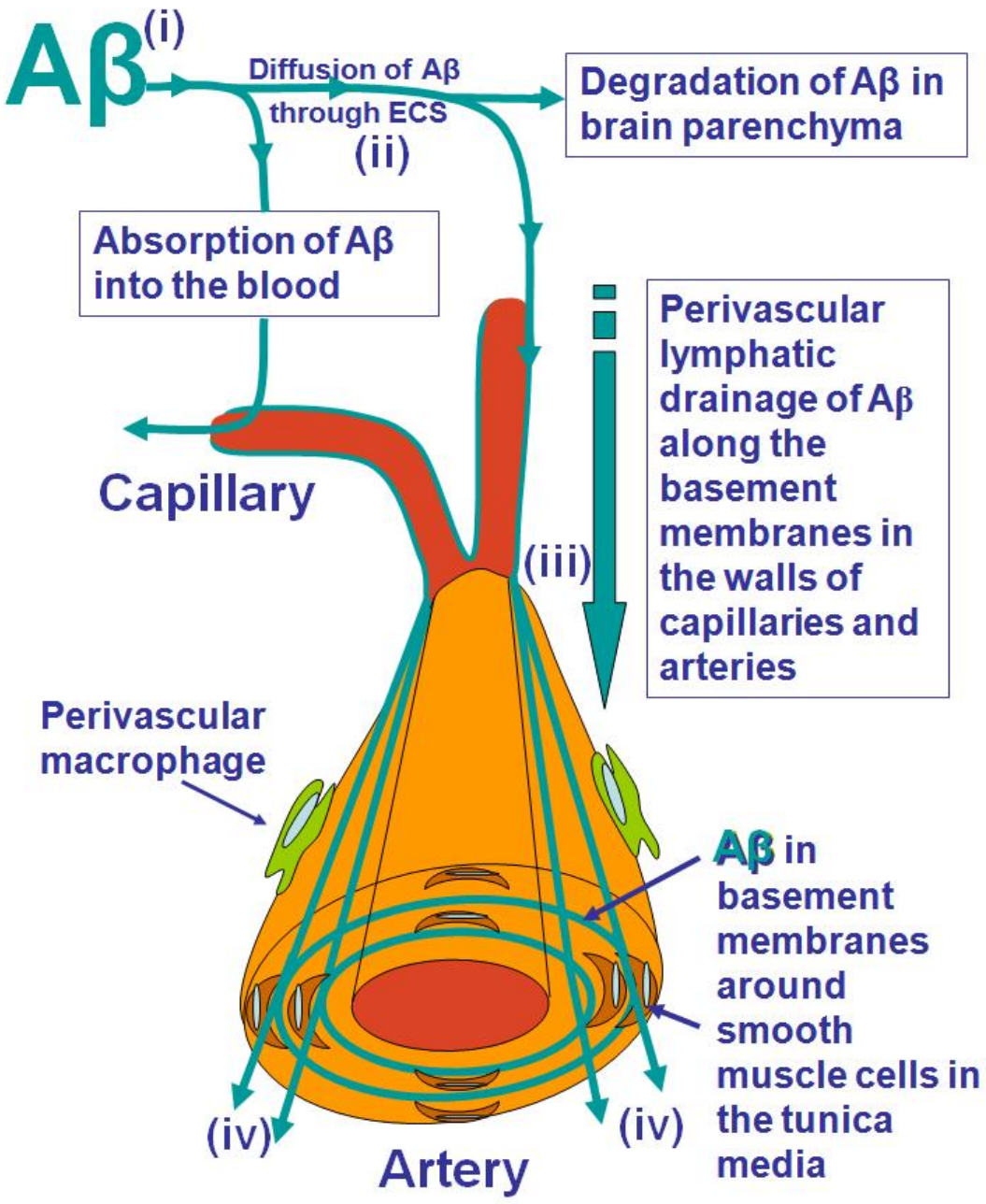

The present study supports the peripheral sink hypothesis in several ways. First, untreated Tg2576 mice develop abeta associated BBB dysfunction due to altered TJ morphology. This would disrupt normal abeta clearance receptor-mediated mechanisms and thus, the mice present disease pathology. Second, abeta active immunization restores BBB integrity as evidenced by normal TJ morphology, implying that BBB clearance of abeta is restored. Third, abeta immunized Tg2576 mice have reduced brain parenchymal and BBB associated abeta. However, larger cerebral blood vessels display TJ dysfunction, leakage and CAA, implying faulty and clogged perivascular drainage mechanisms.

Although a link between vascular pathology and AD exists, a thorough examination of the underlying molecular reasons has yet to be undertaken in human AD and the various AD mouse models. Specifically, studies clarifying how and where BBB leakage occurs at the molecular level would provide new insights into the relationship between AD and CAA. AD mice models known to have BBB dysfunction that could be assessed for brain vascular TJ pathology include the TgCRND8 [179], PDAPP [179] and a variant of the bigenic PSAPP [121] (Tg2576 x PS1M146L line 6.2) (refer to **Table 1.1** and **Table 1.2** for details). The above chosen mice have several disadvantages and advantages compared to Tg2576 mouse.

The TgCRND8, PDAPP and the bigenic PSAPP mice over-express mutant variants of human APP that favour abeta expression. Although the expression of APP is driven by different neuronal specific promoters, these mice are known to present with plaque pathology. With the exception of TgCRND8 that exhibits plaque pathology by three

months of age, the other mice display abeta related pathology at a similar onset age to the Tg2576 mice. Therefore, in the context of examining the effects of abeta plaque pathology on cerebral vasculature, the similar but different abeta over-expression properties of these mice can be compared to the Tg2576. However, the Tg2576, TgCRND8, PDAPP and the bigenic PSAPP don't express significant amounts of CAA-related pathology.

To determine the extent that CAA related vascular pathology influences the expression of TJs and the cerebral vasculature, the Tg-SwDI mice (**Table 1.2**) can be examined. These mice express a human APP variant containing the Swedish, Dutch and Iowa mutations driven by a mouse specific neuronal promoter. Therefore, the Swedish mutation favours abeta production [43] and the Dutch/Iowa mutations prevent clearance of the mutant abeta out of the brain across the BBB [104, 140, 329]. The resulting phenotype of the Tg-SwDI mouse is the presence of robust abeta deposition especially on the cerebral vasculature mimicking CAA-like pathology. With a three month age of abeta pathology onset, the Tg-SwDI could be another useful model to examine.

TJ pathology should also be examined in the various AD mouse immunotherapy (both active [257, 286] and passive [262, 264, 267, 272, 273, 330, 331]) models noted for increased microhemorrhages and various degrees CAA. Ultimately, a human TJ assessment should be performed to include brain tissues from various dementia related patients including AD, vascular dementia and Down's syndrome. This will help to

demonstrate how similar the animal models are in modeling cerebral vascular dysfunction in humans.

This thesis attempted to make to directly correlate abeta induced vascular leakage with presence of TJ abnormalities in the Tg2576 AD mice. The distribution of endogenous mouse albumin staining on the BBB failed to determine if the regions of the BBB that contain TJ abnormalities are sites of vascular leakage. However, evidence of occluded blood vessels was visualized. Future studies should include immunofluorescent staining to costain TJ markers with other markers of vascular leakage, like fibrinogen. Visualizing fluorescent Evans blue and carboxyfluorescein diacetate succinimidyl ester (CFDA-SE) extravasation, similar to the methods used by Ujiie *et al*. [170], with TJ markers via confocal microscopy could be another method.

Another unique vascular pathology noted in the Tg2576 mouse was the presence of obstructed blood vessels and increased microvascular density associated with angiogenesis. These vascular pathologies were absent post abeta immunization suggesting an abeta connection. The cause of the occluded vessels is unknown as is whether the occlusions are a direct or indirect result of angiogenesis. Neovascularization within the BBB could be examined in order to assess the functionality of the cerebral blood vessels. Fluorescent dextran injected *i.v.* into the Tg2576 mice (or any of the AD mouse models mentioned above) could be used to qualify and quantify BBB neovascularization and cerebral blood flow by confocal microscopy. Vascular deposition

of dextran would indicate if and where the cerebral blood vessels are functional. This would also determine the extent of the cerebral occlusions.

Epidemiological evidence suggests that females are at a higher risk for developing AD, however these findings are controversial (reviewed by [332]). Pathologically, female AD patients have been shown to have increased abeta load and distribution compared to male counterparts [333], suggesting a potential hormonal link with abeta pathogenesis. Biochemically, the declining levels of hormone estrogen during menopause has been proposed as a contributing factor. Hormone replacement therapy (HRT) has been investigated clinically in reducing the risks for and minimizing memory deficits in AD. The results of these studies seem to show minimal benefits to HRT (reviewed by [332]). Several AD mouse models have also been shown to have a positive correlation between gender and the degree of abeta pathogenesis including the Tg2576 mouse [334]. In the context of this thesis, gender effects were not investigated in relation to the observed BBB pathology. A future study could be designed to determine if BBB leakiness and TJ dysfunction in the Tg2576 and by extension in AD patients have any gender effects.

Atypical nonvascular associated TJ expression was noted on astrocytes in diseased Tg2576 mice. The atypical expression of ZO-1 was found to be associated with halo-like structures that encircled dense-core plaques. Rare atypical occludin expression was associated with S100β-positive astrocytes. These altered TJ staining patterns have not been previously described in any AD mouse model, but have been described in human AD brain tissues [228, 229]. Explanations for the atypical staining patterns for TJs in the

human brain studies have been vague. However, a novel hypothesis to explain the observations presented in this thesis is that the atypical nonvascular TJ expression on astrocytes could be apart of a glial scar. Astrocytes are critical for structural and metabolic support essential for proper functioning of the brain [335]. During CNS physical injury or disease (like MS), astrocytes can activately aggregate (along with other CNS cell types) to compartmentalize the local site of CNS damage, creating scar-like structure [230]. The glial scar has been proposed to be an important neuroprotective barrier-like structure in CNS repair formed responding, highly activated local astrocytes [230, 232]. Astrocytes in the glial scar are believed to form a mesh-like barrier structure compartmentalizing local damaged area and influence neurovascular remodeling to promote healing. Triggers for scar formation are broad but include physical trauma, infection, systemic inflammation and chronic neurodegeneration.

Although AD is not directly associated with glial scaring, astrocytes do become activated and participate in the inflammatory process during the disease [335]. Some researchers have proposed a “neuro-neglect” hypothesis where the supportive functions of astrocytes are compromised, which can exacerbate AD [335]. Either way, reactive astrocytes have been noted to surround abeta plaques suggesting that these cells may be attempting to create a neuroprotective barrier [232]. Do TJs play an active role in the formation of this neuroprotective glial scar barrier? Although there is no direct experimental evidence, a review by Fawcett and Asher [231] (subsequently mentioned by others [336, 337]) state that TJs are involved in this mechanism. To demonstrate the involvement of TJs in the glial scar, a series of confocal experiments could be performed. First, CNS tissues

bearing glial scaring, like MS and EAE tissues, can be stained and analyzed for TJ, astrocyte and glial scaring (phosphacan [338], neurocan [338] and tenascins [339]) markers. This would show that the TJ proteins are directly associated with glial scaring. Second, human AD, Tg2576 and brains from other AD mouse models could be analyzed for the presence of the same markers. This would give a broad assessment of atypical TJ expression and its association with glial scaring in AD and related tissues. Finally, a promising *in vitro* glial scarring model exists [340]. Briefly, primary astrocytes grown on flexible membranes are subjected to two separate stresses, either a gentle mechanical stretch or co-culture with meningeal cells. The stressed astrocytes have been shown to display glial scar morphology and expression glial scar markers. Again the same TJ, glial scaring and astrocyte markers can be used to analyze TJ expression in severely activated astrocytes.

Dysfunction in the BBB occurs during AD, which could influence cerebral blood flow during the disease [341, 342]. Interruptions in cerebral blood flow could, in turn, influence clotting mechanisms. Therefore, a preliminary examination of clotting abilities in the Tg2576 mouse was examined, which has previously remained uncharacterized. The aged Tg2576 mouse had normal hematology and normal aPTT and PT clotting times. This indicated that the general cellular quantities of the blood constituents and the basic biochemical pathways of the clotting cascade are normal in this mouse. Unexpectedly, whole blood was found to clot faster in the Tg2576 mouse compared to wild-type, suggesting that some anomalous coagulation aspect exists. It is possible that abeta may influence platelet biology to account for the rapid clotting anomaly. Several initial

experiments investigating abeta and platelet interaction in the Tg2576 mouse can be performed. Expression of human APP on circulating platelets in the Tg2576 mouse should be confirmed. This can be done by western blot for the human APP protein using a specific anti-human APP antibody on isolated circulating platelets. Abeta has been shown to enhance human platelet aggregation *in vitro* [325, 343]. The effect of abeta on Tg2576 and wild-type mice platelet aggregation can be examined using similar methods as described by the *in vitro* experiments. For example, the aggregative ability of isolated wild-type platelets in the presence of exogenous fibrillated abeta can be examined and compared to platelet agonists like collagen, ADP and thrombin. Isolated platelet rich plasma from Tg2576 mice could be depleted for soluble serum human abeta using specific antibodies for human abeta. The platelet aggregation of this sample could be assessed in comparison to replicates where exogenous fibrillated abeta is reintroduced. If successful, these studies could be replicated in other AD mouse models to help clarify the potential role of abeta, platelets and hemostasis in the biology of AD.

Strong evidence exists for cerebral microvascular damage occurring during AD. In the popular Tg2576 AD mouse model, the damage extends to the level of disrupted TJs. Alterations in the TJs of the BBB could have profound impacts on blood flow to the brain, clotting mechanisms within the BBB and ultimately brain function. Although the exact relationship between cerebral vascular dysfunction and AD remains to be clarified, this thesis does strength the connection. As the Western world ages, AD represents an ailment that will place a significant burden on all aspects of society. This burden, primarily placed on family caregivers, has been estimated to cost billions in lost productivity and

healthcare costs (both direct and indirect). Currently, there is a lack of understanding regarding the cause(s) of the disease that translates into a lack of a viable treatments or cures. However, researching the biology of the disease, including the prevalent risk factors, especially vascular ones that are believed to contribute to the disease, will provide new entry points for therapeutic intervention.

References

1. Association, T.A.s., *Changing the Trajectory of Alzheimer's Disease: A National Imperative*, 2010.
2. Reger, B. *Alzheimer's Disease: A Brief History and Avenues for Current Research*. The Journal of Young Investigators, 2002. **6**.
3. Graeber, M.B. *History of Neuroscience: Alois Alzheimer (1864-1915)*. IBRO History of Neuroscience 2003.
4. whonamedit.com. *Alois Alzheimer*. 2010 [cited 2010 May 17, 2010]; Available from: http://www.whonamedit.com/doctor.cfm/177.html/.
5. Kraepelin, E., *Klinische Psychiatrie*. Psychiatrie. Ein Lehrbuch für Studierende und Ärzte. Vol. II. 1910, Leipzig: Verlag Johann Ambrosius Barth.
6. Berrios, G.E., *Alzheimer's disease: A conceptual history.* International Journal of Geriatric Psychiatry, 1990. **5**(6): p. 355-365.
7. Grossman, H., C. Bergmann, and S. Parker, *Dementia: a brief review.* Mt Sinai J Med, 2006. **73**(7): p. 985-92.
8. Citron, M., *Alzheimer's disease: strategies for disease modification.* Nat Rev Drug Discov, 2010. **9**(5): p. 387-98.
9. Canada, A.S.o., *Rising Tide: The Impact of Dementia on Canadian Society*, 2009.
10. Zanetti, O., S.B. Solerte, and F. Cantoni, *Life expectancy in Alzheimer's disease (AD).* Arch Gerontol Geriatr, 2009. **49 Suppl 1**: p. 237-43.
11. Minati, L., et al., *Current concepts in Alzheimer's disease: a multidisciplinary review.* Am J Alzheimers Dis Other Demen, 2009. **24**(2): p. 95-121.
12. Mount, C. and C. Downton, *Alzheimer disease: progress or profit?* Nat Med, 2006. **12**(7): p. 780-4.
13. Gearing, M., et al., *The Consortium to Establish a Registry for Alzheimer's Disease (CERAD). Part X. Neuropathology confirmation of the clinical diagnosis of Alzheimer's disease.* Neurology, 1995. **45**(3 Pt 1): p. 461-6.
14. Alzheimer, A., *Über eine eigenartige Erkrankung der Hirnrinde.* Centralblatt für Nervenheilkunde und Psychiatrie 1907. **18**: p. 177-179.
15. Glenner, G.G. and C.W. Wong, *Alzheimer's disease: initial report of the purification and characterization of a novel cerebrovascular amyloid protein.* Biochem Biophys Res Commun, 1984. **120**(3): p. 885-90.
16. Masters, C.L., et al., *Amyloid plaque core protein in Alzheimer disease and Down syndrome.* Proc Natl Acad Sci U S A, 1985. **82**(12): p. 4245-9.
17. Glenner, G.G. and C.W. Wong, *Alzheimer's disease and Down's syndrome: sharing of a unique cerebrovascular amyloid fibril protein.* Biochem Biophys Res Commun, 1984. **122**(3): p. 1131-5.
18. Kang, J., et al., *The precursor of Alzheimer's disease amyloid A4 protein resembles a cell-surface receptor.* Nature, 1987. **325**(6106): p. 733-6.
19. Chow, V.W., et al., *An overview of APP processing enzymes and products.* Neuromolecular Med, 2010. **12**(1): p. 1-12.
20. De Strooper, B., R. Vassar, and T. Golde, *The secretases: enzymes with therapeutic potential in Alzheimer disease.* Nat Rev Neurol, 2010. **6**(2): p. 99-107.

21. Jacobsen, K.T. and K. Iverfeldt, *Amyloid precursor protein and its homologues: a family of proteolysis-dependent receptors.* Cell Mol Life Sci, 2009. **66**(14): p. 2299-318.
22. Bush, A.I., et al., *The amyloid precursor protein of Alzheimer's disease is released by human platelets.* J Biol Chem, 1990. **265**(26): p. 15977-83.
23. Li, Q.X., et al., *Proteolytic processing of Alzheimer's disease beta A4 amyloid precursor protein in human platelets.* J Biol Chem, 1995. **270**(23): p. 14140-7.
24. Dyrks, T., et al., *Identification, transmembrane orientation and biogenesis of the amyloid A4 precursor of Alzheimer's disease.* EMBO J, 1988. **7**(4): p. 949-57.
25. Van Nostrand, W.E., et al., *Immunopurification and protease inhibitory properties of protease nexin-2/amyloid beta-protein precursor.* J Biol Chem, 1990. **265**(17): p. 9591-4.
26. Smith, R.P., D.A. Higuchi, and G.J. Broze, Jr., *Platelet coagulation factor XIa-inhibitor, a form of Alzheimer amyloid precursor protein.* Science, 1990. **248**(4959): p. 1126-8.
27. Schmaier, A.H., et al., *Protease nexin-2/amyloid beta protein precursor. A tight-binding inhibitor of coagulation factor IXa.* J Clin Invest, 1993. **92**(5): p. 2540-5.
28. Mahdi, F., W.E. Van Nostrand, and A.H. Schmaier, *Protease nexin-2/amyloid beta-protein precursor inhibits factor Xa in the prothrombinase complex.* J Biol Chem, 1995. **270**(40): p. 23468-74.
29. Wasco, W., et al., *Identification of a mouse brain cDNA that encodes a protein related to the Alzheimer disease-associated amyloid beta protein precursor.* Proc Natl Acad Sci U S A, 1992. **89**(22): p. 10758-62.
30. Wasco, W., et al., *Isolation and characterization of APLP2 encoding a homologue of the Alzheimer's associated amyloid beta protein precursor.* Nat Genet, 1993. **5**(1): p. 95-100.
31. Hiltunen, M., T. van Groen, and J. Jolkkonen, *Functional roles of amyloid-beta protein precursor and amyloid-beta peptides: evidence from experimental studies.* J Alzheimers Dis, 2009. **18**(2): p. 401-12.
32. Mattson, M.P., et al., *Evidence for excitoprotective and intraneuronal calcium-regulating roles for secreted forms of the beta-amyloid precursor protein.* Neuron, 1993. **10**(2): p. 243-54.
33. Ring, S., et al., *The secreted beta-amyloid precursor protein ectodomain APPs alpha is sufficient to rescue the anatomical, behavioral, and electrophysiological abnormalities of APP-deficient mice.* J Neurosci, 2007. **27**(29): p. 7817-26.
34. Herms, J., et al., *Cortical dysplasia resembling human type 2 lissencephaly in mice lacking all three APP family members.* EMBO J, 2004. **23**(20): p. 4106-15.
35. Haass, C., et al., *Amyloid beta-peptide is produced by cultured cells during normal metabolism.* Nature, 1992. **359**(6393): p. 322-5.
36. Seubert, P., et al., *Isolation and quantification of soluble Alzheimer's beta-peptide from biological fluids.* Nature, 1992. **359**(6393): p. 325-7.
37. Shoji, M., et al., *Production of the Alzheimer amyloid beta protein by normal proteolytic processing.* Science, 1992. **258**(5079): p. 126-9.
38. Thinakaran, G. and E.H. Koo, *Amyloid precursor protein trafficking, processing, and function.* J Biol Chem, 2008. **283**(44): p. 29615-9.

39. Haass, C. and B. De Strooper, *The presenilins in Alzheimer's disease--proteolysis holds the key.* Science, 1999. **286**(5441): p. 916-9.
40. Van Broeck, B., C. Van Broeckhoven, and S. Kumar-Singh, *Current insights into molecular mechanisms of Alzheimer disease and their implications for therapeutic approaches.* Neurodegener Dis, 2007. **4**(5): p. 349-65.
41. Citron, M., et al., *Mutation of the beta-amyloid precursor protein in familial Alzheimer's disease increases beta-protein production.* Nature, 1992. **360**(6405): p. 672-4.
42. Cai, X.D., T.E. Golde, and S.G. Younkin, *Release of excess amyloid beta protein from a mutant amyloid beta protein precursor.* Science, 1993. **259**(5094): p. 514-6.
43. Haass, C., et al., *The Swedish mutation causes early-onset Alzheimer's disease by beta-secretase cleavage within the secretory pathway.* Nat Med, 1995. **1**(12): p. 1291-6.
44. Harrison, R.S., et al., *Amyloid peptides and proteins in review.* Rev Physiol Biochem Pharmacol, 2007. **159**: p. 1-77.
45. Jarrett, J.T., E.P. Berger, and P.T. Lansbury, Jr., *The carboxy terminus of the beta amyloid protein is critical for the seeding of amyloid formation: implications for the pathogenesis of Alzheimer's disease.* Biochemistry, 1993. **32**(18): p. 4693-7.
46. Roher, A.E., et al., *beta-Amyloid-(1-42) is a major component of cerebrovascular amyloid deposits: implications for the pathology of Alzheimer disease.* Proc Natl Acad Sci U S A, 1993. **90**(22): p. 10836-40.
47. Iwatsubo, T., et al., *Visualization of A beta 42(43) and A beta 40 in senile plaques with end-specific A beta monoclonals: evidence that an initially deposited species is A beta 42(43).* Neuron, 1994. **13**(1): p. 45-53.
48. Sakono, M. and T. Zako, *Amyloid oligomers: formation and toxicity of Abeta oligomers.* FEBS J, 2010. **277**(6): p. 1348-58.
49. Robert D. Terry, E.M., Lawrence A. Hansen, *The neuropathology of Alzheimer disease and the structural basis of its cognitive alterations,* in *Alzheimer disease,* R.D. Terry, Editor 1999, Lippincott Williams & Wilkins: Philadelphia. p. 187–206.
50. Lambert, M.P., et al., *Diffusible, nonfibrillar ligands derived from Abeta1-42 are potent central nervous system neurotoxins.* Proc Natl Acad Sci U S A, 1998. **95**(11): p. 6448-53.
51. Lesne, S., et al., *A specific amyloid-beta protein assembly in the brain impairs memory.* Nature, 2006. **440**(7082): p. 352-7.
52. Walsh, D.M., et al., *Naturally secreted oligomers of amyloid beta protein potently inhibit hippocampal long-term potentiation in vivo.* Nature, 2002. **416**(6880): p. 535-9.
53. Wang, H.W., et al., *Soluble oligomers of beta amyloid (1-42) inhibit long-term potentiation but not long-term depression in rat dentate gyrus.* Brain Res, 2002. **924**(2): p. 133-40.
54. Selkoe, D.J., *The molecular pathology of Alzheimer's disease.* Neuron, 1991. **6**(4): p. 487-98.
55. Hardy, J.A. and G.A. Higgins, *Alzheimer's disease: the amyloid cascade hypothesis.* Science, 1992. **256**(5054): p. 184-5.

56. Pimplikar, S.W., *Reassessing the amyloid cascade hypothesis of Alzheimer's disease.* Int J Biochem Cell Biol, 2009. **41**(6): p. 1261-8.
57. Philipson, O., et al., *Animal models of amyloid-beta-related pathologies in Alzheimer's disease.* FEBS J, 2010. **277**(6): p. 1389-409.
58. Hardy, J., *The amyloid hypothesis for Alzheimer's disease: a critical reappraisal.* J Neurochem, 2009. **110**(4): p. 1129-34.
59. Halliwell, B., *Oxidative stress and neurodegeneration: where are we now?* J Neurochem, 2006. **97**(6): p. 1634-58.
60. Sies, H., *Oxidative stress: oxidants and antioxidants.* Exp Physiol, 1997. **82**(2): p. 291-5.
61. Bokov, A., A. Chaudhuri, and A. Richardson, *The role of oxidative damage and stress in aging.* Mech Ageing Dev, 2004. **125**(10-11): p. 811-26.
62. Bennett, S., M.M. Grant, and S. Aldred, *Oxidative stress in vascular dementia and Alzheimer's disease: a common pathology.* J Alzheimers Dis, 2009. **17**(2): p. 245-57.
63. McNaull, B.B., et al., *Inflammation and anti-inflammatory strategies for Alzheimer's disease--a mini-review.* Gerontology, 2010. **56**(1): p. 3-14.
64. Cameron, B. and G.E. Landreth, *Inflammation, microglia, and Alzheimer's disease.* Neurobiol Dis, 2010. **37**(3): p. 503-9.
65. McGeer, P.L. and E.G. McGeer, *NSAIDs and Alzheimer disease: epidemiological, animal model and clinical studies.* Neurobiol Aging, 2007. **28**(5): p. 639-47.
66. Farina, C., F. Aloisi, and E. Meinl, *Astrocytes are active players in cerebral innate immunity.* Trends Immunol, 2007. **28**(3): p. 138-45.
67. Pihlaja, R., et al., *Transplanted astrocytes internalize deposited beta-amyloid peptides in a transgenic mouse model of Alzheimer's disease.* Glia, 2008. **56**(2): p. 154-63.
68. Schwab, C. and P.L. McGeer, *Inflammatory aspects of Alzheimer disease and other neurodegenerative disorders.* J Alzheimers Dis, 2008. **13**(4): p. 359-69.
69. Rogers, J., et al., *Complement activation by beta-amyloid in Alzheimer disease.* Proc Natl Acad Sci U S A, 1992. **89**(21): p. 10016-20.
70. Ballatore, C., V.M. Lee, and J.Q. Trojanowski, *Tau-mediated neurodegeneration in Alzheimer's disease and related disorders.* Nat Rev Neurosci, 2007. **8**(9): p. 663-72.
71. St George-Hyslop, P.H., *Genetic factors in the genesis of Alzheimer's disease.* Ann N Y Acad Sci, 2000. **924**: p. 1-7.
72. Bird, T.D., *Genetic aspects of Alzheimer disease.* Genet Med, 2008. **10**(4): p. 231-9.
73. Kim, J., J.M. Basak, and D.M. Holtzman, *The role of apolipoprotein E in Alzheimer's disease.* Neuron, 2009. **63**(3): p. 287-303.
74. Pitas, R.E., et al., *Lipoproteins and their receptors in the central nervous system. Characterization of the lipoproteins in cerebrospinal fluid and identification of apolipoprotein B,E(LDL) receptors in the brain.* J Biol Chem, 1987. **262**(29): p. 14352-60.
75. Pfrieger, F.W., *Cholesterol homeostasis and function in neurons of the central nervous system.* Cell Mol Life Sci, 2003. **60**(6): p. 1158-71.

76. Nickerson, D.A., et al., *Sequence diversity and large-scale typing of SNPs in the human apolipoprotein E gene.* Genome Res, 2000. **10**(10): p. 1532-45.
77. Roses, A.D., *Apolipoprotein E alleles as risk factors in Alzheimer's disease.* Annu Rev Med, 1996. **47**: p. 387-400.
78. Tokuda, T., et al., *Lipidation of apolipoprotein E influences its isoform-specific interaction with Alzheimer's amyloid beta peptides.* Biochem J, 2000. **348 Pt 2**: p. 359-65.
79. Ma, J., et al., *Amyloid-associated proteins alpha 1-antichymotrypsin and apolipoprotein E promote assembly of Alzheimer beta-protein into filaments.* Nature, 1994. **372**(6501): p. 92-4.
80. Cam, J.A. and G. Bu, *Modulation of beta-amyloid precursor protein trafficking and processing by the low density lipoprotein receptor family.* Mol Neurodegener, 2006. **1**: p. 8.
81. Sagare, A., et al., *Clearance of amyloid-beta by circulating lipoprotein receptors.* Nat Med, 2007. **13**(9): p. 1029-31.
82. Forstl, H. and R. Howard, *Recent studies on dementia senilis and brain disorders caused by atheromatous vascular disease: by A. Alzheimer, 1898.* Alzheimer Dis Assoc Disord, 1991. **5**(4): p. 257-64.
83. de la Torre, J.C., *How do heart disease and stroke become risk factors for Alzheimer's disease?* Neurol Res, 2006. **28**(6): p. 637-44.
84. Duron, E. and O. Hanon, *Vascular risk factors, cognitive decline, and dementia.* Vasc Health Risk Manag, 2008. **4**(2): p. 363-81.
85. Dickstein, D.L., et al., *Role of vascular risk factors and vascular dysfunction in Alzheimer's disease.* Mt Sinai J Med, 2010. **77**(1): p. 82-102.
86. Johnson, V.E., W. Stewart, and D.H. Smith, *Traumatic brain injury and amyloid-beta pathology: a link to Alzheimer's disease?* Nat Rev Neurosci, 2010.
87. Guskiewicz, K.M., et al., *Association between recurrent concussion and late-life cognitive impairment in retired professional football players.* Neurosurgery, 2005. **57**(4): p. 719-26; discussion 719-26.
88. Roberts, G.W., et al., *Beta amyloid protein deposition in the brain after severe head injury: implications for the pathogenesis of Alzheimer's disease.* J Neurol Neurosurg Psychiatry, 1994. **57**(4): p. 419-25.
89. Eichner, J.E., et al., *Apolipoprotein E polymorphism and cardiovascular disease: a HuGE review.* Am J Epidemiol, 2002. **155**(6): p. 487-95.
90. Love, S., et al., *Insights into the pathogenesis and pathogenicity of cerebral amyloid angiopathy.* Front Biosci, 2009. **14**: p. 4778-92.
91. Weller, R.O., et al., *Cerebral amyloid angiopathy in the aetiology and immunotherapy of Alzheimer disease.* Alzheimers Res Ther, 2009. **1**(2): p. 6.
92. de Toledo Ferraz Alves, T.C., et al., *Cardiac disorders as risk factors for Alzheimer's disease.* J Alzheimers Dis, 2010. **20**(3): p. 749-63.
93. McGowan, E., et al., *Abeta42 is essential for parenchymal and vascular amyloid deposition in mice.* Neuron, 2005. **47**(2): p. 191-9.
94. Games, D., et al., *Alzheimer-type neuropathology in transgenic mice overexpressing V717F beta-amyloid precursor protein.* Nature, 1995. **373**(6514): p. 523-7.

95. Moechars, D., et al., *Early phenotypic changes in transgenic mice that overexpress different mutants of amyloid precursor protein in brain.* J Biol Chem, 1999. **274**(10): p. 6483-92.
96. Hsiao, K., et al., *Correlative memory deficits, Abeta elevation, and amyloid plaques in transgenic mice.* Science, 1996. **274**(5284): p. 99-102.
97. Reaume, A.G., et al., *Enhanced amyloidogenic processing of the beta-amyloid precursor protein in gene-targeted mice bearing the Swedish familial Alzheimer's disease mutations and a "humanized" Abeta sequence.* J Biol Chem, 1996. **271**(38): p. 23380-8.
98. Flood, D.G., et al., *FAD mutant PS-1 gene-targeted mice: increased A beta 42 and A beta deposition without APP overproduction.* Neurobiol Aging, 2002. **23**(3): p. 335-48.
99. Borchelt, D.R., et al., *Familial Alzheimer's disease-linked presenilin 1 variants elevate Abeta1-42/1-40 ratio in vitro and in vivo.* Neuron, 1996. **17**(5): p. 1005-13.
100. Lamb, B.T., et al., *Amyloid production and deposition in mutant amyloid precursor protein and presenilin-1 yeast artificial chromosome transgenic mice.* Nat Neurosci, 1999. **2**(8): p. 695-7.
101. Sturchler-Pierrat, C., et al., *Two amyloid precursor protein transgenic mouse models with Alzheimer disease-like pathology.* Proc Natl Acad Sci U S A, 1997. **94**(24): p. 13287-92.
102. Chishti, M.A., et al., *Early-onset amyloid deposition and cognitive deficits in transgenic mice expressing a double mutant form of amyloid precursor protein 695.* J Biol Chem, 2001. **276**(24): p. 21562-70.
103. Herzig, M.C., et al., *Abeta is targeted to the vasculature in a mouse model of hereditary cerebral hemorrhage with amyloidosis.* Nat Neurosci, 2004. **7**(9): p. 954-60.
104. Davis, J., et al., *Early-onset and robust cerebral microvascular accumulation of amyloid beta-protein in transgenic mice expressing low levels of a vasculotropic Dutch/Iowa mutant form of amyloid beta-protein precursor.* J Biol Chem, 2004. **279**(19): p. 20296-306.
105. Lord, A., et al., *The Arctic Alzheimer mutation facilitates early intraneuronal Abeta aggregation and senile plaque formation in transgenic mice.* Neurobiol Aging, 2006. **27**(1): p. 67-77.
106. McQuail, J.A., D.R. Riddle, and M.M. Nicolle, *Neuroinflammation not associated with cholinergic degeneration in aged-impaired brain.* Neurobiol Aging, 2010.
107. Holcomb, L., et al., *Accelerated Alzheimer-type phenotype in transgenic mice carrying both mutant amyloid precursor protein and presenilin 1 transgenes.* Nat Med, 1998. **4**(1): p. 97-100.
108. Oddo, S., et al., *Triple-transgenic model of Alzheimer's disease with plaques and tangles: intracellular Abeta and synaptic dysfunction.* Neuron, 2003. **39**(3): p. 409-21.
109. Oakley, H., et al., *Intraneuronal beta-amyloid aggregates, neurodegeneration, and neuron loss in transgenic mice with five familial Alzheimer's disease mutations: potential factors in amyloid plaque formation.* J Neurosci, 2006. **26**(40): p. 10129-40.

110. Casas, C., et al., *Massive CA1/2 neuronal loss with intraneuronal and N-terminal truncated Abeta42 accumulation in a novel Alzheimer transgenic model.* Am J Pathol, 2004. **165**(4): p. 1289-300.
111. Wirths, O., et al., *Intraneuronal pyroglutamate-Abeta 3-42 triggers neurodegeneration and lethal neurological deficits in a transgenic mouse model.* Acta Neuropathol, 2009. **118**(4): p. 487-96.
112. Mullan, M., et al., *A pathogenic mutation for probable Alzheimer's disease in the APP gene at the N-terminus of beta-amyloid.* Nat Genet, 1992. **1**(5): p. 345-7.
113. Vassar, R., et al., *Beta-secretase cleavage of Alzheimer's amyloid precursor protein by the transmembrane aspartic protease BACE.* Science, 1999. **286**(5440): p. 735-41.
114. Van Dam, D., et al., *Age-dependent cognitive decline in the APP23 model precedes amyloid deposition.* Eur J Neurosci, 2003. **17**(2): p. 388-96.
115. Winkler, D.T., et al., *Spontaneous hemorrhagic stroke in a mouse model of cerebral amyloid angiopathy.* J Neurosci, 2001. **21**(5): p. 1619-27.
116. Hsiao, K.K., et al., *Age-related CNS disorder and early death in transgenic FVB/N mice overexpressing Alzheimer amyloid precursor proteins.* Neuron, 1995. **15**(5): p. 1203-18.
117. Domnitz, S.B., et al., *Progression of cerebral amyloid angiopathy in transgenic mouse models of Alzheimer disease.* J Neuropathol Exp Neurol, 2005. **64**(7): p. 588-94.
118. Ujiie, M., et al., *Blood-brain barrier permeability precedes senile plaque formation in an Alzheimer disease model.* Microcirculation, 2003. **10**: p. 463-70.
119. Dickstein, D.L., et al., *A{beta} peptide immunization restores blood-brain barrier integrity in Alzheimer disease.* Faseb J, 2006. **20**(3): p. 426-33.
120. Lee, E.B., et al., *Meningoencephalitis associated with passive immunization of a transgenic murine model of Alzheimer's amyloidosis.* FEBS Lett, 2005. **579**(12): p. 2564-8.
121. Kumar-Singh, S., et al., *Dense-core plaques in Tg2576 and PSAPP mouse models of Alzheimer's disease are centered on vessel walls.* Am J Pathol, 2005. **167**(2): p. 527-43.
122. Irizarry, M.C., et al., *APPSw transgenic mice develop age-related A beta deposits and neuropil abnormalities, but no neuronal loss in CA1.* J Neuropathol Exp Neurol, 1997. **56**(9): p. 965-73.
123. Frautschy, S.A., et al., *Microglial response to amyloid plaques in APPsw transgenic mice.* Am J Pathol, 1998. **152**(1): p. 307-17.
124. Pappolla, M.A., et al., *Evidence of oxidative stress and in vivo neurotoxicity of beta-amyloid in a transgenic mouse model of Alzheimer's disease: a chronic oxidative paradigm for testing antioxidant therapies in vivo.* Am J Pathol, 1998. **152**(4): p. 871-7.
125. Zlokovic, B.V., *The blood-brain barrier in health and chronic neurodegenerative disorders.* Neuron, 2008. **57**(2): p. 178-201.
126. Begley, D.J. and M.W. Brightman, *Structural and functional aspects of the blood-brain barrier.* Prog Drug Res, 2003. **61**: p. 39-78.
127. Cecchelli, R., et al., *Modelling of the blood-brain barrier in drug discovery and development.* Nat Rev Drug Discov, 2007. **6**(8): p. 650-61.

128. Abbott, N.J., et al., *Structure and function of the blood-brain barrier.* Neurobiol Dis, 2010. **37**(1): p. 13-25.
129. Simard, M., et al., *Signaling at the gliovascular interface.* J Neurosci, 2003. **23**(27): p. 9254-62.
130. Armulik, A., et al., *Pericytes regulate the blood-brain barrier.* Nature, 2010. **468**(7323): p. 557-61.
131. Abbott, N.J., L. Ronnback, and E. Hansson, *Astrocyte-endothelial interactions at the blood-brain barrier.* Nat Rev Neurosci, 2006. **7**(1): p. 41-53.
132. Engelhardt, B. and L. Sorokin, *The blood-brain and the blood-cerebrospinal fluid barriers: function and dysfunction.* Semin Immunopathol, 2009. **31**(4): p. 497-511.
133. Forster, C., *Tight junctions and the modulation of barrier function in disease.* Histochem Cell Biol, 2008. **130**(1): p. 55-70.
134. Terry, S., et al., *Rho signaling and tight junction functions.* Physiology (Bethesda), 2010. **25**(1): p. 16-26.
135. Bowman, G.L. and J.F. Quinn, *Alzheimer's disease and the blood-brain barrier: past, present and future.* Aging Health, 2008. **4**(1): p. 47-57.
136. Farrall, A.J. and J.M. Wardlaw, *Blood-brain barrier: ageing and microvascular disease - systematic review and meta-analysis.* Neurobiol Aging, 2009. **30**(3): p. 337-52.
137. Simpson, I.A., et al., *Decreased concentrations of GLUT1 and GLUT3 glucose transporters in the brains of patients with Alzheimer's disease.* Ann Neurol, 1994. **35**(5): p. 546-51.
138. Mooradian, A.D., H.C. Chung, and G.N. Shah, *GLUT-1 expression in the cerebra of patients with Alzheimer's disease.* Neurobiol Aging, 1997. **18**(5): p. 469-74.
139. Deane, R., et al., *RAGE mediates amyloid-beta peptide transport across the blood-brain barrier and accumulation in brain.* Nat Med, 2003. **9**(7): p. 907-13.
140. Deane, R., et al., *LRP/amyloid beta-peptide interaction mediates differential brain efflux of Abeta isoforms.* Neuron, 2004. **43**(3): p. 333-44.
141. Shibata, M., et al., *Clearance of Alzheimer's amyloid-ss(1-40) peptide from brain by LDL receptor-related protein-1 at the blood-brain barrier.* J Clin Invest, 2000. **106**(12): p. 1489-99.
142. Bradl, M. and H. Lassmann, *Progressive multiple sclerosis.* Semin Immunopathol, 2009. **31**(4): p. 455-65.
143. Kirk, J., et al., *Tight junctional abnormality in multiple sclerosis white matter affects all calibres of vessel and is associated with blood-brain barrier leakage and active demyelination.* J Pathol, 2003. **201**(2): p. 319-27.
144. Plumb, J., et al., *Abnormal endothelial tight junctions in active lesions and normal-appearing white matter in multiple sclerosis.* Brain Pathol, 2002. **12**(2): p. 154-69.
145. Wolburg, H., et al., *Localization of claudin-3 in tight junctions of the blood-brain barrier is selectively lost during experimental autoimmune encephalomyelitis and human glioblastoma multiforme.* Acta Neuropathol, 2003. **105**(6): p. 586-92.
146. Morgan, L., et al., *Inflammation and dephosphorylation of the tight junction protein occludin in an experimental model of multiple sclerosis.* Neuroscience, 2007. **147**(3): p. 664-73.

147. Fabis, M.J., et al., *Loss of blood-brain barrier integrity in the spinal cord is common to experimental allergic encephalomyelitis in knockout mouse models.* Proc Natl Acad Sci U S A, 2007. **104**(13): p. 5656-61.
148. Teller, P. and T.K. White, *The physiology of wound healing: injury through maturation.* Surg Clin North Am, 2009. **89**(3): p. 599-610.
149. Monaco, J.L. and W.T. Lawrence, *Acute wound healing an overview.* Clin Plast Surg, 2003. **30**(1): p. 1-12.
150. Stassen, J.M., J. Arnout, and H. Deckmyn, *The hemostatic system.* Curr Med Chem, 2004. **11**(17): p. 2245-60.
151. Furie, B. and B.C. Furie, *Mechanisms of thrombus formation.* N Engl J Med, 2008. **359**(9): p. 938-49.
152. Ruggeri, Z.M., *Platelets in atherothrombosis.* Nat Med, 2002. **8**(11): p. 1227-34.
153. Gailani, D. and T. Renne, *The intrinsic pathway of coagulation: a target for treating thromboembolic disease?* J Thromb Haemost, 2007. **5**(6): p. 1106-12.
154. Tanaka, K.A., N.S. Key, and J.H. Levy, *Blood coagulation: hemostasis and thrombin regulation.* Anesth Analg, 2009. **108**(5): p. 1433-46.
155. Wolberg, A.S. and R.A. Campbell, *Thrombin generation, fibrin clot formation and hemostasis.* Transfus Apher Sci, 2008. **38**(1): p. 15-23.
156. Gailani, D. and T. Renne, *Intrinsic pathway of coagulation and arterial thrombosis.* Arterioscler Thromb Vasc Biol, 2007. **27**(12): p. 2507-13.
157. Mackman, N., R.E. Tilley, and N.S. Key, *Role of the extrinsic pathway of blood coagulation in hemostasis and thrombosis.* Arterioscler Thromb Vasc Biol, 2007. **27**(8): p. 1687-93.
158. Furie, B. and B.C. Furie, *Molecular and cellular biology of blood coagulation.* N Engl J Med, 1992. **326**(12): p. 800-6.
159. Bennett, J.L., et al., *Bone marrow-derived mast cells accumulate in the central nervous system during inflammation but are dispensable for experimental autoimmune encephalomyelitis pathogenesis.* J Immunol, 2009. **182**(9): p. 5507-14.
160. Bennett, J., et al., *Blood-brain barrier disruption and enhanced vascular permeability in the multiple sclerosis model EAE.* J Neuroimmunol, 2010.
161. Dickstein, D.L., et al., *Abeta peptide immunization restores blood-brain barrier integrity in Alzheimer disease.* FASEB J, 2006. **20**(3): p. 426-33.
162. Schenk, D., et al., *Immunization with amyloid-beta attenuates Alzheimer-disease-like pathology in the PDAPP mouse.* Nature, 1999. **400**(6740): p. 173-7.
163. Ajami, B., et al., *Local self-renewal can sustain CNS microglia maintenance and function throughout adult life.* Nat Neurosci, 2007. **10**(12): p. 1538-43.
164. Guo, L., et al., *Quantitative analysis of angiogenesis using confocal laser scanning microscopy.* Angiogenesis, 2001. **4**(3): p. 187-91.
165. Weidner, N., et al., *Tumor angiogenesis and metastasis--correlation in invasive breast carcinoma.* N Engl J Med, 1991. **324**(1): p. 1-8.
166. Wang, X., et al., *Effects of factor IX or factor XI deficiency on ferric chloride-induced carotid artery occlusion in mice.* J Thromb Haemost, 2005. **3**(4): p. 695-702.
167. Denis, C., et al., *A mouse model of severe von Willebrand disease: defects in hemostasis and thrombosis.* Proc Natl Acad Sci U S A, 1998. **95**(16): p. 9524-9.

168. Subramaniam, M., et al., *Defects in hemostasis in P-selectin-deficient mice.* Blood, 1996. **87**(4): p. 1238-42.
169. Harris, J.O., et al., *Serial gadolinium-enhanced magnetic resonance imaging scans in patients with early, relapsing-remitting multiple sclerosis: implications for clinical trials and natural history.* Ann Neurol, 1991. **29**(5): p. 548-55.
170. Ujiie, M., et al., *Blood-brain barrier permeability precedes senile plaque formation in an Alzheimer disease model.* Microcirculation, 2003. **10**(6): p. 463-70.
171. Claudio, L., *Ultrastructural features of the blood-brain barrier in biopsy tissue from Alzheimer's disease patients.* Acta Neuropathol, 1996. **91**(1): p. 6-14.
172. Fiala, M., et al., *Cyclooxygenase-2-positive macrophages infiltrate the Alzheimer's disease brain and damage the blood-brain barrier.* Eur J Clin Invest, 2002. **32**(5): p. 360-71.
173. Harik, S.I. and R.N. Kalaria, *Blood-brain barrier abnormalities in Alzheimer's disease.* Ann N Y Acad Sci, 1991. **640**: p. 47-52.
174. Stewart, P.A., et al., *A morphometric study of the blood-brain barrier in Alzheimer's disease.* Lab Invest, 1992. **67**(6): p. 734-42.
175. Tomimoto, H., et al., *Alterations of the blood-brain barrier and glial cells in white-matter lesions in cerebrovascular and Alzheimer's disease patients.* Stroke, 1996. **27**(11): p. 2069-74.
176. Starr, J.M., et al., *Blood-brain barrier permeability in Alzheimer's disease: a case-control MRI study.* Psychiatry Res, 2009. **171**(3): p. 232-41.
177. Bowman, G.L., et al., *Blood-brain barrier impairment in Alzheimer disease: stability and functional significance.* Neurology, 2007. **68**(21): p. 1809-14.
178. Algotsson, A. and B. Winblad, *The integrity of the blood-brain barrier in Alzheimer's disease.* Acta Neurol Scand, 2007. **115**(6): p. 403-8.
179. Paul, J., S. Strickland, and J.P. Melchor, *Fibrin deposition accelerates neurovascular damage and neuroinflammation in mouse models of Alzheimer's disease.* J Exp Med, 2007. **204**(8): p. 1999-2008.
180. Bourasset, F., et al., *Reduction of the cerebrovascular volume in a transgenic mouse model of Alzheimer's disease.* Neuropharmacology, 2009. **56**(4): p. 808-13.
181. Rubin, L.L. and J.M. Staddon, *The cell biology of the blood-brain barrier.* Annu Rev Neurosci, 1999. **22**: p. 11-28.
182. Wolburg, H. and A. Lippoldt, *Tight junctions of the blood-brain barrier: development, composition and regulation.* Vascul Pharmacol, 2002. **38**(6): p. 323-37.
183. Bell, R.D. and B.V. Zlokovic, *Neurovascular mechanisms and blood-brain barrier disorder in Alzheimer's disease.* Acta Neuropathol, 2009. **118**(1): p. 103-13.
184. Cortes-Canteli, M., et al., *Fibrinogen and beta-amyloid association alters thrombosis and fibrinolysis: a possible contributing factor to Alzheimer's disease.* Neuron, 2010. **66**(5): p. 695-709.
185. Thal, D.R., et al., *Capillary cerebral amyloid angiopathy is associated with vessel occlusion and cerebral blood flow disturbances.* Neurobiol Aging, 2009. **30**(12): p. 1936-48.

186. Lee, P.H., et al., *Effect of ischemic neuronal insults on amyloid precursor protein processing.* Neurochem Res, 2006. **31**(6): p. 821-7.
187. Zhang, X. and W. Le, *Pathological role of hypoxia in Alzheimer's disease.* Exp Neurol, 2010. **223**(2): p. 299-303.
188. Marco, S. and S.D. Skaper, *Amyloid beta-peptide1-42 alters tight junction protein distribution and expression in brain microvessel endothelial cells.* Neurosci Lett, 2006. **401**(3): p. 219-24.
189. Gonzalez-Velasquez, F.J., J.A. Kotarek, and M.A. Moss, *Soluble aggregates of the amyloid-beta protein selectively stimulate permeability in human brain microvascular endothelial monolayers.* J Neurochem, 2008. **107**(2): p. 466-77.
190. Nagababu, E., et al., *Vascular Endothelial Barrier Dysfunction Mediated by Amyloid-beta Proteins.* J Alzheimers Dis, 2009.
191. Pun, P.B., J. Lu, and S. Moochhala, *Involvement of ROS in BBB dysfunction.* Free Radic Res, 2009. **43**(4): p. 348-64.
192. Calissano, P., C. Matrone, and G. Amadoro, *Apoptosis and in vitro Alzheimer disease neuronal models.* Commun Integr Biol, 2009. **2**(2): p. 163-9.
193. Rohn, T.T. and E. Head, *Caspase activation in Alzheimer's disease: early to rise and late to bed.* Rev Neurosci, 2008. **19**(6): p. 383-93.
194. Elmore, S., *Apoptosis: a review of programmed cell death.* Toxicol Pathol, 2007. **35**(4): p. 495-516.
195. Mattson, M.P. and T. Magnus, *Ageing and neuronal vulnerability.* Nat Rev Neurosci, 2006. **7**(4): p. 278-94.
196. Gamblin, T.C., et al., *Caspase cleavage of tau: linking amyloid and neurofibrillary tangles in Alzheimer's disease.* Proc Natl Acad Sci U S A, 2003. **100**(17): p. 10032-7.
197. Rissman, R.A., et al., *Caspase-cleavage of tau is an early event in Alzheimer disease tangle pathology.* J Clin Invest, 2004. **114**(1): p. 121-30.
198. Rohn, T.T., *The role of caspases in Alzheimer's disease; potential novel therapeutic opportunities.* Apoptosis, 2010.
199. Niu, Y.L., et al., *Expression of the apoptosis-related proteins caspase-3 and NF-kappaB in the hippocampus of Tg2576 mice.* Neurosci Bull, 2010. **26**(1): p. 37-46.
200. Deng, W., J.B. Aimone, and F.H. Gage, *New neurons and new memories: how does adult hippocampal neurogenesis affect learning and memory?* Nat Rev Neurosci, 2010. **11**(5): p. 339-50.
201. Puig, B., et al., *Expression of stress-activated kinases c-Jun N-terminal kinase (SAPK/JNK-P) and p38 kinase (p38-P), and tau hyperphosphorylation in neurites surrounding betaA plaques in APP Tg2576 mice.* Neuropathol Appl Neurobiol, 2004. **30**(5): p. 491-502.
202. Blanc, E.M., et al., *Amyloid beta-peptide induces cell monolayer albumin permeability, impairs glucose transport, and induces apoptosis in vascular endothelial cells.* J Neurochem, 1997. **68**(5): p. 1870-81.
203. Hase, M., S. Araki, and H. Hayashi, *Fragments of amyloid beta induce apoptosis in vascular endothelial cells.* Endothelium, 1997. **5**(4): p. 221-9.
204. Fossati, S., et al., *Differential activation of mitochondrial apoptotic pathways by vasculotropic amyloid-beta variants in cells composing the cerebral vessel walls.* FASEB J, 2010. **24**(1): p. 229-41.

205. Streit, W.J., R.E. Mrak, and W.S. Griffin, *Microglia and neuroinflammation: a pathological perspective.* J Neuroinflammation, 2004. **1**(1): p. 14.
206. Pogue, A.I. and W.J. Lukiw, *Angiogenic signaling in Alzheimer's disease.* Neuroreport, 2004. **15**(9): p. 1507-10.
207. Naldini, A. and F. Carraro, *Role of inflammatory mediators in angiogenesis.* Curr Drug Targets Inflamm Allergy, 2005. **4**(1): p. 3-8.
208. Schultheiss, C., et al., *In vivo characterization of endothelial cell activation in a transgenic mouse model of Alzheimer's disease.* Angiogenesis, 2006. **9**(2): p. 59-65.
209. Tarkowski, E., et al., *Increased intrathecal levels of the angiogenic factors VEGF and TGF-beta in Alzheimer's disease and vascular dementia.* Neurobiol Aging, 2002. **23**(2): p. 237-43.
210. Shibuya, M., *Brain angiogenesis in developmental and pathological processes: therapeutic aspects of vascular endothelial growth factor.* FEBS J, 2009. **276**(17): p. 4636-43.
211. Boscolo, E., et al., *Beta amyloid angiogenic activity in vitro and in vivo.* Int J Mol Med, 2007. **19**(4): p. 581-7.
212. Somanath, P.R., N.L. Malinin, and T.V. Byzova, *Cooperation between integrin alphavbeta3 and VEGFR2 in angiogenesis.* Angiogenesis, 2009. **12**(2): p. 177-85.
213. ten Dijke, P., M.J. Goumans, and E. Pardali, *Endoglin in angiogenesis and vascular diseases.* Angiogenesis, 2008. **11**(1): p. 79-89.
214. Barresi, V., et al., *Density of microvessels positive for CD105 (endoglin) is related to prognosis in meningiomas.* Acta Neuropathol, 2007. **114**(2): p. 147-56.
215. Holley, J.E., et al., *Increased blood vessel density and endothelial cell proliferation in multiple sclerosis cerebral white matter.* Neurosci Lett, 2010. **470**(1): p. 65-70.
216. Duff, S.E., et al., *CD105 is important for angiogenesis: evidence and potential applications.* FASEB J, 2003. **17**(9): p. 984-92.
217. Goddard, J.C., et al., *A computer image analysis system for microvessel density measurement in solid tumours.* Angiogenesis, 2002. **5**(1-2): p. 15-20.
218. Burger, S., et al., *Vascular endothelial growth factor (VEGF) affects processing of amyloid precursor protein and beta-amyloidogenesis in brain slice cultures derived from transgenic Tg2576 mouse brain.* Int J Dev Neurosci, 2009. **27**(6): p. 517-23.
219. Paris, D., et al., *Impaired angiogenesis in a transgenic mouse model of cerebral amyloidosis.* Neurosci Lett, 2004. **366**(1): p. 80-5.
220. Charpin, C., et al., *Tumor neoangiogenesis by CD31 and CD105 expression evaluation in breast carcinoma tissue microarrays.* Clin Cancer Res, 2004. **10**(17): p. 5815-9.
221. Vermeulen, P.B., et al., *Second international consensus on the methodology and criteria of evaluation of angiogenesis quantification in solid human tumours.* Eur J Cancer, 2002. **38**(12): p. 1564-79.
222. Behrem, S., et al., *Endoglin is a better marker than CD31 in evaluation of angiogenesis in glioblastoma.* Croat Med J, 2005. **46**(3): p. 417-22.

223. El-Gohary, Y.M., et al., *Endoglin (CD105) and vascular endothelial growth factor as prognostic markers in prostatic adenocarcinoma.* Am J Clin Pathol, 2007. **127**(4): p. 572-9.
224. Desai, B.S., et al., *Evidence of angiogenic vessels in Alzheimer's disease.* J Neural Transm, 2009. **116**(5): p. 587-97.
225. D'Andrea, M. and R. Nagele, *Morphologically distinct types of amyloid plaques point the way to a better understanding of Alzheimer's disease pathogenesis.* Biotech Histochem, 2010. **85**(2): p. 133-47.
226. Howarth, A.G., M.R. Hughes, and B.R. Stevenson, *Detection of the tight junction-associated protein ZO-1 in astrocytes and other nonepithelial cell types.* Am J Physiol, 1992. **262**(2 Pt 1): p. C461-9.
227. Bauer, H., et al., *Astrocytes and neurons express the tight junction-specific protein occludin in vitro.* Exp Cell Res, 1999. **250**(2): p. 434-8.
228. Romanitan, M.O., et al., *Occludin is overexpressed in Alzheimer's disease and vascular dementia.* J Cell Mol Med, 2007. **11**(3): p. 569-79.
229. Romanitan, M.O., et al., *Altered expression of claudin family proteins in Alzheimer's disease and vascular dementia brains.* J Cell Mol Med, 2009.
230. Rolls, A., R. Shechter, and M. Schwartz, *The bright side of the glial scar in CNS repair.* Nat Rev Neurosci, 2009. **10**(3): p. 235-41.
231. Fawcett, J.W. and R.A. Asher, *The glial scar and central nervous system repair.* Brain Res Bull, 1999. **49**(6): p. 377-91.
232. Sofroniew, M.V. and H.V. Vinters, *Astrocytes: biology and pathology.* Acta Neuropathol, 2010. **119**(1): p. 7-35.
233. Van Elzen, R., L. Moens, and S. Dewilde, *Expression profiling of the cerebral ischemic and hypoxic response.* Expert Rev Proteomics, 2008. **5**(2): p. 263-82.
234. Donato, R., et al., *S100B's double life: intracellular regulator and extracellular signal.* Biochim Biophys Acta, 2009. **1793**(6): p. 1008-22.
235. Mori, T., et al., *Overexpression of human S100B exacerbates cerebral amyloidosis and gliosis in the Tg2576 mouse model of Alzheimer's disease.* Glia, 2010. **58**(3): p. 300-14.
236. Baker, C., et al., *Effects of Alzheimer's peptide and alpha1-antichymotrypsin on astrocyte gene expression.* Neurobiol Aging, 2007. **28**(1): p. 51-61.
237. Neugroschl, J. and M. Sano, *Current treatment and recent clinical research in Alzheimer's disease.* Mt Sinai J Med, 2010. **77**(1): p. 3-16.
238. Solomon, B., et al., *Disaggregation of Alzheimer beta-amyloid by site-directed mAb.* Proc Natl Acad Sci U S A, 1997. **94**(8): p. 4109-12.
239. Solomon, B., et al., *Monoclonal antibodies inhibit in vitro fibrillar aggregation of the Alzheimer beta-amyloid peptide.* Proc Natl Acad Sci U S A, 1996. **93**(1): p. 452-5.
240. Golde, T.E., P. Das, and Y. Levites, *Quantitative and mechanistic studies of Abeta immunotherapy.* CNS Neurol Disord Drug Targets, 2009. **8**(1): p. 31-49.
241. Janus, C., et al., *A beta peptide immunization reduces behavioural impairment and plaques in a model of Alzheimer's disease.* Nature, 2000. **408**(6815): p. 979-82.
242. Morgan, D., et al., *A beta peptide vaccination prevents memory loss in an animal model of Alzheimer's disease.* Nature, 2000. **408**(6815): p. 982-5.

243. Weiner, H.L., et al., *Nasal administration of amyloid-beta peptide decreases cerebral amyloid burden in a mouse model of Alzheimer's disease.* Ann Neurol, 2000. **48**(4): p. 567-79.
244. Das, P., et al., *Reduced effectiveness of Abeta1-42 immunization in APP transgenic mice with significant amyloid deposition.* Neurobiol Aging, 2001. **22**(5): p. 721-7.
245. Arendash, G.W., et al., *Behavioral assessment of Alzheimer's transgenic mice following long-term Abeta vaccination: task specificity and correlations between Abeta deposition and spatial memory.* DNA Cell Biol, 2001. **20**(11): p. 737-44.
246. Bard, F., et al., *Epitope and isotype specificities of antibodies to beta -amyloid peptide for protection against Alzheimer's disease-like neuropathology.* Proc Natl Acad Sci U S A, 2003. **100**(4): p. 2023-8.
247. Das, P., et al., *Amyloid-beta immunization effectively reduces amyloid deposition in FcRgamma-/- knock-out mice.* J Neurosci, 2003. **23**(24): p. 8532-8.
248. Austin, L., et al., *Short-term beta-amyloid vaccinations do not improve cognitive performance in cognitively impaired APP + PS1 mice.* Behav Neurosci, 2003. **117**(3): p. 478-84.
249. Lemere, C.A., et al., *Alzheimer's disease abeta vaccine reduces central nervous system abeta levels in a non-human primate, the Caribbean vervet.* Am J Pathol, 2004. **165**(1): p. 283-97.
250. Maier, M., et al., *Short amyloid-beta (Abeta) immunogens reduce cerebral Abeta load and learning deficits in an Alzheimer's disease mouse model in the absence of an Abeta-specific cellular immune response.* J Neurosci, 2006. **26**(18): p. 4717-28.
251. Oddo, S., et al., *Reduction of soluble Abeta and tau, but not soluble Abeta alone, ameliorates cognitive decline in transgenic mice with plaques and tangles.* J Biol Chem, 2006. **281**(51): p. 39413-23.
252. Oddo, S., et al., *Abeta immunotherapy leads to clearance of early, but not late, hyperphosphorylated tau aggregates via the proteasome.* Neuron, 2004. **43**(3): p. 321-32.
253. Buckwalter, M.S., et al., *Increased T cell recruitment to the CNS after amyloid beta 1-42 immunization in Alzheimer's mice overproducing transforming growth factor-beta 1.* J Neurosci, 2006. **26**(44): p. 11437-41.
254. Chen, G., et al., *Active beta-amyloid immunization restores spatial learning in PDAPP mice displaying very low levels of beta-amyloid.* J Neurosci, 2007. **27**(10): p. 2654-62.
255. Nikolic, W.V., et al., *Transcutaneous beta-amyloid immunization reduces cerebral beta-amyloid deposits without T cell infiltration and microhemorrhage.* Proc Natl Acad Sci U S A, 2007. **104**(7): p. 2507-12.
256. Vasilevko, V., et al., *Experimental investigation of antibody-mediated clearance mechanisms of amyloid-beta in CNS of Tg-SwDI transgenic mice.* J Neurosci, 2007. **27**(49): p. 13376-83.
257. Petrushina, I., et al., *Mannan-Abeta28 conjugate prevents Abeta-plaque deposition, but increases microhemorrhages in the brains of vaccinated Tg2576 (APPsw) mice.* J Neuroinflammation, 2008. **5**: p. 42.

258. Bard, F., et al., *Peripherally administered antibodies against amyloid beta-peptide enter the central nervous system and reduce pathology in a mouse model of Alzheimer disease.* Nat Med, 2000. **6**(8): p. 916-9.
259. DeMattos, R.B., et al., *Peripheral anti-A beta antibody alters CNS and plasma A beta clearance and decreases brain A beta burden in a mouse model of Alzheimer's disease.* Proc Natl Acad Sci U S A, 2001. **98**(15): p. 8850-5.
260. Dodart, J.C., et al., *Immunization reverses memory deficits without reducing brain Abeta burden in Alzheimer's disease model.* Nat Neurosci, 2002. **5**(5): p. 452-7.
261. Kotilinek, L.A., et al., *Reversible memory loss in a mouse transgenic model of Alzheimer's disease.* J Neurosci, 2002. **22**(15): p. 6331-5.
262. Pfeifer, M., et al., *Cerebral hemorrhage after passive anti-Abeta immunotherapy.* Science, 2002. **298**(5597): p. 1379.
263. Wilcock, D.M., et al., *Passive amyloid immunotherapy clears amyloid and transiently activates microglia in a transgenic mouse model of amyloid deposition.* J Neurosci, 2004. **24**(27): p. 6144-51.
264. Wilcock, D.M., et al., *Passive immunotherapy against Abeta in aged APP-transgenic mice reverses cognitive deficits and depletes parenchymal amyloid deposits in spite of increased vascular amyloid and microhemorrhage.* J Neuroinflammation, 2004. **1**(1): p. 24.
265. Tamura, Y., et al., *The F(ab)'2 fragment of an Abeta-specific monoclonal antibody reduces Abeta deposits in the brain.* Neurobiol Dis, 2005. **20**(2): p. 541-9.
266. Hartman, R.E., et al., *Treatment with an amyloid-beta antibody ameliorates plaque load, learning deficits, and hippocampal long-term potentiation in a mouse model of Alzheimer's disease.* J Neurosci, 2005. **25**(26): p. 6213-20.
267. Racke, M.M., et al., *Exacerbation of cerebral amyloid angiopathy-associated microhemorrhage in amyloid precursor protein transgenic mice by immunotherapy is dependent on antibody recognition of deposited forms of amyloid beta.* J Neurosci, 2005. **25**(3): p. 629-36.
268. Asami-Odaka, A., et al., *Passive immunization of the Abeta42(43) C-terminal-specific antibody BC05 in a mouse model of Alzheimer's disease.* Neurodegener Dis, 2005. **2**(1): p. 36-43.
269. Lee, E.B., et al., *Targeting amyloid-beta peptide (Abeta) oligomers by passive immunization with a conformation-selective monoclonal antibody improves learning and memory in Abeta precursor protein (APP) transgenic mice.* J Biol Chem, 2006. **281**(7): p. 4292-9.
270. Levites, Y., et al., *Insights into the mechanisms of action of anti-Abeta antibodies in Alzheimer's disease mouse models.* FASEB J, 2006. **20**(14): p. 2576-8.
271. Levites, Y., et al., *Anti-Abeta42- and anti-Abeta40-specific mAbs attenuate amyloid deposition in an Alzheimer disease mouse model.* J Clin Invest, 2006. **116**(1): p. 193-201.
272. Wilcock, D.M., et al., *Deglycosylated anti-amyloid-beta antibodies eliminate cognitive deficits and reduce parenchymal amyloid with minimal vascular consequences in aged amyloid precursor protein transgenic mice.* J Neurosci, 2006. **26**(20): p. 5340-6.

273. Schroeter, S., et al., *Immunotherapy reduces vascular amyloid-beta in PDAPP mice.* J Neurosci, 2008. **28**(27): p. 6787-93.
274. Seubert, P., et al., *Antibody capture of soluble Abeta does not reduce cortical Abeta amyloidosis in the PDAPP mouse.* Neurodegener Dis, 2008. **5**(2): p. 65-71.
275. Wilcock, D.M. and C.A. Colton, *Anti-amyloid-beta immunotherapy in Alzheimer's disease: relevance of transgenic mouse studies to clinical trials.* J Alzheimers Dis, 2008. **15**(4): p. 555-69.
276. Gilman, S., et al., *Clinical effects of Abeta immunization (AN1792) in patients with AD in an interrupted trial.* Neurology, 2005. **64**(9): p. 1553-62.
277. Orgogozo, J.M., et al., *Subacute meningoencephalitis in a subset of patients with AD after Abeta42 immunization.* Neurology, 2003. **61**(1): p. 46-54.
278. Han, B.H., et al., *Cerebrovascular dysfunction in amyloid precursor protein transgenic mice: contribution of soluble and insoluble amyloid-beta peptide, partial restoration via gamma-secretase inhibition.* J Neurosci, 2008. **28**(50): p. 13542-50.
279. Masliah, E., et al., *Abeta vaccination effects on plaque pathology in the absence of encephalitis in Alzheimer disease.* Neurology, 2005. **64**(1): p. 129-31.
280. Bombois, S., et al., *Absence of beta-amyloid deposits after immunization in Alzheimer disease with Lewy body dementia.* Arch Neurol, 2007. **64**(4): p. 583-7.
281. Holmes, C., et al., *Long-term effects of Abeta42 immunisation in Alzheimer's disease: follow-up of a randomised, placebo-controlled phase I trial.* Lancet, 2008. **372**(9634): p. 216-23.
282. Nicoll, J.A., et al., *Abeta species removal after abeta42 immunization.* J Neuropathol Exp Neurol, 2006. **65**(11): p. 1040-8.
283. Nicoll, J.A., et al., *Neuropathology of human Alzheimer disease after immunization with amyloid-beta peptide: a case report.* Nat Med, 2003. **9**(4): p. 448-52.
284. Ferrer, I., et al., *Neuropathology and pathogenesis of encephalitis following amyloid-beta immunization in Alzheimer's disease.* Brain Pathol, 2004. **14**(1): p. 11-20.
285. Boche, D., et al., *Consequence of Abeta immunization on the vasculature of human Alzheimer's disease brain.* Brain, 2008. **131**(Pt 12): p. 3299-310.
286. Wilcock, D.M., et al., *Amyloid-beta vaccination, but not nitro-nonsteroidal anti-inflammatory drug treatment, increases vascular amyloid and microhemorrhage while both reduce parenchymal amyloid.* Neuroscience, 2007. **144**(3): p. 950-60.
287. Wilcock, D.M., et al., *Amyloid reduction by amyloid-beta vaccination also reduces mouse tau pathology and protects from neuron loss in two mouse models of Alzheimer's disease.* J Neurosci, 2009. **29**(25): p. 7957-65.
288. Denic, A., et al., *The relevance of animal models in multiple sclerosis research.* Pathophysiology, 2010.
289. Skundric, D.S., *Experimental models of relapsing-remitting multiple sclerosis: current concepts and perspective.* Curr Neurovasc Res, 2005. **2**(4): p. 349-62.
290. Dickstein, D.L., *The role of inflammation and amyloid beta in Alzheimer disease pathology*, in *Medical Genetics*2005, University of British Columbia: Vancouver. p. xiii, 158.

291. Braak, H. and E. Braak, *Neuropathological stageing of Alzheimer-related changes.* Acta Neuropathol, 1991. **82**(4): p. 239-59.
292. Morgan, D., *The role of microglia in antibody-mediated clearance of amyloid-beta from the brain.* CNS Neurol Disord Drug Targets, 2009. **8**(1): p. 7-15.
293. Herzig, M.C., W.E. Van Nostrand, and M. Jucker, *Mechanism of cerebral beta-amyloid angiopathy: murine and cellular models.* Brain Pathol, 2006. **16**(1): p. 40-54.
294. Park, L., et al., *NADPH-oxidase-derived reactive oxygen species mediate the cerebrovascular dysfunction induced by the amyloid beta peptide.* J Neurosci, 2005. **25**(7): p. 1769-77.
295. Perry, V.H., J.A. Nicoll, and C. Holmes, *Microglia in neurodegenerative disease.* Nat Rev Neurol, 2010. **6**(4): p. 193-201.
296. Biscaro, B., et al., *Abeta immunotherapy protects morphology and survival of adult-born neurons in doubly transgenic APP/PS1 mice.* J Neurosci, 2009. **29**(45): p. 14108-19.
297. Schmitz, C., et al., *Age-related changes of DNA repair and mitochondrial DNA synthesis in the mouse brain.* Acta Neuropathol, 1999. **97**(1): p. 71-81.
298. Schreiner, B., F.L. Heppner, and B. Becher, *Modeling multiple sclerosis in laboratory animals.* Semin Immunopathol, 2009. **31**(4): p. 479-95.
299. Leech, S., et al., *Persistent endothelial abnormalities and blood-brain barrier leak in primary and secondary progressive multiple sclerosis.* Neuropathol Appl Neurobiol, 2007. **33**(1): p. 86-98.
300. Kniesel, U. and H. Wolburg, *Tight junctions of the blood-brain barrier.* Cell Mol Neurobiol, 2000. **20**(1): p. 57-76.
301. Mankertz, J., et al., *Expression from the human occludin promoter is affected by tumor necrosis factor alpha and interferon gamma.* J Cell Sci, 2000. **113 (Pt 11)**: p. 2085-90.
302. Zamboni, P., et al., *A prospective open-label study of endovascular treatment of chronic cerebrospinal venous insufficiency.* J Vasc Surg, 2009. **50**(6): p. 1348-58 e1-3.
303. Tanzi, R.E., et al., *Protease inhibitor domain encoded by an amyloid protein precursor mRNA associated with Alzheimer's disease.* Nature, 1988. **331**(6156): p. 528-30.
304. Xu, F., M.L. Previti, and W.E. Van Nostrand, *Increased severity of hemorrhage in transgenic mice expressing cerebral protease nexin-2/amyloid beta-protein precursor.* Stroke, 2007. **38**(9): p. 2598-601.
305. Xu, F., et al., *AbetaPP/APLP2 family of Kunitz serine proteinase inhibitors regulate cerebral thrombosis.* J Neurosci, 2009. **29**(17): p. 5666-70.
306. Chen, M., et al., *Platelets are the primary source of amyloid beta-peptide in human blood.* Biochem Biophys Res Commun, 1995. **213**(1): p. 96-103.
307. Tang, K., et al., *Platelet amyloid precursor protein processing: a bio-marker for Alzheimer's disease.* J Neurol Sci, 2006. **240**(1-2): p. 53-8.
308. Atwood, C.S., et al., *Cerebrovascular requirement for sealant, anti-coagulant and remodeling molecules that allow for the maintenance of vascular integrity and blood supply.* Brain Res Brain Res Rev, 2003. **43**(1): p. 164-78.

309. Jeynes, B. and J. Provias, *The possible role of capillary cerebral amyloid angiopathy in Alzheimer lesion development: a regional comparison.* Acta Neuropathol (Berl), 2006. **112**(4): p. 417-27.
310. Merkle, D.L., et al., *Modulation of fibrin assembly and polymerization by the beta-amyloid of Alzheimer's disease.* Blood Coagul Fibrinolysis, 1996. **7**(6): p. 650-8.
311. Lee, W.H., Jr., et al., *Effects of extracorporeal circulation upon behavior, personality, and brain function. II. Hemodynamic, metabolic, and psychometric correlations.* Ann Surg, 1971. **173**(6): p. 1013-23.
312. Pardridge, W.M., R.J. Boado, and C.R. Farrell, *Brain-type glucose transporter (GLUT-1) is selectively localized to the blood-brain barrier. Studies with quantitative western blotting and in situ hybridization.* J Biol Chem, 1990. **265**(29): p. 18035-40.
313. Gupta, A. and K. Pansari, *The association between blood coagulation markers, atherothrombosis and dementia.* Int J Clin Pract, 2003. **57**(2): p. 107-11.
314. Gupta, A., et al., *Coagulation and inflammatory markers in Alzheimer's and vascular dementia.* Int J Clin Pract, 2005. **59**(1): p. 52-7.
315. Gallacher, J., et al., *Is sticky blood bad for the brain?: Hemostatic and inflammatory systems and dementia in the Caerphilly Prospective Study.* Arterioscler Thromb Vasc Biol, 2010. **30**(3): p. 599-604.
316. Stott, D.J., et al., *Activation of hemostasis and decline in cognitive function in older people.* Arterioscler Thromb Vasc Biol, 2010. **30**(3): p. 605-11.
317. Ledesma, M.D., et al., *Brain plasmin enhances APP alpha-cleavage and Abeta degradation and is reduced in Alzheimer's disease brains.* EMBO Rep, 2000. **1**(6): p. 530-5.
318. van Oijen, M., et al., *Fibrinogen is associated with an increased risk of Alzheimer disease and vascular dementia.* Stroke, 2005. **36**(12): p. 2637-41.
319. Melchor, J.P., R. Pawlak, and S. Strickland, *The tissue plasminogen activator-plasminogen proteolytic cascade accelerates amyloid-beta (Abeta) degradation and inhibits Abeta-induced neurodegeneration.* J Neurosci, 2003. **23**(26): p. 8867-71.
320. Sales, N., et al., *Cellular prion protein localization in rodent and primate brain.* Eur J Neurosci, 1998. **10**(7): p. 2464-71.
321. Bendheim, P.E., et al., *Nearly ubiquitous tissue distribution of the scrapie agent precursor protein.* Neurology, 1992. **42**(1): p. 149-56.
322. Kawarabayashi, T., et al., *Age-dependent changes in brain, CSF, and plasma amyloid (beta) protein in the Tg2576 transgenic mouse model of Alzheimer's disease.* J Neurosci, 2001. **21**(2): p. 372-81.
323. Barclay, G.R., et al., *Comparative analysis of normal prion protein expression on human, rodent, and ruminant blood cells by using a panel of prion antibodies.* Transfusion, 2002. **42**(5): p. 517-26.
324. Holada, K. and J.G. Vostal, *Different levels of prion protein (PrPc) expression on hamster, mouse and human blood cells.* Br J Haematol, 2000. **110**(2): p. 472-80.
325. Kowalska, M.A. and K. Badellino, *beta-Amyloid protein induces platelet aggregation and supports platelet adhesion.* Biochem Biophys Res Commun, 1994. **205**(3): p. 1829-35.

326. Shen, M.Y., et al., *Amyloid beta peptide-activated signal pathways in human platelets.* Eur J Pharmacol, 2008. **588**(2-3): p. 259-66.
327. Xu, F., et al., *Protease nexin-2/amyloid beta-protein precursor limits cerebral thrombosis.* Proc Natl Acad Sci U S A, 2005. **102**(50): p. 18135-40.
328. Eckman, E.A. and C.B. Eckman, *Abeta-degrading enzymes: modulators of Alzheimer's disease pathogenesis and targets for therapeutic intervention.* Biochem Soc Trans, 2005. **33**(Pt 5): p. 1101-5.
329. Davis, J., et al., *Deficient cerebral clearance of vasculotropic mutant Dutch/Iowa Double A beta in human A betaPP transgenic mice.* Neurobiology of aging, 2006. **27**(7): p. 946-54.
330. Burbach, G.J., et al., *Vessel ultrastructure in APP23 transgenic mice after passive anti-Abeta immunotherapy and subsequent intracerebral hemorrhage.* Neurobiol Aging, 2007. **28**(2): p. 202-12.
331. Karlnoski, R.A., et al., *Deglycosylated anti-Abeta antibody dose-response effects on pathology and memory in APP transgenic mice.* J Neuroimmune Pharmacol, 2008. **3**(3): p. 187-97.
332. Janicki, S.C. and N. Schupf, *Hormonal influences on cognition and risk for Alzheimer's disease.* Current neurology and neuroscience reports, 2010. **10**(5): p. 359-66.
333. Kraszpulski, M., et al., *The load and distribution of beta-amyloid in brain tissue of patients with Alzheimer's disease.* Acta neurologica Scandinavica, 2001. **103**(2): p. 88-92.
334. Callahan, M.J., et al., *Augmented senile plaque load in aged female beta-amyloid precursor protein-transgenic mice.* The American journal of pathology, 2001. **158**(3): p. 1173-7.
335. Fuller, S., M. Steele, and G. Munch, *Activated astroglia during chronic inflammation in Alzheimer's disease-Do they neglect their neurosupportive roles?* Mutat Res, 2009.
336. Ricci, G., et al., *Astrocyte-neuron interactions in neurological disorders.* J Biol Phys, 2009. **35**(4): p. 317-36.
337. Nash, M., et al., *Central nervous system regeneration inhibitors and their intracellular substrates.* Mol Neurobiol, 2009. **40**(3): p. 224-35.
338. McKeon, R.J., M.J. Jurynec, and C.R. Buck, *The chondroitin sulfate proteoglycans neurocan and phosphacan are expressed by reactive astrocytes in the chronic CNS glial scar.* J Neurosci, 1999. **19**(24): p. 10778-88.
339. Tang, X., J.E. Davies, and S.J. Davies, *Changes in distribution, cell associations, and protein expression levels of NG2, neurocan, phosphacan, brevican, versican V2, and tenascin-C during acute to chronic maturation of spinal cord scar tissue.* J Neurosci Res, 2003. **71**(3): p. 427-44.
340. Wanner, I.B., et al., *A new in vitro model of the glial scar inhibits axon growth.* Glia, 2008. **56**(15): p. 1691-709.
341. Johnson, N.A., et al., *Pattern of cerebral hypoperfusion in Alzheimer disease and mild cognitive impairment measured with arterial spin-labeling MR imaging: initial experience.* Radiology, 2005. **234**(3): p. 851-9.
342. Staffen, W., et al., *Cerebral perfusion (HMPAO-SPECT) in patients with depression with cognitive impairment versus those with mild cognitive*

impairment and dementia of Alzheimer's type: a semiquantitative and automated evaluation. Eur J Nucl Med Mol Imaging, 2009. **36**(5): p. 801-10.
343. Wolozin, B., et al., *Beta-amyloid augments platelet aggregation: reduced activity of familial angiopathy-associated mutants.* Mol Psychiatry, 1998. **3**(6): p. 500-7.